



<https://theses.gla.ac.uk/>

Theses Digitisation:

<https://www.gla.ac.uk/myglasgow/research/enlighten/theses/digitisation/>

This is a digitised version of the original print thesis.

Copyright and moral rights for this work are retained by the author

A copy can be downloaded for personal non-commercial research or study, without prior permission or charge

This work cannot be reproduced or quoted extensively from without first obtaining permission in writing from the author

The content must not be changed in any way or sold commercially in any format or medium without the formal permission of the author

When referring to this work, full bibliographic details including the author, title, awarding institution and date of the thesis must be given

Enlighten: Theses

<https://theses.gla.ac.uk/>
research-enlighten@glasgow.ac.uk

**Cell Engineering the
Osteoblast Response to Topography**

Diana Marshall Ferris

Sc. B., Brown University, 1996

Submitted for the degree of:

Master of Science (M.Sc.)

December, 1997

Supervisor: Adam S. G. Curtis

Centre for Cell Engineering, University of Glasgow

ProQuest Number: 10394691

All rights reserved

INFORMATION TO ALL USERS

The quality of this reproduction is dependent upon the quality of the copy submitted.

In the unlikely event that the author did not send a complete manuscript and there are missing pages, these will be noted. Also, if material had to be removed, a note will indicate the deletion.



ProQuest 10394691

Published by ProQuest LLC (2017). Copyright of the Dissertation is held by the Author.

All rights reserved.

This work is protected against unauthorized copying under Title 17, United States Code
Microform Edition © ProQuest LLC.

ProQuest LLC.
789 East Eisenhower Parkway
P.O. Box 1346
Ann Arbor, MI 48106 – 1346

GLASGOW UNIVERSITY
LIBRARY

1109 (copy 2)

GLASGOW
UNIVERSITY
LIBRARY

ABSTRACT

Grooved, rough, and porous surfaces are in use clinically to stabilise the bone/implant interface and encourage osseointegration for hip and knee replacements and dental implants. To date, there is no one topographical surface that is considered superior. No one has ever directly observed the process of bone formation by cells in three dimensional spaces. Also, little work on the response of cells to curved surfaces exists.

The aim of this work was two-fold: to isolate and characterise primary osteoblasts from rat and human sources, and to study the response of those cells to different topographies. Fused silica grooved surfaces (width = 2 - 100 μm , depth = 10 nm - 6.0 μm), polyurethane replicas, and fine quartz tubes (diameter = 150 - 700 μm , length = 5 mm - 2.5 cm) provided an array of topographical environments. Besides conventional techniques like video time lapse scanning cinemicrography, scanning electron microscopy, immunofluorescent (confocal scanning laser microscopy) and histological staining, two new techniques were used to assess osteoblast extracellular matrix production and orientation: polarised light microscopy and atomic force microscopy.

Findings included rat and human osteoblast sensitivity to grooved features greater than 80 and 100 nm in depth respectively. Furthermore, preliminary results suggested that grooved surfaces (width: 5 μm , depth: 6 μm) influence extracellular matrix production, i.e. the alignment of collagen and mineral with the groove long axis. The ability to influence and control the orientation of new bone via topography is the first step towards tissue engineering organised bone. In addition, the ability to control new bone growth could have an impact in the acceleration and enhancement of the wound healing and repair process.

Video time lapse cinemicrography revealed that within an hour of seeding, osteoblasts in tubes had extended towards each other and formed dynamic cord-like structures that spanned the tube diameter and along its length. Furthermore, after a few days, cells had formed nodule-like structures usually associated with two dimensional tissue culture despite the lack of ascorbic acid and β -glycerophosphate. Examination of these tubular environments with polarised light revealed birefringent particles present in some of these nodules. Osteocalcin staining showed brightly stained globules produced along cell cords and suggested the inner wall of the tube was coated by small mineralised particles.

In summary, the findings presented in this work demonstrate the ability of both material surfaces modified in a regular manner (grooves) and extended concave surfaces of small diameter (tubes) to influence osteoblast behaviour and mineralisation *in vitro*. There is some evidence to suggest that grooved surfaces influence extracellular matrix orientation, i.e. collagen and mineral alignment. Also, cells seeded into a three dimensional tubular environment behaved differently than similar cells on flat surfaces in terms of overall activity, and extracellular matrix production. In conclusion, this work imparts new information on the response of osteoblasts to topographical surfaces and environments that could lead to the tissue engineering of bone and redesign of implant surfaces.

ACKNOWLEDGMENTS

The author wishes to gratefully acknowledge numerous people for their help and support throughout this work. First of all, she would like to acknowledge her supervisor, Adam Curtis, for his challenging skepticism and critical analysis that strengthened the quality of research presented here. She would also like to thank both him and Chris Wilkinson for hospitably welcoming her to Scottish life both in and outside of the laboratory. She would also like to recognize Mathis Riehle for his support, invaluable help and seemingly inexhaustible reservoir of knowledge about almost any technical topic imaginable. She would also like to thank Jim Crossan for a difficult but fair first year viva and also for his support throughout the year. She would like to acknowledge Bill Monaghan for help in making all of the fused silica structures used in this work. Finally, last but certainly not least, she would like to acknowledge Homa Darmaui, Tong Tong Li, Karen MacDonald, Morgan Denyer, Andy Hart, Douglas Hamilton, and especially Carrie McEwen for their help, support, and for making the lab an enjoyable place to work.

TABLE OF CONTENTS

ABSTRACT	i
ACKNOWLEDGMENTS	iii
LIST OF FIGURES.....	v
LIST OF TABLES	viii
CHAPTER 1: <i>AN INTRODUCTION</i>	11
CHAPTER 2: <i>CELL CULTURE AND PHENOTYPE DETERMINATION</i>	41
CHAPTER 3: <i>HUMAN BONE CELLS</i>	63
CHAPTER 4: <i>RAT OSTEObLAST RESPONSE TO GROOVED SURFACES</i>	69
CHAPTER 5: <i>THE BEHAVIOUR OF OSTEObLASTS IN QUARTZ TUBES</i>	100
SUMMARY	121
REFERENCES.....	123

LIST OF FIGURES

Chapter 1:

Figure 1: Schematic depicting the gross structure of the osteon.13

Chapter 2:

Figure 2: a. Phase contrast picture of human osteoblasts migrating from a fragment of bone.
b. Human osteoblasts on tissue culture polystyrene early in culture. Morphological characteristics of osteoblasts include a polygonal shape and the tendency to form multilayered cultures. [Original magnification, 20x].....49

Figure 3: Phase contrast picture of a multilayered culture of rat osteoblasts plated on tissue culture polystyrene. [Original magnification, 10x].....50

Figure 4: Phase contrast picture of an unmineralised nodule found the day after reseeding human osteoblasts into a tissue culture flask. [Original magnification, 10x].....50

Figure 5: Standard curve of the absorbance of p-nitrophenol solutions.....51

Figure 6: Protein absorbance at 280 nm at various dilutions of human bone cell sample I.....51

Figure 7: Group I was incubated with p-nitrophenyl phosphate for 15 minutes while Group II had a 30 minute incubation time. Clearly, there was more alkaline phosphatase activity in human bone cell layers compared to mouse 3T3 cells. The bar above each block represents one standard deviation within that group.....53

Figure 8: von Kossa staining of human osteoblasts plated on fused silica after seven days in culture. [Original magnification: 20x]54

Figure 9: Osteocalcin staining of cells plated on fused silica [Original magnification: 40x]....55

Chapter 3:

Figure 10: Structure design for df003-df010.....66

Chapter 4:

Figure 11: Schematic depicting fused silica “mini-structures” used in mineralisation experiments (top view).....	71
Figure 12: Schematic depicting fused silica thin (150 µm) structures used in mineralisation experiments (top view).....	74
Figure 13: Computerised image of primary rat calvarial osteoblasts stained with Coomassie blue and plated onto a structure with a groove depth of 1.23 µm and groove widths of 2, 5, 10, & 20 µm. Note cell elongation in a direction parallel to the long axis of the grooves (long axis for all groove widths is horizontal with respect to the page).....	75
Figure 14: Deviation in degrees of primary rat osteoblasts from the groove long axis of various structures.	77
Figure 15: These graphs depict the number of rat calvaria osteoblasts that aligned within a range of degrees (i.e. bars @ 9° denote cells aligned 0-9° to the groove long axis) on grooved areas that are 80 nm deep and 2, 5, 10, or 20 µm wide. Note that more cells are aligned on 2 and 5 µm wide grooves, and that as the grooves become wider there is an increase in alignment variability.....	78
Figure 16: Osteoblast alignment on a structure with grooves 200 nm deeper than the structure results showed in grooved features. The alignment variability increased proportionally to groove width, but compared to Figure 15, the overall variability decreased significantly.	79
Figure 17: Osteoblast cell length on a range of groove widths and depths. Cell length tended to increase on most grooves.....	82
Figure 18: Osteoblast cell width generally decreased compared to the control.....	82
Figure 19: Phase contrast picture of live cells on a polyurethane surface (grooves 10 µm wide and 2 µm deep).....	84
Figure 20: SEM photograph of a polyurethane surface (grooves 10 µm wide and 100 nm deep) after aggregates of cells were washed off during the fixing process. Numerous, mineral-like globules ranged in size from 0.5 - 2.0 µm.....	84
Figure 21: SEM photograph of a polyurethane surface (grooves 2 µm wide and 1.23 µm deep) after aggregates of cells were washed off during the fixing process. Mineral-like globules ranged in size from 0.5 - 3.0 µm.....	85
Figure 22: Rat calvarial osteoblasts after 11 days in culture aligned along a 5 µm wide, 6.0 µm deep grooved area. Cells are secreting mineral-like extracellular matrix. Inset close-up is at x12.5K magnification.....	86
Figure 23: Bone marrow cells and some extracellular matrix found in a groove and across ridges of a 20µm wide, 5.6 µm deep patterned mini-structure. Note no overall order of extracellular matrix or cells. Inset close-up is x6.0K magnification.....	86
Figure 24: Bone marrow cells and mineral-like deposits on a 20 µm wide, 5.6 µm deep structure of fused silica.....	87
Figure 25: Bone marrow cells on grooved surface (5.0 µm wide, 5.6 µm deep) after 3 days in culture. Cells aligned and formed a nodule which was manually disrupted in order to view	

the grooved interface. There was evidence of extracellular matrix production that looked like calcium phosphate and collagen (see close up at x2.5K).	88
Figure 26: Along the periphery of the nodule (Figure 25), cells were highly aligned to the grooves (5.0 μm wide, 5.6 μm deep). Collagen-like fibrils (see inset for close-up at x11.0K) were found along cells and grooves. The overall direction of the fibrils was parallel to the grooves.	89
Figure 27: Grooved surface (5 μm wide, 3.3 μm deep) exposed to polarised light after cell sheet removal. Birefringent material along grooves appeared yellow at 90° intervals. [Original magnification = 20x]	90
Figure 28: AFM overview scan of area along a groove or ridge on a 2 μm wide, 3.3 μm deep grooved region (Field area = 7.5 μm x 7.5 μm).	91
Figure 29: Close up scan of area explored in Figure 28 (Field area = 40 nm x 40 nm).	91
Figure 30: Fine view scan of the same region (Field area = 10 nm x 10 nm).	92

Chapter 5:

Figure 31: Time lapse cinemicrography of osteoblasts seeded into a 300 μm diameter tube. [Original magnification = 20x]. Frames shown are approximately 30 minutes apart. Frame 1 represents the time just after seeding. Note, cells do not spread out individually. By 1 hour after seeding (frame 3) cells had begun to reach out to each other and formed dynamic sheets/clusters of cells. Note the dynamic detachment from the tube of one side of the bottom clump of cells from frame 7 to frame 8. By frame 9 the bottom cluster had detached from the top cluster of cells as well.	106
Figure 32: Time lapse video frames of osteoblasts after four days in culture in a 300 μm diameter quartz tube. Frames 1-12 are 1 hour apart with the exception of frames 1-2 (42 minutes apart). Note tendency of cells to form aggregate/nodule-like structures (frame 1) that move as a unit through out the tube and interact with other similar structures (frame 12). [Original magnification = 20x]	107
Figure 33: Continuation of frames in Figure 32. Frame 13 is 1 hour after frame 12 in time. Note dynamic movement of cells and cell clusters from frame 13 to frame 24. The two clusters actually merge by frame 14 and begin to move as a unit after frame 16. [Original magnification = 20x]	108
Figure 34: Time lapse cinemicrography of osteoblasts seeded into a 700 μm diameter tube after 72 hours in culture. [Original magnification = 20x]. Frames shown are approximately 1 hour apart. Note formation of cell clusters/ nodule-like structures similar to those found in 300 μm diameter tubes (Figures 31-33).	109
Figure 35: Phase contrast picture of cells in tube fixed after 18 days. Tube diameter = 270 μm . [Original magnification = 20x]	110
Figure 36: Nodule formation - phase contrast picture of live cells on Day 7 in a 700 μm diameter tube (tube length = 2.3 cm) [Original magnification = 10x]	111
Figure 37: Nodular formation - phase contrast picture of live cells spanning the tube diameter (700 μm) on Day 7 (tube length = 1.7 cm) [Original magnification = 10x]	111
Figure 38: Tube (diameter = 220 μm) full of cells and extracellular material at Day 18. [Original magnification = 40x]	112

Figure 39: Cord of cells in a tube with an inner diameter of 280 μm fixed after 18 days in culture. Confocal laser scanning image [Original magnification: 40x]. Note the globules that formed along the cord and the highly stained particles along the inner wall of the tube (see bottom of picture).....	112
Figure 40: Osteocalcin staining of cell cord spanning across a 700 μm diameter tube. Cells were fixed at 12 days of culture after 5 days of exposure to supplemented media. Confocal laser scanning image [Original magnification: 40x].	113
Figure 41: Photograph of nodule found in tube after 16 days of unsupplemented culture under polarised light [Original magnification = 20x]. Note yellow birefringent material in centre of nodule.....	114
Figure 42: Photograph of the same nodule in Figure 41 under polarised light and after 90° of rotation [Original magnification = 20x]. Note blue birefringent material in centre of nodule.....	115
Figure 43: Nodule found in 700 μm diameter tube (length = 1.4 cm) after 12 days of culture and exposure to polarised light (ascorbic acid and β -glycerophosphate added at Day 5) [Original magnification = 20x].....	116
Figure 44: Photograph of large nodule found after 12 days of culture (ascorbic acid and β -glycerophosphate added at Day 5). After exposure to polarised light, most of nodule contained regions of birefringent material. Tube diameter = 700 μm , length = 1.5 cm. [Original magnification = 10x].....	117

LIST OF TABLES

Chapter 1:

Table 1: The location of glycoproteins in bone tissue and their possible function in bone formation (Marks & Popoff ¹ , 1988; Boskey ² , 1989; Stanford & Keller ³ , 1991; Grzesik & Robey ⁴ , 1994; Davies ⁵ , 1996; Reddi ⁶ , 1997; Robey ⁷ , 1989; Boden ⁸ , et al, 1996; Mundy ⁹ , 1993).....	16
Table 2: The integrin receptors thought to bind to specific glycoproteins (Stanford & Keller, 1991; Saito, et al, 1994).....	17
Table 3: Four stages of the <i>in vitro</i> development of a mineralised matrix (Stein, et al, 1996).....	24

Chapter 2:

Table 4: Concentration (nmol/mg protein) of p-nitrophenol produced by human bone cells exposed to the p-nitrophenyl phosphate for either 15 minutes (Sample HB I) or 30 minutes (Sample HB II). The sample designations, HB a-d or HB e-h, represent cell layers from individual petri dishes.....	52
Table 5: Concentration (nmol/mg protein) of p-nitrophenol produced by mouse 3T3 cells exposed to the p-nitrophenyl phosphate substrate for either 15 minutes (Sample 3T3 I) or 30 minutes (Sample 3T3 II). The sample designations, 3T3 a-c or 3T3 d-f represent cell layers from individual petri dishes.....	52

Chapter 3:

Table 6: Groove dimensions of fused silica structures used for experiments with human bone cells.....	66
---	----

Chapter 4:

Table 7: Grooved dimensions for "mini-structures".....	71
Table 8: Grooved dimensions for thin (150 nm) structures.....	74
Table 9: Deviation in degrees from groove long axis. A measurement of 0° would be a perfectly aligned cell.....	76

Table 10: Cell major and minor axis lengths.....	80
Table 11: Cell area and perimeter on various grooved features.	81
Table 12: Statistical results for quantitative response of osteoblasts to grooved surfaces of varying dimensions.	83

Chapter 5:

Table 13: Tube dimensions.....	104
Table 14: Nodule size and number in tubes with cells cultured in the absence of β -glycerophosphate and ascorbic acid. <i>Note “*” denotes tube with flared end approximately 1.5 mm wide. All nodules presented were found in 700 μm wide end....</i>	115
Table 15: Polarised light analysis of tubes cultured in the absence of β -glycerophosphate and ascorbic acid.....	115
Table 16: Nodule size and number in tubes with cells cultured in the presence of β -glycerophosphate and ascorbic acid. <i>Note “*” denotes tube with flared end approximately 1 mm wide. All nodules presented were found in 700 μm wide end.....</i>	117
Table 17: Polarised light analysis of tubes exposed to β -glycerophosphate and ascorbic acid.	118

Chapter 1: *An Introduction*

BONE PHYSIOLOGY	12
TISSUE LEVEL MORPHOLOGY.....	12
OSTEOGENESIS.....	17
DYNAMIC NATURE OF BONE/ BONE REMODELING	19
WOUND REPAIR - HUMAN.....	21
OSTEOBLAST DIFFERENTIATION AND PHENOTYPE EXPRESSION DURING CELL CULTURE	23
DIFFERENTIATION.....	23
PHENOTYPE EXPRESSION.....	25
THE BIOMATERIAL/BONE CELL INTERFACE	26
OSTEOBLAST RESPONSE TO SURFACES	28
SURFACE ENERGY AND CHEMISTRY	28
TOPOGRAPHY.....	29
MECHANICAL STRETCHING OF OSTEOBLASTS	37
PROJECT AIMS	38
GENERAL GOALS	38
SPECIFIC GOALS.....	38

BONE PHYSIOLOGY

Tissue Level Morphology

Macroscopic Structure

All of the long bones in the human body have similar global features. Each bone consists of two regions, the epiphyses or bone ends, and the diaphysis or midshaft of the bone. The diaphysis is a long, hollow cylinder of bone with the medullary canal located in its centre. The epiphyses are comprised of cortical bone along the outer perimeter and cancellous bone in their interior (please see next section for description of cancellous and cortical bone). The surrounding “skin” of the long bone, referred to as the periosteum, consists of an outer layer of dense tissue, while osteoblasts (bone making cells) and osteoclasts (bone eating cells) are found in the osteogenic inner layer. Tendons and ligaments attach to the bone along this tissue. A similar tissue, also rich in osteoblasts and osteoclasts, the endosteum, lines the canals in bone, including both the medullary canal, and the trabeculae in cancellous bone that contact marrow (Marieb, 1995).

Microscopic Structure

Bone tissue can be classified into two types: cortical (compact), and cancellous (trabecular). Cortical bone is comprised of unit structures of oriented collagen and mineral. Cancellous bone, on the other hand, is mainly distinguishable by trabecular struts amidst a sea of marrow.

Cortical bone is teeming with channels and passages that provide pathways for nerves, blood vessels and lymphatic vessels. The structural unit of compact bone, the osteon, (**Figure 1**) is also known as a haversian system. These “tiny weight-bearing pillars” are

oriented parallel to the long axis of the cortical bone, and each is a hollow tube of bone matrix. Structurally, they are comprised of 3-7 μm thick concentric sheets of oriented collagen known as lamellae. Each sheet of collagen is oriented in the opposite direction (90°) from the one on either side of it. This structure allows bone to withstand torsional stresses - each lamellae reinforces the other. Each osteon is comprised of 4-20 lamellae and has an average diameter between 150 and 250 μm (Marieb, 1995, & Park and Lakes, 1992).

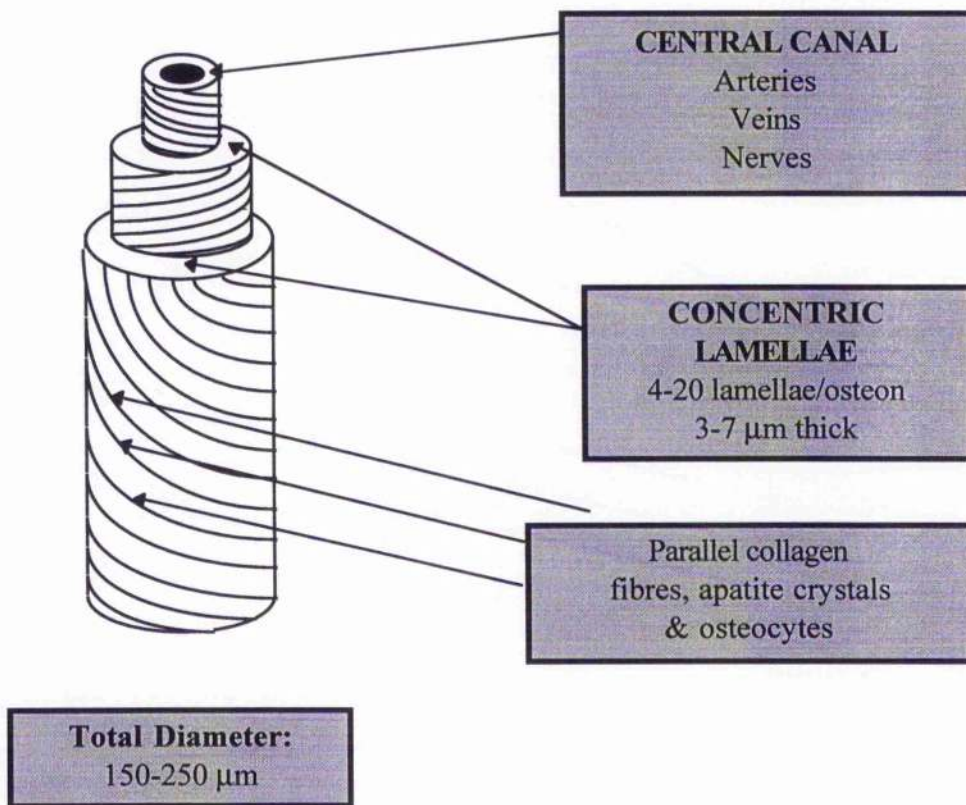


Figure 1: Schematic depicting the gross structure of the osteon.

There are two type of canals in cortical bone. Haversian canals are found in the direct centre of the osteon and contain small blood vessels and nerve fibres. Volkmann's canals, orientated perpendicular to the Haversian system, serve to connect the vascular and nerve

supplies of the periosteum to the central canals of various osteons and ultimately the medullary cavity (Webster, 1988).

At lamellae junctions, spider-shaped bone cells occupy lacunae. As the matrix hardens during bone formation, osteoblasts become trapped and mature into osteocytes in these tiny cavities. These trapped cells maintain connections with one another via long tentacle-like projections and gap junctions through tiny canals or canaliculi which also serve to connect the cells to the central canal in the osteon and enable nutrients and wastes to be delivered and removed. This network of cells and canaliculi established in the osteon is also known as the osteocytic-osteoblastic bone membrane, and separates the mineralised matrix from the plasma in the central canal (Sherwood, 1993).

Cancellous bone consists of trabeculae organised along directions of stress that act similarly to struts to support the bone. No osteons are present, instead cells are randomly arranged and interconnected via canaliculi like those canals found in cortical bone. Cancellous bone is best visualised as a sponge, with the interconnected interstices filled with bone marrow (Marieb, 1995).

Biochemical Composition:

Bone consists of both organic and inorganic parts, each contributing to its unique mechanical properties. Wet bone contains approximately 22 wt% organic matrix, of which 90-96 wt% is collagen. This organic matrix also consists of cells including osteoblasts, osteoclasts, and osteocytes, and osteoid. The mechanical properties conferred by this organic matrix include the great tensile strength of bone, its flexibility and its ability to resist stretching and twisting (Park & Lakes, 1992). The osteoid secreted by the

osteoblasts comprises about one third of the bone matrix and includes proteoglycans, glycoproteins, and collagen.

Recent research has involved the identification of glycoproteins located within bone matrix and the integrins involved in mediating cell attachment to these proteins (Tables 1 & 2). Skeletal development, bone matrix production, and pathological processes like fractures, osteogenic tumours, and metabolic bone diseases are influenced by the interactions of bone cells and their extracellular environment (Saito, et al, 1994).

Glycoprotein in Bone (*contains RGD sequence)	Location in Human Bone	Suggested Function
Fibronectin*	Mature & immature bone matrix, appears early in osteogenesis ¹	Cell adhesion ^{1,6} Multiple cell attachment mitogen ³ Differentiation ¹
Thrombospondin*	Mature bone matrix - osteoid layer (osteoblasts & osteocytes), cambial layer of periosteum, primitive woven bone, appears early in osteogenesis ⁷	Multifunctional cell adhesion modulator ⁶ Binds to calcium ⁷ Binds to osteonectin ^{3,7} Binds to hydroxyapatite ^{3,7}
Fibrillin	Bone matrix ⁶	Assembly of elastic fibre ⁶
Osteopontin* (SPP1, BSP I)	Bone matrix (secreted mostly by osteoblasts), appears later in osteogenesis ¹	Regulates & nucleates mineralisation ⁵ , involved in cell attachment ^{2,3} & tissue remodeling ⁵ , binds to hydroxyapatite ¹
Type I collagen*	Bone matrix ¹	Principal (>90%) ECM ⁶
Type III, V, X, XI, XIII collagens	Bone matrix ¹	Minor collagens ⁶
Osteonectin (SPARC)	Soft and hard tissues ^{2,3}	Modulates cell-matrix interactions ³ Links mineral to matrix ⁶
Vitronectin*	Mature bone matrix ⁴	Cell attachment ⁶
Bone sialoprotein* (BSP II)	Localised to osteoblasts primarily but has been found in platelets and cancer cells ⁵	Nucleator for mineralisation ^{5,6} Matrix organisation ³ Cell attachment ^{2,3,7}
Bone-associated glycoprotein- 75	Bone matrix ⁶	Binds calcium ⁶ and hydroxyapatite ³
Osteocalcin (bone Gla protein, BGP)	Mineralised tissues ² , but mRNA has been found in platelets ¹	Role in mineralisation ² Role in remodeling ⁶ Calcium binding protein ³ Calcium homeostasis ² Binds strongly to hydroxyapatite ¹
Matrix Gla Protein	Soft and hard tissues ^{2,3}	Regulates mineralisation ^{2,5} Calcium homeostasis ²
Bone morphogenetic proteins (BMPs)	Bone matrix ⁸	Role in differentiation ⁷ , morphogenesis ²
CS-PG I (biglycan)	Chondroitin sulphate form is unique to bone, but core protein same as dermatan sulphate PG biglycan in many soft tissues ⁵	Tissue remodelling & wound healing ⁵ Binds to collagen ⁶
CS-PG II (decorin)	Same as above	Regulates fibrillogenesis ³ Binds to TGF- β ⁶
CS-PG III	Restricted to bone (?) ⁵	Regulates mineralisation ⁵
alpha-2HS-glycoprotein	Synthesised in liver ² & found everywhere ⁵	Bone remodelling & resorption ^{2,3}
Osteoadherin	Bone matrix ⁶	Cell attachment ⁶
Osteoglycin	Bone matrix ⁶	TGF β /BMP binding ⁶

Table 1: The location of glycoproteins in bone tissue and their possible function in bone formation (Marks & Popoff¹, 1988; Boskey², 1989; Stanford & Keller³, 1991; Grzesik & Robey⁴, 1994; Davies⁵, 1996; Reddi⁶, 1997; Robey⁷, 1989; Boden⁸, et al, 1996; Mundy⁹, 1993).

Glycoprotein(s)	Integrin receptor(s)
type I or IV collagen, gelatin, laminin	$\alpha_1\beta_1$ and $\alpha_3\beta_1$
fibronectin	$\alpha_5\beta_1, \alpha_5\beta_5$ and poss. $\alpha_3\beta_1, \alpha_v\beta_1, \alpha_v\beta_3$
osteopontin, bone sialoprotein	$\alpha_v\beta_3$
vitronectin	$\alpha_v\beta_3, \alpha_v\beta_5$
fibrinogen	$\alpha_v\beta_3$
vitronectin, fibronectin, fibrinogen, thrombospondin, von Willebrand factor, bone sialoprotein & osteopontin	$\alpha_5\beta_3$

Table 2: The integrin receptors thought to bind to specific glycoproteins (Stanford & Keller, 1991; Saito, et al, 1994).

The inorganic portion of bone is responsible for 69 wt % of the bone mass and is comprised mostly of hydroxyapatite ($\text{Ca}_{10}(\text{PO}_4)_6(\text{OH})_2$) with a few other ions including citrate ($\text{C}_6\text{H}_5\text{O}_7^{4-}$), carbonate (CO_3^{2-}), fluoride (F^-), and hydroxyl ions (OH^-). Tiny calcium phosphate salt crystals on the order of 20-40 nm in length and 1.5-3 nm in width are interspersed among the collagen in the extracellular matrix. The inorganic portion of bone is responsible for conferring the mechanical property of hardness and the ability of bone to resist compression (Park & Lakes, 1992).

Ostcogenesis

In the developing human embryo, the fibrous and cartilaginous skeleton starts to be replaced by bone around week six. This ossification occurs by two processes: intramembranous and endochondral bone formation. In the former type, flat bones like those of the skull and clavicles are formed while in the case of the latter, the long bones of the skeleton are made.

At week 8, mesenchymal cells cluster together in the fibrous framework of a central ossification centre in the membrane, differentiate into osteoblasts and secrete osteoid, thus

beginning the intramembranous ossification process. After a few days, the osteoid becomes mineralised and is identical to true bone matrix. During this process some osteoblasts become trapped in the lacunae of the developing bone and mature into osteocytes. This process occurs simultaneously at multiple ossification centres until an interconnected network of trabeculae are formed. This type of bone is called woven bone because the blood vessels and collagen are arranged randomly in an overlapping fashion throughout the structure. Concomitantly, the periosteal sheet is formed at the surface of the woven bone. Eventually the woven bone around the perimeter of the bone organises itself into lamellar bone, but the interior of the bone retains its trabecular structure permanently with spaces filled with marrow (Marieb, 1995).

The second type of developmental bone formation is endochondral ossification and begins late in the second month of development. This type of bone formation involves the transformation of an existing hyaline cartilage "skeleton" into bone, and begins at a primary ossification centre. The first step is the vascularisation of the perichondrium, the outer layer covering the hyaline cartilage. This change in nutrition results in the transformation of the osteoprogenitor cells just below the perichondrium to osteoblasts. The osteoblasts secrete osteoid that encases the hyaline cartilage. During the formation of this "bone collar," the underlying cartilage cells hypertrophy and signal the surrounding matrix to calcify. The calcification of the matrix prevents nutrients from diffusing to the interior cartilage cells who subsequently die. Despite the deterioration of the interior of the forming bone, its overall structural integrity is maintained by the outer collar of bone (Marieb, 1995).

During the third month of development, the interior deteriorated matrix is invaded by a periosteal bud which includes a nutrient artery and vein, lymphatics, nerve fibres, red marrow elements, osteoblasts, and osteoclasts. The osteoblasts secrete osteoid around the hyaline cartilage remnants forming a cancellous bone structure. The region of this structure in the centre of the developing bone is broken down by osteoclasts to form the medullary canal. The bone grows distally and proximally along the epiphyseal lines by the division of cartilage cells. At birth or shortly thereafter, the epiphyses ossify via secondary ossification centres. This process differs from formation of the diaphysis in that the trabecular interior structure is retained. At the end of the entire process, cartilage cells are only found at the epiphyseal plates and the articular surfaces (Marieb, 1995).

Dynamic nature of bone/ bone remodelling

In most tissues, tissue is regenerated cell by cell. In bone however, the tissue as a whole including extracellular matrix is renewed and revitalised continuously. Between 5-7% of human bone mass is regenerated each week and the influx and outflux of calcium per day can be as much as one half a gram. Amazingly, the distal portion of the human femur is completely replaced every 5-6 months (Marieb, 1995). Thus, bone is an extremely dynamic and complex tissue that is continuously modified throughout development and life.

During the process of bone remodelling, new bone is laid down on the surface of old bone. Factors that promote bone deposition include ascorbic acid necessary for collagen synthesis, vitamin A, and minerals including calcium, phosphorus, magnesium, and manganese. These junctions of new and old bone are sometimes referred to as cement lines in the literature. The deposition of bone *in vivo* is delineated by the presence of an osteoid

seam, a 0.2-12 μm wide “gauzy-looking” band of unmineralised bone matrix. There is evidence that this region is morphologically distinct from normal mineralised bone tissue because these areas do not contain collagen, but instead consist of ground substances rich in sulphur (Marieb, 1995; Davies, 1996) Davies quotes work by Frasca (1981) that suggests these regions are sulphated protein polysaccharide complexes.

Because the transition between unmineralised and mineralised areas is quite sudden, it is speculated that some unknown factor triggers mineralisation after the 10-12 day maturation of the matrix. Known information regarding mineralisation includes the fact that specific local concentrations of calcium and phosphate ions are necessary in order for hydroxyapatite crystallised nuclei to form spontaneously. These precursor nuclei catalyse the crystallisation of calcium salts. Other factors that contribute to the matrix calcification process include the secretion of extracellular matrix proteins like osteonectin and osteocalcin which bind and concentrate calcium and high levels of alkaline phosphatase. Even though it always precedes mineralisation, the exact function of alkaline phosphatase in the mineralisation process remains a mystery.

Therefore, not only are the specifics of mineralisation not well understood, the exact mechanism by which bone responds to mechanical stress remains unknown as well. Known facts include increases in mechanical stress are directly proportional to bone deposition as evidenced by more bone mass in athletes and decreases in bedridden patients (Sherwood, 1993). Also, the deposition of bone occurs in regions of negative charge, while resorption occurs in regions of positive charge. Information obtained experimentally includes the facts that electrical current produced by bone deformation is proportional to the applied force, and compressed and stretched regions are oppositely charged.

Furthermore, electrical stimulation of fracture sites has led to the theory that these fields prevent parathyroid hormone from stimulating osteoclasts at the fracture site thereby promoting bone formation (Marieb, 1995).

Thus, bone is a dynamic tissue that is continuously undergoing the process of remodelling. It is responsible for controlling the availability of ionic calcium, a crucial player in numerous biological processes. The exact mechanisms by which mineralisation occurs *in vivo* or *in vitro* and how bone responds to mechanical influences are not well understood to date.

Wound repair - human

The healing time for a fracture in human bone is 8-12 weeks, but can last much longer for larger, weight bearing bones and older people (Marieb, 1995). Twenty-four hours from the time of fracture, a blood clot or hematoma forms at the fracture site. Osteocytes closest to the fracture are resorbed, osteoblasts deprived of nutrition die, the periosteum becomes swollen with oedema and proliferating fibroblasts. However, there is little change in the endosteum. After two days, the clot is invaded by capillaries, phagocytic cells that clean up debris, and fibroblasts that begin to lay down new osteoid. At four days, the blood clot has been mostly replaced by vascularised fibroblastic tissue (soft granulation tissue) containing nests of cartilage cells that extends down the medullary canal from the fracture line in both directions.

The next stage, callus formation, is crucial to the expeditious and successful repair of the fracture site. By the fifth day of repair, a callus produced by fibroblasts making collagen, has formed smoothly connecting the bone sides externally. The success of this stage and the next, depend on a mostly intact periosteum as a source of osteogenic, reparative cells.

Some osteogenic cells migrate from the endosteal surface and the marrow, but if the periosteum has been severely disrupted, callus bridging will not occur, an essential component of proper fracture healing. Other notes regarding callus formation include the fact that flat bones like the ribs that form via intermembranous ossification do not progress through a callus cartilaginous stage like most long bones do (Webster, 1988).

The successful and timely replacement of the callus scaffold with bone depends on immobilisation (rigid fixation favours bone formation), age, and nutrition. Bone formation at fracture sites can be stimulated with electrical fields and bone morphogenetic proteins (Webster, 1988). At the end of the week during repair, the central cartilage nests have started to calcify and osteogenic cells appear underneath the periosteum, increasing its thickness. By the tenth day, the process of replacing the fibroblastic tissue with immature woven bone has begun. At two weeks, remodelling events have created a medullary canal and endochondral bone formation is well progressed. By the eighteenth day, the periosteum is back to a normal size and a new cortical bone collar surrounds the callus remnants which include the newly formed woven bone and in the centre, the remains of the original cortex. At the end of the fourth week, the outer cortical bone collar is the same thickness as the original cortex and a red marrow medullary canal exists between the old and new cortex. Along the fracture line, the old and new cortices are bridged by foci of cartilage or fibrous tissue. By the seventh week, the fractured bone is basically back to normal (Byers, et al, 1981; Marieb, 1995). Thus, the time for wound healing to occur depends directly on the mechanical stability of the site and on the existence of an intact source of osteogenic cells.

OSTEOBLAST DIFFERENTIATION AND PHENOTYPE EXPRESSION DURING CELL CULTURE

Differentiation

ECM protein temporal markers:

Characteristics of osteoblasts include their ability to synthesise type I collagen, SPARC/osteonectin, osteopontin, bone sialoprotein and osteocalcin, in addition to high alkaline phosphatase (AIP) activity. These factors appear to be properties of cells at different maturation levels. For instance, AIP levels increase initially, but drop off as mineralisation progresses. Other observations include: osteopontin appears prior to bone sialoprotein and osteocalcin, bone sialoprotein is first detected in differentiated osteoblasts forming bone, and osteocalcin appears concomitant with mineralisation.

Gene expression:

Numerous studies reviewed recently by Stein, et al, (1996) used analytical techniques including northern blot analysis, in situ hybridisation, nuclear run-on transcription and histochemistry to paint a picture of the genes expressed during the development of osteoblasts *in vitro*. Essentially, there are four stages on route to a mature, mineralised matrix (Table 3).

During the initial proliferative stage, requisite genes like *c-myc*, *c-fos*, and *c-jun* along with histones and cyclins are expressed. In addition, genes associated with the regulation of extracellular matrix biosynthesis like TGF- β and type I collagen, integrin expression and cell adhesion markers like fibronectin can be detected. Genes for alkaline phosphatase appear during the second phase as the matrix begins to mature and prepare itself for mineralisation. Osteocalcin and osteopontin genes are expressed at maximal levels during

the third stage which is denoted by hydroxyapatite deposition. The fourth and final stage of bone matrix synthesis is hypothesised to have a editing or remodelling role. Genes for collagenase and type I collagen are expressed, and apoptosis and proliferative compensation are characteristic of this stage.

Stages of mineralised matrix formation <i>in vitro</i>	Genes expressed and matrix characteristics
Stage 1: Proliferation	<ul style="list-style-type: none"> • Expression of proliferation genes • Integrin expression • Adhesion mediators, i.e. fibronectin
Stage 2: Preparation for mineralisation	<ul style="list-style-type: none"> • Alkaline phosphatase
Stage 3: Matrix maturation	<ul style="list-style-type: none"> • Hydroxyapatite deposition • Osteocalcin & osteopontin genes @ maximal levels
Stage 4: Matrix Maintenance	<ul style="list-style-type: none"> • Type I collagen & collagenase • Apoptosis & proliferation

Table 3: Four stages of the *in vitro* development of a mineralised matrix (Stein, et al, 1996).

External factors:

Once cell attachment to an *in vivo* surface occurs, growth factors present in the bone like acidic and basic fibroblast growth factor, insulin-like growth factors I and II, platelet-derived growth factor, transforming growth factor β , and bone morphogenetic proteins influence osteoblastic functions. These factors and proteins may effect proliferation, maturation and / or differentiation of progenitor cell lines, and the formation or composition of the extracellular matrix (Stanford & Keller, 1991).

An exciting family of proteins that is the most promising in the clinical realm in terms of inducing new bone formation is the bone morphogenetic proteins (BMPs). This class of

proteins are members of the transforming growth factor- β (TGF- β) superfamily. Wang, et al, in (Boden, et al, 1996) report that these proteins have the capability to induce “full osteoblast differentiation” *in vivo*. Studies of bone development have revealed that BMP-2, BMP-4, and BMP-7 are important in earlier stages (endochondral ossification), whereas later events (membranous bone formation) are mediated by BMP-6 and BMP-7. Furthermore, BMPs are able to drive uncommitted mesenchymal or bone marrow stromal cells down the osteoblast lineage in culture (Boden, et al, 1996). Another member of the bone morphogenetic family, osteogenic protein-1, has been demonstrated to initiate and/or promote bone formation both *in vitro* and *in vivo* (Dee, et al, 1996).

Phenotype expression

Morphological appearance and mineralisation:

Osteoblasts are anchorage-dependent cells meaning they must first adhere to a surface in order for cellular functions to occur like proliferation and mineralised matrix deposition (Dee, et al, 1996). Furthermore, these cells can be defined morphologically as early (polygonal cells with refractile matrix), intermediate (polygonal cells, refractile matrix, multilayered cellular system) and mature (similar to intermediate, but with matrix visibly mineralised) (Aubin, et al, 1995).

In general, osteoblast development has three steps: proliferation, matrix synthesis and maturation, and mineralisation. The enzyme alkaline phosphatase located in matrix vesicles of chondrocytes and osteoblasts is a calcium-binding glycoprotein. In cartilage, these vesicles serve as focal points for mineralisation. During mineralisation, alkaline phosphate actually provides phosphates for immediate mineralisation in the vesicle membrane. One theory of mineralisation in bone proposes that the activation of alkaline

phosphatase and the localisation of calcium cause the first mineral crystals to be produced inside matrix vesicles. Subsequent mineralisation occurs between and along collagen fibrils (Marks & Popoff, 1988).

THE BIOMATERIAL/BONE CELL INTERFACE

When an implant is placed in the body its surface chemistry, charge density and topography immediately determine which macromolecules, i.e. proteins, sugars, ions and lipids, adsorb to its surface during the first few minutes and even seconds of implantation. Boyan, et al, (1996) suggest initial cell recruitment is determined by chemotactic factors provided by the newly conditioned implant surface, whereas recently bound proteins determine cell attachment. Martin, et al, (1995) propose that this initial cellular attachment leads to the production of cytokines and chemotactic and growth factors, thereby influencing the overall tissue response to the implant.

The surface chemistry or topography of an implant are not the only factors determining implant success *in vivo*. For example, a local factor like high oxygen tension which favours osteogenesis over chondrogenesis can be important as well. In addition, if micromotion occurs after implant placement, fibrocartilage could form. Thus, while surface characteristics may dominate the body's initial response to the implant, environmental or outer mechanical factors may play a significant role in determining overall implant success (Boyan, et al, 1996).

Besides implant surface design and external factors, it is also important to consider the site of implantation and the cell populations that could come in contact with the implant. Every surgical site will contain blood, an instant source of mesenchymal and osteoprogenitor cells. The first cells to see an implant are most likely to be

undifferentiated mesenchymal cells instead of fully mature and secretory osteoblasts. These stem cells can differentiate into osteoblasts, chondrocytes, muscle cells and adipocytes (Boyan, et al, 1996).

How accurately does *in vitro* cell culture mimic the real situation? There is some evidence that the interface constructed by osteoblasts (rat bone marrow cells) *in vitro* is similar to the one found *in vivo*. *In vitro* studies have revealed the presence of a 0.5 μm thick layer similar to the cementing line found *in vivo*. This continuous layer of globular accretions is rich in calcium, phosphorous, osteopontin and bone sialoprotein (Davies, 1996).

Despite more detailed information regarding the interface itself, Davies (1996) asserts there is a dearth of information regarding a mechanistic explanation of how materials elicit a specific bone cell response and how this interface is formed. He argues the following questions remain unsatisfactorily answered:

- How do cells make bone on foreign surfaces?
- What is the differentiation state of the osteogenic cells that colonise an implant?
- How do these cells adhere to the implant surface in a manner that permits maturation of the osteoblastic phenotype?
- Is there an identifiable sequence of matrix formation events that characterises this bone formation at an interface?
- Can the sequence of matrix formation events on implant surfaces be affected in either subtle or overt ways by the surface properties of the material?

Thus, there remains a gap in fundamental information about the biomaterial / bone cell interface and its formation.

OSTEOBLAST RESPONSE TO SURFACES

Cells are exquisitely sensitive to material surfaces. Previous studies have shown that surfaces sputter coated with various implant materials effect metabolism and phenotypic expression of osteoblasts and chondrocytes (Cooley, et al, 1992; Hambleton, et al, 1994). There is even evidence to suggest that cells are sensitive to surfaces of varying crystallinities. A study performed by Boyan, et al, (1995) indicated that alkaline phosphatase, [³H] uridine incorporation and collagen production differed significantly for chondrocytes cultured on highly ordered TiO₂ (rutile) versus amorphous TiO₂. Furthermore, Boyan, et al, quotes the work of Hanein, et al, (1994), stating that cells can differentiate between the two {011} faces (R,R) and (S,S) of calcium tartrate hemihydrate crystals. The authors suggest that protein adsorption may be different for each surface, and that this might have been the dominating factor influencing the cell response to the different surfaces.

Surface energy and chemistry

The surface energy of a material is defined as positive/negative hydrophilic or neutral hydrophobic. The surface charge creates a local environment with a specific surface tension, surface energy and adhesion energy (Boyan, et al, 1996). Hydrophilic or "wetttable" surfaces are high in energy, and encourage more cell attachment and spreading than hydrophobic surfaces. One suggested reason for this ability to induce a favourable cell response is the high amount of proteins that become adsorbed to the surface over time. For example, Chesmel and Black (1995) believe their polymeric biomaterial surfaces adsorb as much as 10-20 molecular layers of protein from media supplemented with 10% serum.

The two popular methods of altering the surface chemistry and energy of implants for orthopaedic applications with the goal of encouraging or enhancing mineralisation have been hydroxyapatite coatings and bioactive glasses. Both of these surfaces have showed increases in bone deposition but their mechanical integrity and dissolution properties are suspect (Chehroudi, et al, 1997). Thus, osteoblasts are sensitive to changes to general surface chemistry and energy. How is this response related to or similar to their response to different topographical surfaces?

Topography

Bowers, et al, (1992) report that studies involving dental implant surfaces suggest that topography plays a crucial role in implant success, rather than surface chemistry alone. A reason why surface topography may be a critical factor in determining cell response to the surface is the undeniable link between surface energy and topography. Hence, by altering the topography, and thus surface energy, one could change the proteins and other molecules that become adsorbed to the implant surface and control cell attachment later (Boyan, et al, 1996).

Clinical Implications/Motivation:

The long-term stability of orthopaedic implants for younger patients and those with active lifestyles remains an elusive goal. Polymethylmethacrylate (PMMA) cement and porous-coated structures designed to promote bone ingrowth are used clinically to stabilise the implant/bone interface (Thomas, et al, 1987). Researchers continue to search for innovative methods to improve stability and enhance bone ingrowth. In the 1980s and 1990s, researchers attempted numerous surface macro and micro textures including sintered beads, fibre meshes, plasma-spray coatings, and sand blasted or acid etched surfaces to

further stabilise the implant-bone interface (Rashmir-Raven, et al, 1995; Chae, et al, 1992; Tisdell, et al, 1994; Hayashi, et al, 1989; Wong, et al, 1995; Nimb, et al, 1995; Friedman, et al, 1995).

In each of these studies, researchers tried to improve the osseointegration of the implant and bone. Osseointegration is the attachment of bone directly to the implant surface via chemical or biochemical means (Wong, et al, 1995). It ought to be noted that other groups have defined it as the contact between bone and the implant on a light microscope level (Keller, et al, 1987). The primary goal of osseointegration is to produce a mechanically stable and long-lasting interface between the implant surface and bone. Well-osseointegrated implants will transfer the load directly to bone, potentially reducing stress shielding and bone resorption. In addition, less reaming may be necessary for fixation, leaving more of the patient's viable bone stock available for future operations. The chief factors affecting osseointegration in addition to overall implant design include the vigour of the bone remodelling response or the quality of the implant bed, the surgical skill in insertion, the physical activity level of the patient after surgery, and the overall biocompatibility of the implant materials (Wong, et al, 1995).

Surface topography also plays a role in the design of dental implants. A recent analysis of thirteen commercially available dental implants revealed large variability in terms of surface roughness/ topography, indicating that there is no consensus for the best topographical surface at this time (Wennerberg, et al, 1993). Thus, topography is an important variable in device design, and may significantly effect long term clinical success.

General discussion:

Interest in cell response to topography has spanned most of the 20th century. As early as 1911, Harrison described cell orientation and guided movement in reaction to spider web threads. In the 1940s and 50s, it was discovered that cells align to fibres and grooves (Weiss, 1945,1956). Cell sensitivity to curvature was demonstrated through experiments with cells and glass fibres by Curtis and Varde (1964). In the 1980s and 1990s, developments within the microelectronics field have enabled researchers to study cell sensitivity to the precisely defined features of multiple grooved substrata, in some cases with topographical dimensions on the order of nanometers (Clark, et al, 1987,1990; Wojciak & Crossan, 1994; Wojciak-Stothard, et al, 1995, 1996; Wojciak, et al, 1995). These developments have facilitated new bioengineering approaches to problems in the areas of tendon repair, signalling in neural networks, dental implant stability and bone formation (Wilkinson & Curtis, 1996; Chehroudi & Brunette, 1995).

Influence on cell shape:

Chehroudi, et al, (1997) suggest that one explanation for altered cell behaviour on topography may be due to the change in cell shape. Thus, the ability to control cell polarity and shape could enhance or favour osteogenesis *in vivo*.

It is believed that one of the primary regulators of the proliferative rate in anchorage dependent cells is cell shape. Rounded cells tend to divide at a lower rate compared to those that are flattened and well spread on the substrate (Boyan, et al, 1995). Furthermore, cell shape may influence protein production. Changes in cell shape are sensed through integrins on the cell membrane. These changes are then translated to the

cytoskeleton and eventually relayed to the nucleus, potentially altering phenotypic expression.

If osteoblasts display a fibroblastic morphology in culture, they secrete matrix products into the medium. However, bone-like matrices occur if the cells are rounded and multilayered at a high density (Hunter, et al, 1995). *In vivo*, osteoblasts exist in a 3-D matrix multilayered structure that is essential for terminal osteoblastic differentiation and matrix calcification (Bellows, et al, 1986). "For this reason it may be of use if an orthopaedic biomaterial does not allow spreading to a degree which may favour a change in phenotype from osteoblastic to fibroblastic at the implant-bone interface" (Ricci, et al, 1994). Thus, the ability to directly control cell shape via topography may enhance bone formation along the interface.

Rough surfaces:

Acid etching, sandblasting, sanding and polishing are non-specific methods used to alter the topography of implant surfaces. Initial studies of the osteoblast response to rough surfaces focused on cell attachment as indicative of a positive overall cell reaction to the surface. Some *in vitro* studies have demonstrated that osteoblasts prefer rough surfaces over smooth ones (Michaels, et al, 1989; Bowers, et al, 1992). Recent research, however, has suggested that cell shape may be a more important factor than attachment in terms of enhanced extracellular matrix production. Furthermore, more groups are examining the long term response of osteoblasts to the surfaces, i.e. mineralisation, as more indicative of implant success.

Martin, et al, (1995) considered the effect of roughening titanium on osteoblast proliferation, differentiation, and matrix production. Cell replication and alkaline

phosphatase activity (nonconfluent cells) were inversely related to roughness. However, osteoblasts preferred rough over smooth titanium surfaces as demonstrated by the inhibition of protein production and matrix synthesis on the smooth surfaces, and higher collagen synthesis and better matrix production on the rougher surfaces. A reason why cells preferred this rougher surface could be the increased adsorption of a cell mediator of attachment like fibronectin.

Boyan, et al, (1995) also found a decrease in cell proliferation on rough titanium surfaces and argue that this indicates an acceleration of cell differentiation. The formation of multilayered aggregates supported this theory. Furthermore, Bowers, et al, (1992) found mineralisation and alkaline phosphatase activity of confluent osteoblasts to increase proportionally to increasing roughness.

One interesting finding of Martin, et al, (1995) was that the most "regular" rough surface, i.e., a surface with 1 μm pits and 10 μm craters, seemed to stimulate calcification and matrix production and/or cell differentiation. Cell number, proliferation and cell layer alkaline phosphatase results were similar to those of osteoblasts plated on smooth surfaces. However, matrix production and cellular alkaline phosphatase results were similar to results from osteoblasts seeded onto rough surfaces. This finding offers support to the idea of using of grooved substrata with rigidly defined topography to control cell shape and influence mineralisation (discussed in the next section).

Finally, by roughening the surface unidirectionally, one is able to influence the orientation of mineralisation macroscopically. Gomi and Davies (1993) demonstrated that polystyrene dishes roughened in one direction with 600 or 320 grit sandpaper which had grain sizes of 26 μm and 46 μm respectively, produced oriented bone *in vitro* after 2 weeks

ascertained via the von Kossa staining method. Thus, roughening the surface can affect cell attachment, proliferation, protein synthesis, and may be able to orient extracellular matrix production *in vitro* and *in vivo*.

Microfabricated surfaces:

It was not until the 1990s that a few groups began to publish papers on the response of osteoblasts both *in vivo* and *in vitro* to grooved, microfabricated surfaces. In 1991, Brunette, et al, first reported the ability of these surfaces to orient osteoblasts derived from foetal rat calvaria. Epoxy resin surfaces with v-shaped grooves 18 or 30 μm deep were sputter coated with a 50 nm layer of titanium. Time lapse cinemicrography revealed that cells oriented with their long axis parallel to the grooves and moved along the long axis. *In vivo* experiments with a percutaneous/skull rat model were also conducted. No bone was present next to the smooth surfaces (12 total), and only 6 out of the 26 grooved surfaces studied exhibited bone-like tissue. Also, the authors noted oblique or perpendicular orientation of collagen to the grooves.

This work was continued by Chehroudi, et al, in 1992. Implants were identical to those used by Brunette, et al, 1991. Both rat calvarial cells (passages II & III) and calvarial explants were seeded onto microfabricated surfaces. Using compressed air to remove the outer cell layer, the authors discovered mineralised globules greater than 10 μm on the grooved surfaces, whereas smaller globules (0.5 - 3 μm) were found only on smooth surfaces after four weeks of culture. Mineralised globules 5 μm in diameter appeared only on the grooved explant surface system and not on the smooth control. No bone-like tissue was found next to smooth surfaces after implantation *in vivo*. Although this has not been rigorously confirmed, the authors found differences in the collagen fibril alignment next to

grooved surfaces versus smooth *in vivo*, and suggest that the enhanced mineralisation seen next to grooved surfaces *in vivo* may be a result of this orientation of collagen.

Qu, et al, (1996), continuing work in Brunette and Chehroudi's laboratory with cells derived from foetal rat calvaria looked at the effect of v-shaped grooved surfaces 3 μm deep (pitch ranging from 6-8 μm) on cell adhesion, cytoskeleton arrangement, and bone nodule formation *in vitro*. Significantly more osteoblast-like cells attached to the grooved surfaces and after 6 hours cells had aligned to the grooved surface. The authors report tissue orientation in the form of bone-like tissue nodules *in vitro*, and by using digital radiography methods showed tissue alignment with the groove long axis *in vivo*.

Chehroudi, et al, (1997) describe a successful *in vivo* model to quantify the amount of bone produced on grooved and pitted surfaces. The region of implantation was again, the parietal portion of male Sprague Dawley rat skulls. A total of 316 implant surfaces were analysed for bone formation after 8 weeks. Findings included the decrease of bone-like foci as groove depth increased, and the orientation of these foci with the groove long axis. In summary, grooved surfaces have demonstrated the ability to influence the production of more bone-like tissue and may influence the orientation of the tissue formed as well.

Two other groups in the 1990s have demonstrated the influence of grooved surfaces on bone cells. Gray, et al, (1996) cut 350 μm wide grooves of depths up to 200 μm into thick slabs of dental tissues with a diamond wheel. Rat calvarial osteoblasts were seeded onto the surface and examined over 2-4 weeks. The researchers found that bone formation occurred in places of "cellular condensation," i.e. within the grooves, at the junction between the slab and the culture dish, the dish periphery, and in cracks where dissimilar tissues separated. Bone formation occurred fastest in the deeper grooves.

The authors felt the results of this study demonstrated “unequivocally that the topography of the substratum affects the siting, timing and extent of new bone formation.” Furthermore, surface topography effected differentiation and cell activity in the absence of mechanical stress, a stimulus for bone formation *in vivo*. The authors also viewed that the fact the amount of new bone was proportional to increasing depth highly significant, indicating that there may be an optimum depth for bone formation.

Chesmel, et al, (1995a,b), used solvent-cast polystyrene to produce a topography of 5 μm wide grooves with depths of either 0.5 or 5 μm arranged radially around a central cell source. The surface chemistry of these structures was altered by varying the amount of styrene monomer introduced during the casting.

Various combinations of surface chemistry and topography did not significantly effect the growth rates of cells during the experiment. Surprisingly, there was no increase in the number of cells that migrated to the 0.5 and 5 μm deep grooves compared to a smooth surface. A significant difference in the amount of collagenous and noncollagenous protein produced by the cells was found between the surfaces with 0 and 1% of the styrene monomer versus the surface with 2% of the monomer, indicating cell sensitivity to the surface chemistry. There were no striking differences in protein production between the controls and the 0.5 and 5 μm deep grooves.

No qualitative differences were observed between the amount of contact guidance of cells on the 0.5 μm deep grooves versus cells on the 5 μm deep grooves. Cells in both cases were aligned along the long axis of the grooves. Grooves enhanced the radial movement of cells as measured by the radial outgrowth area, as well as the overall migration rate. This observation is supported by other studies that have shown increased

cell migration in the direction of the grooves (Ricci, et al, 1990; Ricci, et al, 1994). The fact that migration speed and orientation, and extracellular matrix production varied on different surface chemistries and topographies but were not correlated with each other suggests separate cell controls for each of these responses. In conclusion, the authors found that grooved surfaces caused confluent regions of cells and extracellular matrix to form in an “orderly” manner and that expressions of extracellular matrix proteins varied from surface to surface. Further work is necessary to clarify exactly which extracellular matrix proteins are affected.

Thus, previous work regarding the osteoblast response to grooved surfaces has determined that (1) osteoblasts are sensitive to grooved surfaces as shallow as 0.5 μm , (2) osteoblasts are responsive to grooves and surface chemistry but neither clearly dominates the other, (3) grooved surfaces promote bone formation *in vivo* and *in vitro* but the mechanism by which this occurs remains unknown, and (4) grooved surfaces influence alignment of cells and bone-like nodules and tissue in culture.

Mechanical Stretching of osteoblasts

Proto-oncogene mRNA like c-fos, c-jun and zif/268 are actively synthesised during mechanical stretching of substrates seeded with osteoblasts (Dolce, et al, 1995). These results suggest these genes are involved in the initial signal transduction during mechanical stimulus. Further support for this hypothesis is found in the work of Copley, et al, (1994) who discovered osteoblasts cultured on poly-l-lysine versus fibronectin and subjected to biaxial mechanical strain displayed significantly different proliferation rates. The reader is referred to the work of Brighton, et al, (1991, 1992, 1996); Hasegawa, et al,

(1985); Somjen, et al, (1980); Duncan, et al, (1995); and Buckley, et al, (1988) for more information regarding the influence of mechanical phenomena on osteoblast behaviour.

PROJECT AIMS

General goals

The ability to influence and control the orientation and growth of new bone via topography two and three dimensionally is the first step toward the tissue engineering of organised bone. In addition, the ability to guide new bone growth could have an impact in the acceleration and enhancement of the wound healing and repair process. This work examines the influence of micron and nanometric grooved features on cell behaviour and extracellular matrix production - namely collagen and mineral orientation.

Furthermore, this work addresses the behavioural differences of osteoblasts to flat versus extended concave surfaces (tubes). Osteoblast mineralisation has never been observed continuously in a three dimensional environment before. The diameter of these tubes is similar to that of porous surfaces used clinically, and it is hoped new, more specific information regarding mineralisation in these tubular structures can be learned that will help to optimise future prostheses.

Specific goals

Successful isolation of primary osteoblasts:

The initial aim of this project was to establish a repeatable, dependable protocol for the isolation of primary osteoblasts from human and rat sources.

Osteoblast response to grooved topography:

With a few exceptions, the majority of published literature on osteoblasts and grooved surfaces has focused on grooved dimensions on the order of tens or hundreds of microns. This work focused on smaller grooves as a method of influencing cell behaviour and matrix production. Dimensions of grooves assessed in this work are similar to those being analysed in industry (Harold Alexander, personal communication). In addition, most analysis of tissue orientation has been macroscopic in nature. This work attempted to answer the following questions that have been hitherto unsatisfactorily or unaddressed in the literature:

- How sensitive are osteoblasts to grooved topography, i.e. features as shallow as 80 nanometers?
- What is the effect on osteoblasts of varying the width of the grooves - specifically of those smaller than the average width of a bone cell, 2 and 5 μm , those the same size as the width of a bone cell, 10 μm , and those 2x the width of a bone cell?
- How is the osteoblast response different in terms of alignment or mineral production on polyurethane (a flexible surface of higher biocompatibility) versus fused silica grooved surfaces?
- How do grooved surfaces effect the extracellular matrix production of osteoblasts, i.e. do oriented osteoblasts produce oriented collagen or hydroxyapatite?

Osteoblast response to curved surfaces/tubes:

There have been few reports in the literature regarding cell behaviour in extended concave surfaces (tubes), and no one has monitored cell behaviour continuously in tubes before.

This work addressed the following questions:

- What is the effect of small diameter (150-700 μm) tubes on osteoblast behaviour?

- Does the tubular environment effect the osteoblasts' extracellular matrix production over time?
- Does varying the diameter or length of the tube have an effect on cell behaviour or extracellular matrix production?

Chapter 2: *Cell Culture and Phenotype Determination*

INTRODUCTION.....	42
MATERIALS AND METHODS.....	42
HUMAN CELL ISOLATION PROTOCOL.....	42
RAT CALVARIAL CELL ISOLATION PROTOCOL.....	43
ADULT RAT BONE MARROW CELL ISOLATION PROTOCOL.....	44
IMMUNOFLUORESCENCE.....	44
CONFOCAL LASER SCANNING MICROSCOPY.....	45
SCANNING ELECTRON MICROSCOPY.....	45
SPECTROPHOTOMETRIC ALKALINE PHOSPHATASE ASSAY.....	45
HISTOLOGICAL STAINING.....	46
RESULTS.....	47
PHENOTYPE CONFIRMATION.....	47
DISCUSSION.....	55
CELL ISOLATION PROTOCOL & MEDIA.....	55
PHENOTYPE CONFIRMATION.....	59
CONCLUSION.....	61

INTRODUCTION

A review of published protocols in the literature about the isolation of human and rat bone cells was conducted, and modified methods were developed for this work. The primary objective was to develop a repeatable isolation method that resulted in the maximum number of viable osteoblasts. Once these cells were obtained, their phenotype was examined using published criteria as a standard, i.e. alkaline phosphatase activity, osteocalcin staining, and of course, their mineralisation capability. A variety of techniques, including a spectrophotometric assay (alkaline phosphatase), polarised light microscopy, scanning electron microscopy, histological staining (von Kossa and Alizarin Red S methods) and immunofluorescence (osteocalcin and type I collagen) were used.

MATERIALS AND METHODS

Human Cell Isolation Protocol

The following isolation method was adapted from protocols discussed by Gallagher, et al, (1996). Cells were isolated from bone obtained from the iliac crest of a 27 year old male. Bone fragments were placed into a solution of Dulbecco's Modified Eagle Medium (DMEM, Sigma, UK) supplemented with 5% antibiotics, and cut into 1-3 mm pieces with sterile scissors after periosteum and soft tissue were removed. The fragments, suspended in fresh DMEM/antibiotic solution, were vortexed successively with fresh solutions until they appeared white and no blood remained.

These bone fragments were separated into two groups with approximately 1.25g of bone per group. Group A was immediately suspended in 8 ml of DMEM supplemented with 10% new-born calf serum, 2.5% glutamine/ penicillin/ streptomycin/ amphotenicin B

and 10 nM dexamethasone (Sigma, UK) and plated into 10 cm petri dishes. Group B was exposed to 2 mg/ml collagenase (Type VIII, Sigma, UK) for 1 hour at 37°C. The supernatant was discarded and the fragments were suspended in 8 ml of media and placed into 10 cm petri dishes. 50 µm/ml of L-ascorbic acid (Sigma, UK) was added fresh every 2-3 days of culture after 10 initial days of undisturbed culture. After 14 days, cells were fed as needed, usually every 2-4 days. On Day 20, fragments were resuspended manually into 10 cm petri dishes for further culture.

Rat Calvarial Cell Isolation Protocol

Isolation of calvaria from neonate (between 2-7 days old) Sprague Dawley rat pups was performed using a modified version of a protocol found in Hung, et al, (1995). The endosteum and periosteum were scraped from the frontal, parietal and occipital bones which were chopped into 1-2 mm fragments and vortexed in a DMEM/ 10 % antibiotics solution until fragments appeared white. Five 20 minute digestions at 37°C using collagenase 2 mg/ml (Type VIII or Type IA, Sigma, UK) followed. The first population released after 20 minutes was discarded. After each digestion, the supernatant was collected, media added, the solution centrifuged and cells collected in a pellet. Cells were plated into 75 cm² culture flasks in DMEM supplemented with 10% calf serum and 5% glutamine/ penicillin/ streptomycin/ amphotenicin B. Media was changed on Day 1 after plating and every 48-72 hours afterwards, and at each media changing fresh 50 µg/ml ascorbic acid was added. Either primary cells or cells no greater than passage III were used for reported experiments.

Adult Rat Bone marrow Cell Isolation Protocol

Heterogeneous cell populations were isolated from adult 125-150 g Sprague Dawley rats using a modified version of a protocol found in Herbertson and Aubin (1995). Briefly, the femurs were dissected out and placed into a solution of 10% glutamine/ penicillin/ streptomycin/ amphotenicin in Hepes saline. The proximal and distal ends were removed and the interior flushed out with the Hepes solution. This cell suspension was collected and centrifuged at 2000 rpm, and 4°C for 2 minutes. The cells from both femurs were resuspended in a T-75 tissue culture flask into DMEM supplemented with 10% calf serum and 5% glutamine/ penicillin/ streptomycin/ amphotenicin B, 50 µg/ml L-ascorbic acid (Sigma, UK) and 10 mM of β-glycerophosphate (Sigma, UK). The ascorbic acid and β-glycerophosphate were added fresh to the media at each changing (every 48-72 hours). Cells from passages I-III were used for all experiments discussed.

Immunofluorescence

The detection of osteocalcin and type I collagen of confluent rat osteoblast layers was conducted using immunofluorescent techniques. Structures and tubes were rinsed in phosphate buffered saline (PBS), and fixed in buffered formalin for 15 minutes (structures) to 1 hour (tubes). Cells were rinsed in PBS and allowed to remain in PBS at 4°C overnight. Cells were incubated in a 0.5% PBS solution of bovine albumin (Sigma, UK) for 20 minutes, followed by an incubation with anti-human osteocalcin antibody (Biogenesis) 1:25 for 1 hour, washed 2-3x with the 0.5% bovine albumin solution and incubated 1-2 hours with FITC anti-rabbit or FITC anti-mouse secondary antibody 1:50 (Sapu, Law Hospital Carluk-Lanarkshire, Scotland) 1:50.

Confocal Laser Scanning Microscopy

Cells were examined for the presence of osteocalcin and type I collagen using the Odyssey Real Time Laser Scanning Microscope Model No. VSM-LSM (Noran Instruments, Inc., Milton Keynes, UK) equipped with an argon-ion laser, and the MetaMorph Imaging System (Universal Imaging Corporation). Cells were examined under a 488 nm excitation wavelength, a 0.5 μm aperture, a 15 μm slit and a 40x objective. Proper controls for second antibody and immunofluorescence were tested with each new antibody combination.

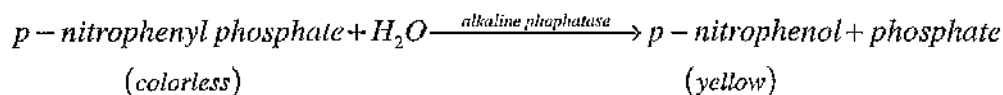
Scanning Electron Microscopy

Cells layers were washed 3-6x in warm PBS and fixed in 1% glutaraldehyde / PBS for 1 hour at 37°C. Cells were rinsed in PBS and fixed with a 1% osmium tetroxide solution in PBS for 15 minutes. Osmic acid was rinsed off with deionized water 10x. Then cells were dehydrated in the following solutions: 50% ethanol/deionized water for 10 minutes, and 2 times 100% ethanol for 10 minutes. The cells were placed in hexamethyldisilazane (HMDS, Sigma, UK) for 5 minutes followed by a final rinse in HMDS. The remaining HMDS was poured off and the samples were allowed to dry overnight and then coated with a 200 Å layer of gold/palladium using a sputter coater (SC500, Emscope). Samples were viewed with a scanning electron microscope (S-800, Hitachi).

Spectrophotometric alkaline phosphatase assay

Confluent cultures of primary human bone cells and rat calvarial osteoblasts were tested for alkaline phosphatase activity. Cultures of mouse 3T3 fibroblast cells served as an

initial control. The principle behind the alkaline phosphatase assay is to determine the amount of p-nitrophenol produced during the reaction:



The rate of increase in absorbance at 405-410 nm is directly proportional to the alkaline phosphate activity in the sample.

Cell layers were lysed just after confluency was reached using a 0.1% Triton X-100 solution of 0.1 M 2-amino-2-methyl-1-propanol. 200 µl of cell extract was added to 800 µm of a 7 mM solution of p-nitrophenyl phosphate (Sigma, UK) and 500 µm of 0.1 M 2-amino-2-methyl-1-propanol. The reaction was carried out for group I (human cells) at 37°C for 15 minutes and for group II (human cells) for 30 minutes at 37°C. The reaction was quenched on ice and 1 ml of 0.2 N NaOH was added to halt the reaction. The production of p-nitrophenol was measured at 410 nm using a UV-visible recording spectrophotometer (Shimadzu, UV-160). Standard curves were obtained using p-nitrophenol solutions (Sigma, UK). All values were normalised with respect to the amount of protein present in each sample as determined by measuring the absorbance of cell extracts at 280 nm.

Histological Staining

von Kossa method

The objective of the von Kossa method is to identify calcium phosphate mineralisation in osteoblast culture. This method depends on a salt substitution reaction between silver

nitrate and calcium phosphate. The silver phosphate is reduced to black metallic silver by the action of light (Culling, et al, 1985; Lillie, et al, 1976; Kiernan, 1981).

Briefly, after cell layer confluency, "mineralising media" including 50 µg/ml ascorbic acid and 10 mM β-glycerol phosphate was added. When mineralised nodules appeared, the cells were prepared for von Kossa staining. The cell layer was rinsed 2x in HEPES saline or PBS, fixed in 95% ethanol at 4°C for 5 minutes and rinsed in distilled water 3x. A 5% solution of silver nitrate was added to the cell layer, and the reaction was carried out in sunlight and/or bench top light for approximately 1 hour. The layer was washed well with distilled water and counter stained with neutral red (0.5%) for 60 seconds.

Alizarin Red S

The objective of the Alizarin Red S method is also the detection of calcium deposits. The following protocol was adapted from methods by Drury & Wallington (1967) and Kiernan (1981). After fixation, cell layers were rinsed in distilled water. A 2% alizarin red S (Sigma, UK) solution (pH 4.2) was added for 1-5 minutes and the reaction monitored under a microscope until completion. The layers were differentiated in a 0.05% hydrochloric acid/95% ethanol solution for 15 seconds. The layer was rinsed in 100% ethanol two times and rinsed in histoclear twice for 5 minutes.

RESULTS

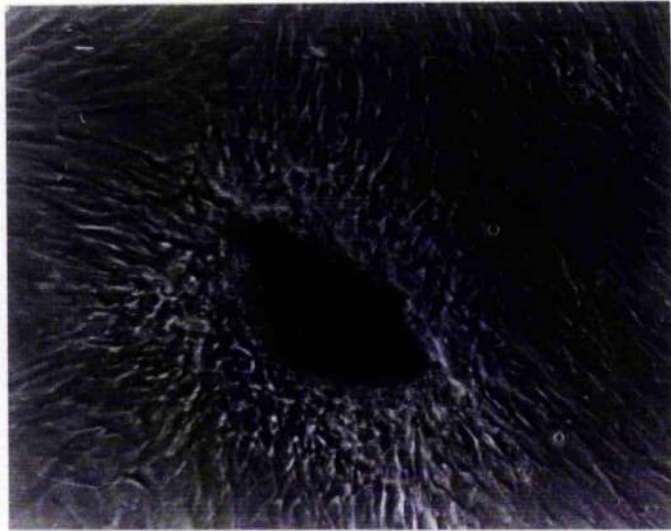
Phenotype confirmation

Cell phenotype was confirmed by typical osteoblast morphology, the high activity of alkaline phosphatase, positive staining for osteocalcin, and the ability of these cells to form

mineralised nodules in culture as ascertained by von Kossa and Alizarin Red S staining, and polarised light microscopy (see sections below).

General morphology:

Isolated rat and human osteoblasts displayed osteoblastic morphology in culture. Typical characteristics included a polygonal shape (**Figure 2**), and the tendency to form multilayered tissue (**Figure 3**). Furthermore, osteoblasts formed nodules several days after reaching confluency in culture (**Figure 4**).



a.



b.

Figure 2: **a.** Phase contrast picture of human osteoblasts migrating from a fragment of bone. **b.** Human osteoblasts on tissue culture polystyrene early in culture. Morphological characteristics of osteoblasts include a polygonal shape and the tendency to form multilayered cultures. [Original magnification, 20x]

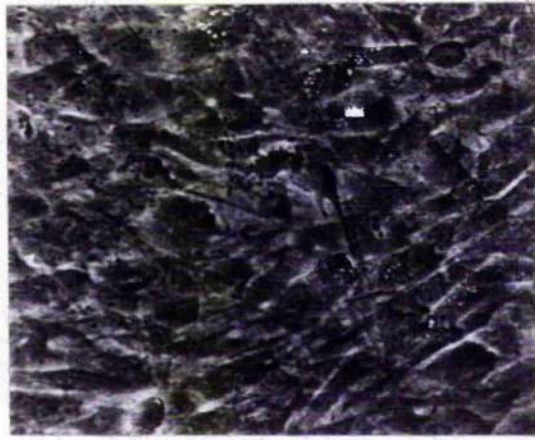


Figure 3: Phase contrast picture of a multilayered culture of rat osteoblasts plated on tissue culture polystyrene. [Original magnification, 10x]

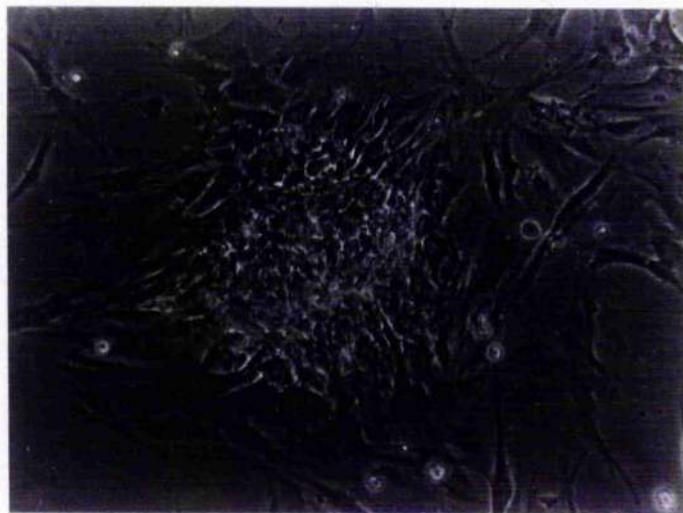


Figure 4: Phase contrast picture of an unmineralised nodule found the day after reseeding human osteoblasts into a tissue culture flask. [Original magnification, 10x]

Alkaline phosphatase assay:

Alkaline phosphatase activity was confirmed for both human and rat cells using a spectrophotometric assay and mouse 3T3 fibroblasts as negative controls. The following

results compare human versus 3T3 mouse fibroblast alkaline phosphatase activity. A standard curve was obtained using p-nitrophenol solutions (**Figure 5**).

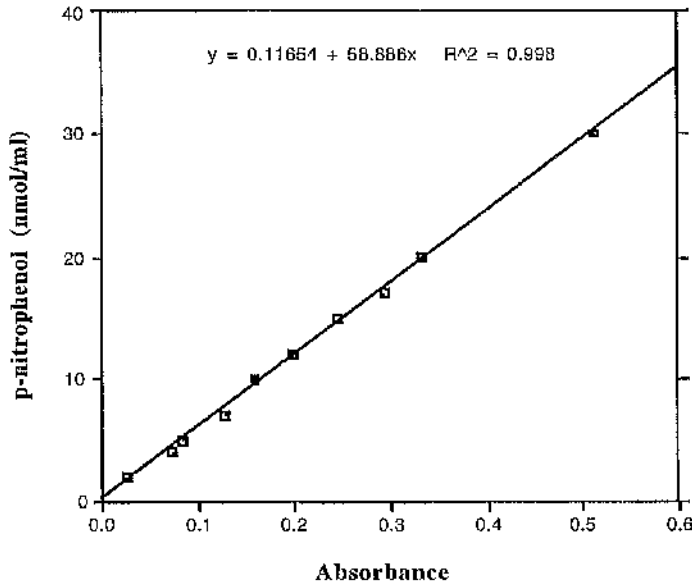


Figure 5: Standard curve of the absorbance of p-nitrophenol solutions.

The linear region of the absorbance curve for protein measured at 280 nm was determined based on the following curve (**Figure 6**).

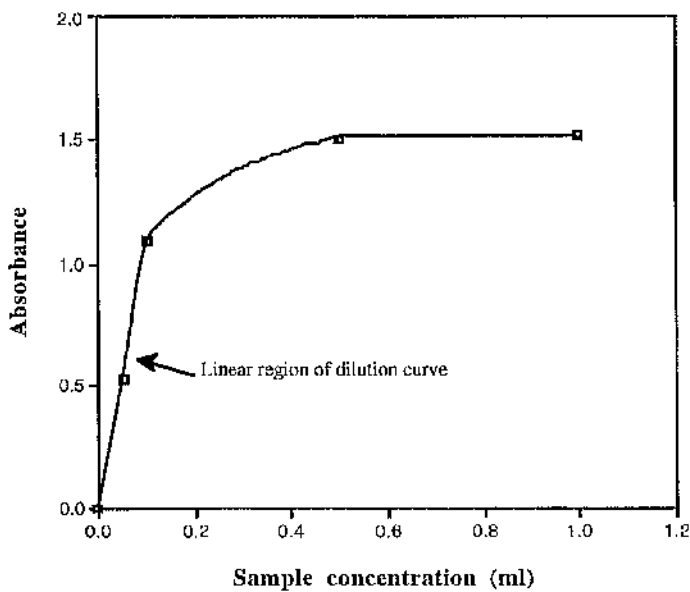


Figure 6: Protein absorbance at 280 nm at various dilutions of human bone cell sample I.

Thus, 0.05 ml of sample was used for each protein measurement.

The spectrophotometric measurements of individual cell layer extracts represented in the following tables as HB x or 3T3 x clearly showed a higher alkaline phosphatase activity for human bone cell cultures compared to mouse 3T3 fibroblast cultures (Tables 4-5, Figure 7).

Sample HB I	[p-nitrophenol] (nmol/mg protein)	Sample HB II	[p-nitrophenol] (nmol/mg protein)
HB a	0.51	HB e	1.32
HB b	0.45	HB f	0.78
HB c	0.46	HB g	0.92
HB d	0.69	HB h	1.66
Average	0.53	Average	1.17
SD	0.11	SD	0.40

Table 4: Concentration (nmol/mg protein) of p-nitrophenol produced by human bone cells exposed to the p-nitrophenyl phosphate for either 15 minutes (Sample HB I) or 30 minutes (Sample HB II). The sample designations, HB a-d or HB e-h, represent cell layers from individual petri dishes.

Sample 3T3 I	[p-nitrophenol] (nmol/mg protein)	Sample 3T3 II	[p-nitrophenol] (nmol/mg protein)
3T3 a	0.07	3T3 d	0.04
3T3 b	0.09	3T3 e	0.03
3T3 c	0.09	3T3 f	0.06
Average	0.08	Average	0.04
SD	0.01	SD	0.01

Table 5: Concentration (nmol/mg protein) of p-nitrophenol produced by mouse 3T3 cells exposed to the p-nitrophenyl phosphate substrate for either 15 minutes (Sample 3T3 I) or 30 minutes (Sample 3T3 II). The sample designations, 3T3 a-c or 3T3 d-f represent cell layers from individual petri dishes.

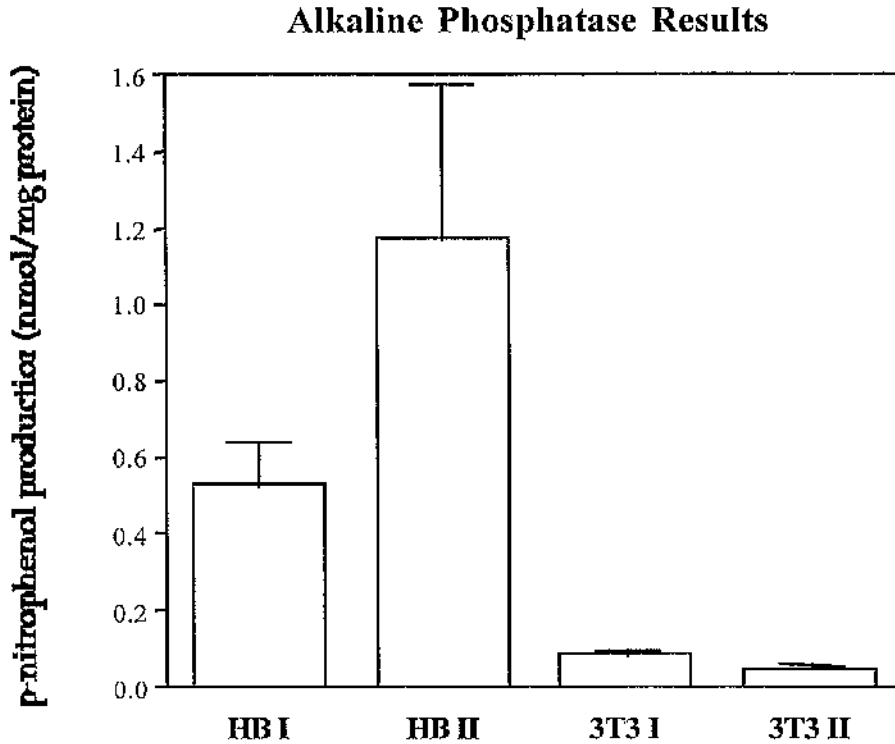


Figure 7: Group I was incubated with p-nitrophenyl phosphate for 15 minutes while Group II had a 30 minute incubation time. Clearly, there was more alkaline phosphatase activity in human bone cell layers compared to mouse 3T3 cells. The bar above each block represents one standard deviation within that group.

As expected, when the incubation time of the human bone cell sample and the p-nitrophenyl phosphate substrate was doubled, the production of p-nitrophenol also doubled. The average production of p-nitrophenol for both groups of human bone cells was greater than the mouse 3T3 cells, and the production of p-nitrophenol by the HB II's was significantly ($P < 0.001$) greater than either 3T3 I or 3T3 II. There was no statistical difference between the I and II groups of the mouse 3T3s.

von Kossa staining:

Confluent cultures of human and rat osteoblasts on fused silica stained positively for the presence of calcium salts using von Kossa histological staining (**Figure 8**).

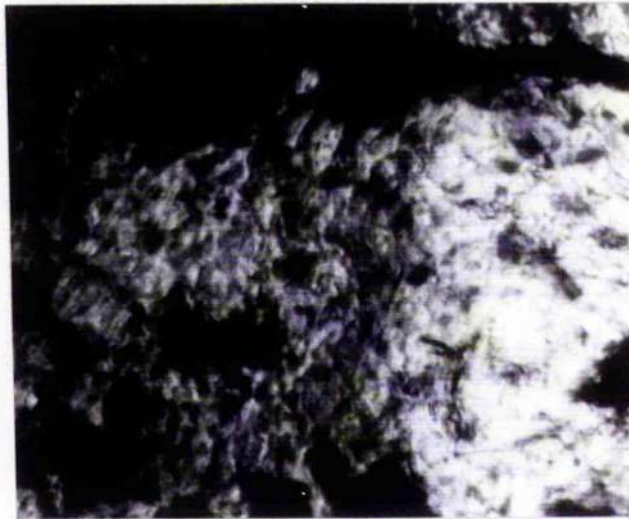


Figure 8: von Kossa staining of human osteoblasts plated on fused silica after seven days in culture. [Original magnification: 20x]

Alizarin Red S staining:

Confluent cultures of rat osteoblasts stained positively for calcium deposits using the Alizarin Red S staining method (not shown).

Immunofluorescence:

Cells on fused silica surfaces and inside quartz tubes were stained for osteocalcin and type I collagen. Autofluorescent and secondary antibody controls for reported results were negative. Type I collagen staining was considered too weak to prove conclusive. Layers of rat osteoblasts and matrix stained heavily for osteocalcin however (**Figure 9**). Refer to tube results section (Chapter 5) for more osteocalcin staining.



Figure 9: Osteocalcin staining of cells plated on fused silica [Original magnification: 40x]

DISCUSSION

Cell Isolation Protocol & Media

In vitro studies of osteoblasts over the last ten-odd years have concluded that specific supplements must be added to the media in order to promote mineralisation in culture. Even the standard use of serum is important. Schmidt and Kulbe (1993) reported loss of osteoblastic phenotype when cells were cultured with foetal calf serum. Thus, calf serum was used to supplement media throughout this work. Another culture supplement, the glucocorticoid dexamethasone, has been reported to increase bone nodule formation (discussed below) by bone marrow stromal cells (Herbertson and Aubin, 1995). The use of this additive remains controversial, however. Majeska, et al, (1981) report glucocorticoids inhibit the biosynthesis of alkaline phosphatase. All human bone cells in this work were cultured in the presence of 10 nM dexamethasone. Because of the unknown effect of this supplement, its use was discontinued for all rat bone marrow and calvarial cell cultures discussed.

Two other culture supplements, ascorbic acid and β -glycerophosphate are widely accepted as necessary additives to promote *in vitro* mineralisation (Owen, et al, 1990; Aronow, et al, 1990; Bellows, et al, 1986). L-ascorbic acid (Vitamin C) is a necessary supplement to the media, because it is required during the synthesis of collagen. Specifically, it acts as a cofactor during the hydroxylation of lysine and proline residues (Gallagher, et al, 1996; Chehroudi, et al, 1992). L-ascorbic acid has also been reported to increase proliferation, α 1(I)-procollagen mRNA, and noncollagenous protein (osteocalcin and bone sialoprotein synthesis) production in human osteoblasts (Gallagher, et al, 1996). For these reasons, ascorbic acid was added fresh to the media throughout cell culture.

It should be noted that the addition of β -glycerophosphate in order to promote *in vitro* mineralisation does not necessarily mimic the *in vivo* mineralisation situation. This phosphate is not available physiologically, and it has not been unequivocally demonstrated that it acts similarly to phosphates during *in vivo* mineralisation (Gallagher, et al, 1996). Experimental work (Owen, et al, 1990) has determined the concentrations of 50 μ g/ml ascorbic acid and 10 mM β -glycerophosphate as the most effective in promoting mineralisation. Thus, these concentrations were used throughout this work.

Human Cells:

The decision to use primary human bone cells is not a new one (Begley, et al, 1993; Schmidt and Kulbe, 1993) There are several reasons why this is a difficult system to work with, however. First of all, the isolation and culture of these cells is not trivial. Bone fragments from a patient are placed into media and cells migrate out weeks later, making the culture of these cells time consuming. In addition, there is a limited amount of genetic variability when using cells derived from only one patient. Also, other factors like age and

sex effect the cell pool isolated. Serum levels of osteocalcin are higher in men than women and decrease as the patient ages (Schmidt and Kulbe, 1993). Despite these difficulties, however, the use of human cells is more appealing in terms of species specificity and clinical relevance.

Rat Calvarial Cells:

The rat calvarial model, both foetal and neonatal, is a well established, widely used method for the isolation of osteoblasts enzymatically released with collagenase and/or trypsin (McCabe, et al, 1994; Bizios, 1994; Harris, et al, 1994; Bellows, et al, 1986). In fact, it has been used successfully for several decades (Stein, et al, 1996). When using this isolation method, it is important to consider the osteogenic potential of the various populations of cells released and the effects of passaging those cells. Bellows, et al, (1986) report that cell populations released after ten minutes of collagenase digestion were unable to form mineralised bone nodules due to the high proportion of fibroblasts. Secondly, groups report loss of phenotype after more than three passages (Valentini, personal communication) in culture. Thus, in order to maximise the osteogenic potential of cells used in this work, cells released from the first twenty minutes of the enzymatic isolation were discarded and cell populations were only used for experiments until passage III.

There is published evidence that cells released from rat calvaria accurately mimic their *in vivo* properties. Cells obtained from osteopetrotic rats retained *in vivo* pathological characteristics of precocious and intensified mineralisation when studied *in vitro* (Stein, et al, 1996). Thus, the rat calvarial model is a reasonable, relatively straight forward isolation method for the initial assessment of various topographical surfaces.

Adult Rat Bone Marrow cells:

In an effort to more accurately imitate *in vivo* reality, researchers have begun to use adult rat bone marrow as a source of undifferentiated and partially differentiated osteogenic cells (Davies, 1996; Herbertson & Aubin, 1995; Benayahu, et al, 1995; Bruder, et al, 1994). Although this cell source is heterogeneous, including mesenchymal stem cells, fibroblasts, endothelial cells and adipocytes, the mesenchymal stem cells present can be driven down several lineages, namely the osteoblast, chondroblast or adipocyte paths (Benayahu, et al, 1995).

Herbertson and Aubin (1995) report that by altering culture conditions, one is able to promote the differentiation of a specific cell type from those cells that adhere to the tissue culture flask after isolation from the marrow. Specifically, 1/300th (Aubin, et al, 1990) of the cells from rat bone marrow stroma cultured in conditions favouring bone formation were found to be osteoprogenitor cells. When ascorbic acid and β -glycerophosphate were included in the media, these authors reported the ability of these cells to form mineralised nodules. Furthermore, Davies (1996) has demonstrated that the interface formed by these cells on biomaterials is identical to the interface found on retrieved implants and in cement lines.

In an effort to encourage these cells down the osteoblast line, ascorbic acid and β -glycerophosphate were added to the media from day 1 of culture and to each media change during experiments discussed in this work. It is believed that this isolation method more accurately reflects the *in vivo* situation of wound repair and response to implant placement.

Phenotype confirmation

By tailoring cell isolation methods reported in the literature and only using primary cells or at most passage III cells, a cell population of both human and rat osteoblasts was isolated in a reproducible manner. Analysis of cells using standard techniques like an alkaline phosphatase spectrophotometric assay, histological staining including von Kossa and Alizarin Red S methods, immunofluorescent staining for osteocalcin and scanning electron microscopy, polarised light microscopy, and atomic force microscopy to detect extracellular matrix production produced revealed osteoblastic characteristics similar to those reported in the literature.

Alkaline phosphatase assay:

The relative levels of alkaline phosphatase produced by human or rat osteoblasts compared to mouse fibroblasts were different as expected. Mouse 3T3 cells did not produce significant levels of alkaline phosphatase, and human and rat cells produced more levels of the enzyme overall.

The high standard deviations seen in groups I and II of the human osteoblasts may be due to slightly different stages of confluency reached by each dish. As osteoblasts become more multilayered their levels of alkaline phosphatase reach a peak and then tend to drop off as mineralisation occurs (Robey, 1989). Thus, alkaline phosphatase production is directly related to tissue maturity and culture time conditions. In conclusion, cells isolated from a 27 year old male human and rat calvaria displayed significantly higher levels of alkaline phosphatase than mouse fibroblast controls as predicted.

Culture mineralisation characteristics:

It is well documented that cellular condensation precedes bone formation both *in vitro* and *in vivo* (Gray, et al, 1996). The name given to these dense, three dimensional regions of cells, mineral and matrix is *nodule*. Numerous groups have reported that this phenomenon can only be produced in *in vitro* cell culture conditions if the media is supplemented with ascorbic acid and β -glycerophosphate (Bellows, et al, 1986; Aronow, et al, 1990; Harris, et al, 1994; Owen, et al, 1990; Ecarot-Charrier, et al, 1988; Pockinwise, et al, 1992). For example, Bellows, et al, (1986) observed 75 μ m thick, three-dimensional nodules three days after the confluency of osteoblasts derived from foetal calvaria grown in media supplemented with ascorbic acid, and β -glycerophosphate. Aronow, et al, (1990) and Harris, et al, (1994) reported similar findings. Mineralised bone nodules in cell culture can form as early as 24 hours in after the addition of β -glycerophosphate to confluent cell layers (Ecarot-Charrier, et al, 1988). These nodules resemble woven bone, and stain heavily for alkaline phosphatase, type I collagen and mineral (von Kossa technique).

Other analytical techniques have been employed to study nodules formed *in vitro*. Pockinwise, et al, (1992) demonstrated cellular orientation towards the nodule apex and a rough crystalline surface appearance due to deposited mineral and matrix using scanning electron microscopy (SEM). Ultrastructural analysis has revealed that mineralised nodules constructed by foetal or neonatal rat cell populations closely resemble sections of rat calvaria (Owen, et al, 1990) in terms of an ordered deposition of apatite crystals in a matrix of orthogonally organised collagen bundles (Pueleo, et al, 1991).

Thus, various groups have reported that cells isolated from rats and mice form bone nodules under specific *in vitro* culture conditions. These nodules have been examined

histochemically using von Kossa and alkaline phosphatase staining methods, ultrastructurally via TEM analysis, and morphologically with phase contrast techniques and SEM analysis. Most of these techniques in addition to 2 new ones: polarised light microscopy and atomic force microscopy, were used to assess osteoblast mineralisation *in vitro* in this work.

Histological staining:

The von Kossa staining method is a widely used protocol to detect *in vitro* mineralisation by osteoblasts (Dee, et al, 1996; Stein, et al, 1990). In addition to using this method to detect mineralised regions in culture, researchers have used it to determine overall mineralised tissue organisation (Gomi and Davies, 1993) It should be noted, however, that the von Kossa method simply displaces the calcium in any calcium salt, meaning it is not strictly specific for calcium phosphate or hydroxyapatite.

In an effort to confirm von Kossa results, the Alizarin Red S staining method was employed. This stain forms an orange-red chelate complex with calcium, and only stains large deposits of calcium well (Bancroft, et al, 1994). A comparison of cultures stained using each of these staining protocols revealed that similar regions stained with Alizarin Red S were much more diffuse in nature. Thus, the author feels the Alizarin Red S staining method is even more non-specific than the von Kossa staining method.

CONCLUSION

Populations of viable osteoblasts were derived from human and rat sources using repeatable cell isolation methods. Analytical techniques revealed the ability of cell populations to produce alkaline phosphatase and mineralised nodules in culture. Thus, it

was concluded that the majority of cells used to study cell response and mineralisation to topographical surfaces were indeed osteoblasts.

Chapter 3: *Human Bone Cells*

INTRODUCTION.....	64
MATERIALS AND METHODS.....	64
TOPOGRAPHIC SURFACES.....	64
EXPERIMENTS.....	65
RESULTS.....	66
DISCUSSION/CONCLUSIONS.....	67

INTRODUCTION

A protocol for the isolation of human bone cells was developed and carried out. Cell phenotype was assessed by morphological characteristics, alkaline phosphatase activity, and mineralisation (von Kossa staining). This chapter focuses on the reaction of these cells to grooved topography in terms of sensitivity to nanometric size features and the effect these surfaces have, if any, on mineralisation. The results reported below are preliminary in nature. Unfortunately, a lack of cells from one source prevented the author from conducting further experiments.

MATERIALS AND METHODS

***Note**

Please refer to Chapter 2 for the cell isolation method and analytical techniques not reported below but used in this chapter.

Topographic Surfaces

Fused silica surfaces patterned using photolithographic techniques were used for the experiments discussed in this section. One mm fused silica samples (Multilab, Newcastle, UK) were cleaned prior to patterning with a 3:1 solution of sulphuric acid:hydrogen peroxide for 5-10 minutes at 60°C, rinsed in R.O. water and blown dry. A layer of photoresist (AZ 1400-31) was spun on in 30 seconds at 4000 rpm, and the entire sample placed in the oven for 30 minutes at 90°C. A chrome mask with the necessary pattern allowed irradiation with UV light of specific portions of the photoresist. These areas were developed and removed in a 1:1 solution of Shipley developer: R.O. water. Samples were

then dry etched in a Reactive Ion Etching Unit. Acetone was used to remove residual resist and the entire sample was etched for one more minute to ensure even surface chemistry. Before repeat experiments, structures were cleaned again using a 3:1 solution of sulphuric acid:hydrogen peroxide for 15 minutes and rinsed in deionized water. Structures were stored in 100% ethanol, and before use flame sterilised and placed into individual petri dishes or wells.

Experiments

All structures were comprised of fused silica and had varying dimensions (**Table 6**). Some structures had regions of 2, 5, 10, 20 μm grooves separated by control flat surfaces (**Figure 10**). Structures df003, df006, and df009 were seeded with first passage human cells at a concentration of approximately 2.6×10^4 cells/structure. Structures df004, df005, df007, df008, df010, AC018 were seeded with second passage human cells at a concentration of approximately 7.5×10^3 cells/structure. Structures df001, df002 were seeded with second passage cells at a concentration of 1.5×10^4 cells/structure. The cell response to these surfaces was monitored over several weeks. β -glycerophosphate was added fresh to the media at each changing after cell layer confluency. Mineralised nodule formation was assessed with the von Kossa method.

Structure	Depth (μm)	Groove Widths (μm)
AC018	5000	5 & 10
df001	600	12.5
df002	1100	12.5
df003	10	2, 5, 10 & 20
df004	60	2, 5, 10 & 20
df005	80	2, 5, 10 & 20
df006	100	2, 5, 10 & 20
df007	280	2, 5, 10 & 20
df008	670	2, 5, 10 & 20
df009	1230	2, 5, 10 & 20
df010	2000	2, 5, 10 & 20

Table 6: Groove dimensions of fused silica structures used for experiments with human bone cells.

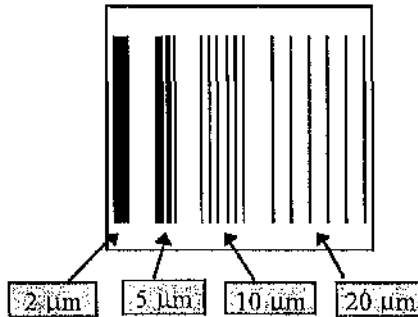


Figure 10: Structure design for df003-df010.

RESULTS

Several experiments were conducted to ascertain the response of human osteoblasts to various grooved surfaces. In general, when grooved features were equal to or greater than 100 nanometers, osteoblasts aligned parallel to the groove long axis. This alignment usually occurred within the first day of seeding. However, during the course of one

experiment, cells did not align until day 11 on the 2 μm and 5 μm wide grooves of structure df005 (depth = 80 nm).

Another observation included the tendency of sheets of osteoblasts to detach from the structure after a certain period of time in culture. Usually nodules lined the leading edge of the sheet and the sheet generally lifted off from the 20 μm end of the structure first.

Nodules appeared on flat surfaces and grooves as early as the day after the addition of β -glycerophosphate to the culture. In one experiment, five days after adding β -glycerophosphate to the media, six mineralised nodules were found on structure df001 (width = 12.5 μm , depth = 0.6 μm) while three were found on df002 (width = 12.5 μm , depth = 1.1 μm).

DISCUSSION/CONCLUSIONS

Two intriguing results emerged from preliminary studies of the human osteoblast response to grooved surfaces. The first result was the time-dependent response in terms of cell alignment linked to features smaller than the average width of a bone cell, 10 μm , i.e. 2 μm and 5 μm and as shallow as 80 nanometers over a period of eleven days. There is evidence for time dependent migration of osteoblasts to carboxyl terminated regions from methyl terminated ones on self assembled monolayers of gold thiol groups (Colin Scotchford, personal communication). Thus, these cells have the capacity to react preferentially over time to biomaterial surfaces in culture.

The second interesting, result included the retained alignment of cell sheets. Other cells, i.e. MDCK cells, form attachments with each other and do not remain aligned after confluency is reached (Clark, et al, 1990). This retention of alignment follows published results by Gomi and Davies (1993), Qu, et al, (1996) and Chehroudi, et al, (1997) who

report overall tissue organisation along the direction parallel to grooves or surface scratches in both *in vitro* and *in vivo* cases. The ability of aligned bone cells to produce oriented tissue is the first step towards the tissue engineering of bone.

The tendency of cell sheets to peel off after significant time in culture implies that the focal attachments of osteoblasts for each are stronger and more appealing than those of the inflexible fused silica surface. This result suggests that the modulus of elasticity of the substrate is crucial, i.e., bone cells might prefer a more flexible surface closer to the material properties of bone. Another interpretation of these results is that this is a simple matter of cell adhesion. If the surface was chemically modified to be more "adhesive," i.e. a more hydrophilic surface, maybe cell attachment could be sustained.

Did the topography presented to the human bone cells influence mineralisation? Twice as many nodules formed when the structure depth was 0.6 μm as on 1.1 μm depth (width = 12.5 μm), suggesting there may be an optimum topography for mineralisation. More work is necessary to confirm this result.

Chapter 4: *Rat Osteoblast Response to Grooved Surfaces*

INTRODUCTION.....	70
MATERIALS AND METHODS.....	70
GROOVED SUBSTRATES.....	70
QUANTITATIVE CELL RESPONSE TO TOPOGRAPHY	72
EXTRACELLULAR MATRIX PRODUCTION	72
RESULTS	74
QUANTITATIVE RESPONSE TO TOPOGRAPHY	74
EXTRACELLULAR MATRIX PRODUCTION	83
DISCUSSION.....	92
QUANTITATIVE RESPONSE TO TOPOGRAPHY	92
EXTRACELLULAR MATRIX PRODUCTION	93
CONCLUSIONS.....	99

INTRODUCTION

The focus of this chapter is to provide fresh information regarding the osteoblast response to grooved surfaces by applying new analytical techniques like polarised light microscopy and atomic force microscopy in order to gain more knowledge regarding extracellular matrix production by osteoblasts *in vitro*. In addition, this work investigates how sensitive rat osteoblasts are to nanometric size features.

MATERIALS AND METHODS

*Note

Please refer to Chapter 2 for the cell isolation method and analytical techniques not reported below but used in this chapter.

Grooved Substrates

Fused silica surfaces patterned using photolithographic techniques (see below) and solvent castings of these surfaces with polyurethane (see below) were used for the experiments discussed in this work.

Photolithographic techniques:

Please refer to Chapter 3 for photolithography fabrication process details. “Mini-structures” 7 mm x 7 mm were designed for extracellular matrix production analysis experiments such that half of the structure contained equivalent grooves and ridges and the other half was flat (**Figure 11**). All structures were cut from the same slide of fused silica and had depths ranging from 130 nm to 6.0 μm , and groove widths of 5, 20, or 100 μm (**Table 7**).

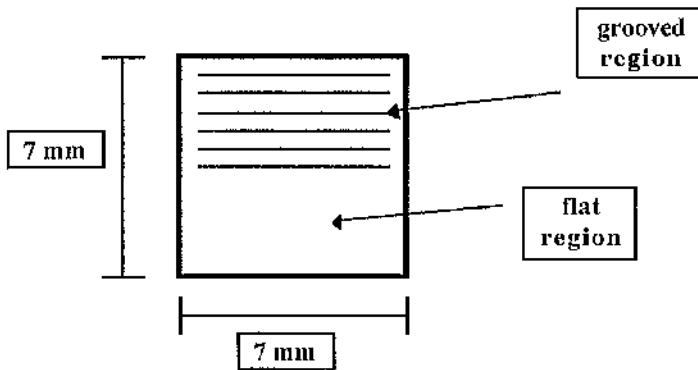


Figure 11: Schematic depicting fused silica “mini-structures” used in mineralisation experiments (top view).

Sample Name	Pattern Size	Etch depth
A1	5 μm line/space	130 nm
A2	“	700 nm
A3	“	1.5 μm
A4	“	3.6 μm
A5	“	5.6 μm
A6	“	6.0 μm
B1	20 μm line/space	130 nm
B2	“	700 nm
B3	“	1.5 μm
B4	“	3.6 μm
B5	“	5.6 μm
B6	“	6.0 μm
C1	100 μm line/space	130 nm
C2	“	1.5 μm
C3	“	3.6 μm
C4	“	6.0 μm

Table 7: Grooved dimensions for “mini-structures.”

Solvent Casting:

Polyurethane replicas of structures were cast by pouring dissolved polyurethane monomer and solvent over fused silica structures in a glass petri dish. The glass dish containing the

polyurethane solvent solution was baked at 80 °C for 24-48 hours. Upon removal and cooling, the dish was left to soak in a Decon solution for 24-48 hours. Structures were removed with a scalpel, rinsed in deionized water, followed by rinsing several times in 70 % ethanol and allowed to air dry in sterile petri dishes. Cloning rings were flame sterilised and placed on top of structures to prevent them from floating during cell seeding and culture.

Quantitative Cell Response to Topography

Primary rat calvaria osteoblasts were seeded multiple times onto structures of fused silica at a concentration of 2.5×10^5 cells/ml. Cells aligned over a 48 hour period, were stained with Brilliant Coomassie blue and analysed using an image analysis program (NIH Image Analysis 1.61). An average of 53 cells were analysed per groove depth/width. Parameters measured included cell area, cell perimeter, the deviation in degrees of the cell major axis from the long axis of the groove, and the length of the cell's major and minor axis. Data was analysed statistically using the nonparametric Mann-Whitney test (Instat 2.0, GraphPad Software).

Extracellular Matrix Production

Three analytical techniques were used to assess extracellular matrix production on grooved surfaces: scanning electron microscopy (SEM), polarised light microscopy (PLM), and atomic force microscopy (AFM).

SEM Analysis:

Rat calvarial osteoblasts and bone marrow cells were seeded onto structures at a density of $1.0-2.4 \times 10^5$ cells/ml for mineralisation experiments on fused silica. β -glycerophosphate

(10 mM) was added once rat calvarial cultures became confluent. (Bone marrow cells were cultured continuously in the presence of β -glycerophosphate and ascorbic acid. Rat calvarial cells were cultured continuously in the presence of ascorbic acid.) Rat calvarial cells (Day 11) and bone marrow cells (Day 3) were fixed for SEM analysis (See Chapter 2 for method.).

Rat calvarial osteoblasts were also seeded onto polyurethane replicas of structures df006-10 (see Chapter 3) at a concentration of 10×10^5 cells/ml. The entire experiment with newly cast polyurethane structures was repeated three separate times in order to confirm results.

PLM Analysis:

Extracellular matrix production was also assessed with polarised light microscopy. After fixation in buffered formalin, various samples were suspended in PBS on glass slides and examined under polarised light. In addition to the microscope analyser and the polariser, samples were viewed under a red I plate compensator. Samples were rotated through 360° and addition and subtraction colour changes noted.

AFM Analysis:

Passage 2 rat osteoblasts were plated at a concentration of 2.5×10^5 onto small coverslip structures (**Figure 12, Table 8**). β -glycerophosphate (10 mM) was added to media the day after plating. After fixation (Day 7) in buffered formalin the underlying surface (the confluent cell layer had been removed manually) was examined using contact mode atomic force microscopy.

Sample Name	Pattern Size	Etch depth
C	2 & 5 μm line/space	800 nm
D	10 & 20 μm line/space	800 nm
F	2 & 5 μm line/space	3.3 μm
G	10 & 20 μm line/space	3.3 μm

Table 8: Grooved dimensions for thin (150 μm) structures.

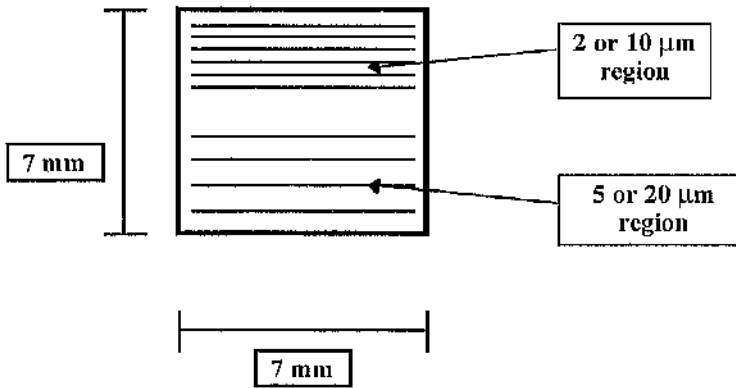


Figure 12: Schematic depicting fused silica thin (150 μm) structures used in mineralisation experiments (top view).

RESULTS

Quantitative response to topography

Rat osteoblasts were sensitive to grooved surfaces as demonstrated by their alignment to the groove long axis (Table 9, Figures 13 & 14). They were guided by features as shallow as 80 nm. As grooves increased in depth by 200 nm, cell alignment increased significantly ($P < 0.0002$) and cells were more sensitive to 2 μm and 5 μm features versus 10 μm and 20 μm ones (Figures 15 & 16). As the grooves became deeper, depth became the controlling factor and groove width ceased to have a significant effect in terms of

alignment, although the mean angle for cell alignment was always lower on the 2 and 5 μm wide grooves versus the 10 and 20 μm ones.

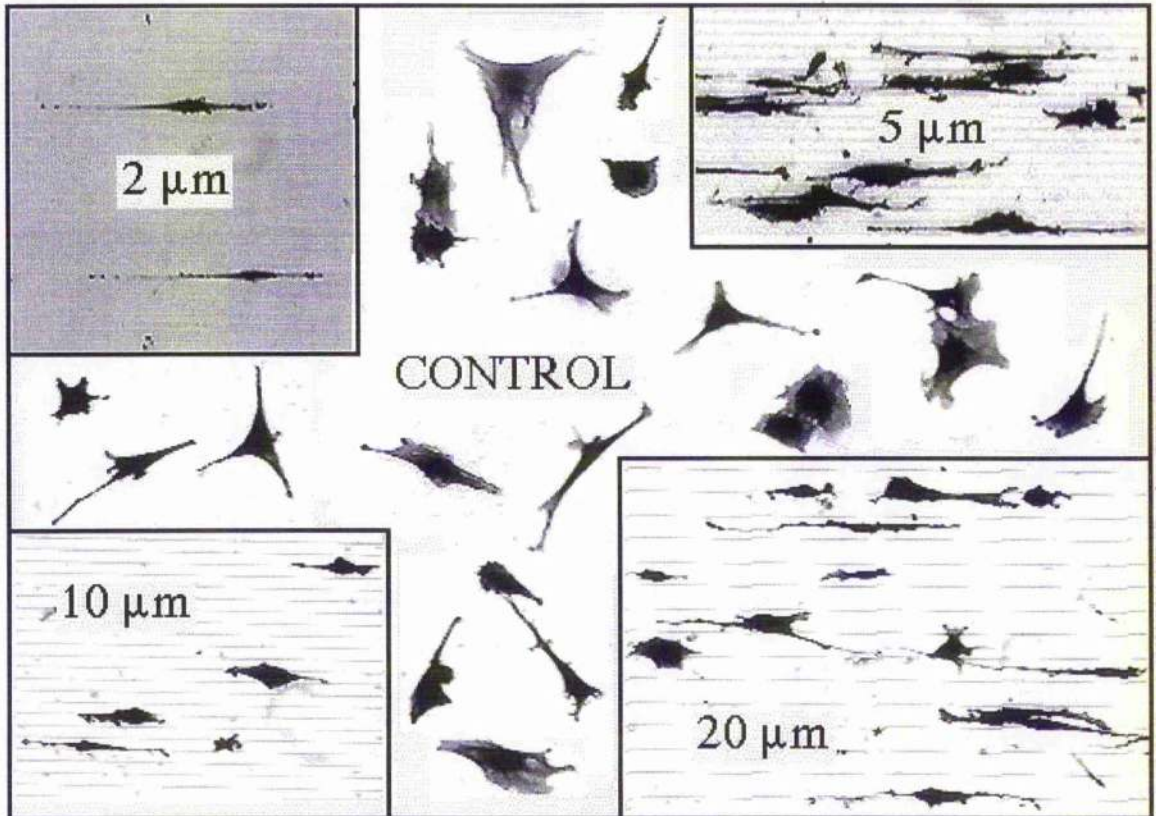


Figure 13: Computerised image of primary rat calvarial osteoblasts stained with Coomassie blue and plated onto a structure with a groove depth of 1.23 μm and groove widths of 2, 5, 10, & 20 μm . Note cell elongation in a direction parallel to the long axis of the grooves (long axis for all groove widths is horizontal with respect to the page).

Structure	Groove width (μm)/ depth (μm)	Cell number examined	Angle mean (degrees)	95% Confidence Limit	
				Minimum	Maximum
Flat Control		124.00	49.58	45.11	54.09
df005	2 / 80	62.00	15.48	11.49	20.23
	5 / 80	39.00	17.55	13.47	21.64
	10 / 80	49.00	36.62	29.56	43.69
	20 / 80	43.00	37.21	29.57	44.85
df007	2 / 280	24.00	3.76	2.03	5.49
	5 / 280	30.00	8.76	3.79	13.74
	10 / 280	36.00	11.38	6.27	16.48
	20 / 280	60.00	14.77	10.13	19.40
df008	2 / 670	42.00	5.70	3.22	8.18
	5 / 670	37.00	6.75	3.83	9.68
	10 / 670	56.00	7.81	5.05	10.57
	20 / 670	46.00	11.97	7.29	16.66
df009	2 / 1230	49.00	3.98	1.33	6.62
	5 / 1230	87.00	4.84	2.97	6.72
	10 / 1230	67.00	7.55	4.36	10.75
	20 / 1230	56.00	7.94	3.94	11.941
df001	12.5 / 600	59.00	5.99	4.20	7.78
df002	12.5 / 1100	36.00	5.42	3.51	7.34

Table 9: Deviation in degrees from groove long axis. A measurement of 0° would be a perfectly aligned cell.

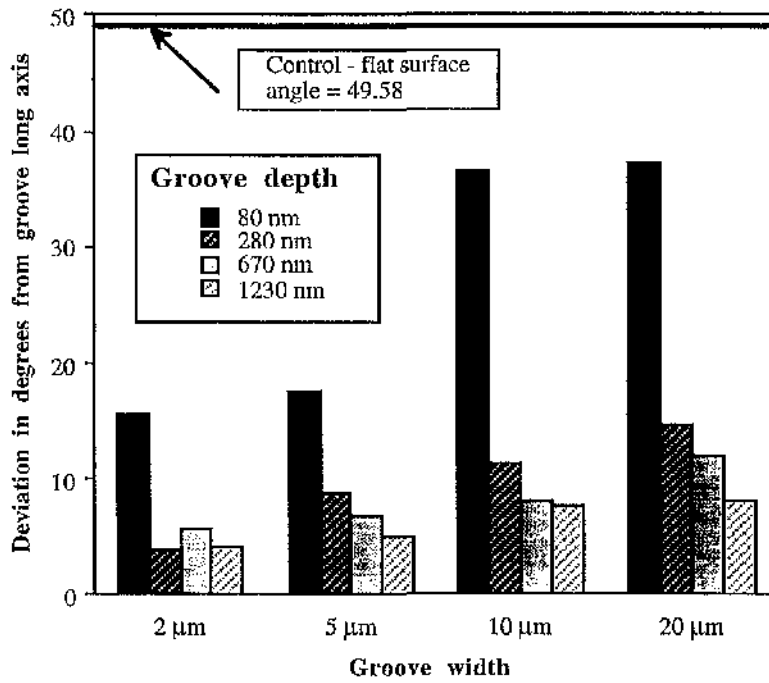


Figure 14: Deviation in degrees of primary rat osteoblasts from the groove long axis of various structures.

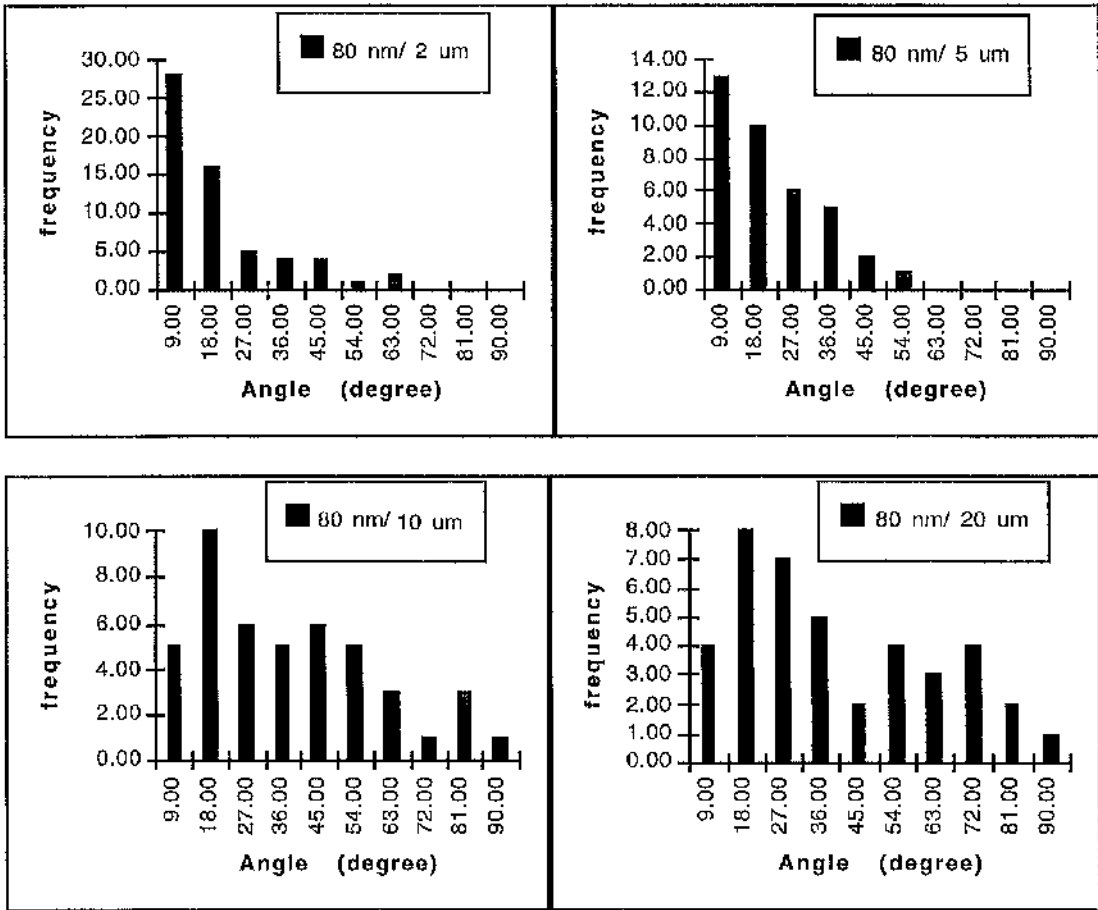


Figure 15: These graphs depict the number of rat calvaria osteoblasts that aligned within a range of degrees (i.e. bars @ 9° denote cells aligned 0-9° to the groove long axis) on grooved areas that are 80 nm deep and 2, 5, 10, or 20 μm wide. Note that more cells are aligned on 2 and 5 μm wide grooves, and that as the grooves become wider there is an increase in alignment variability.

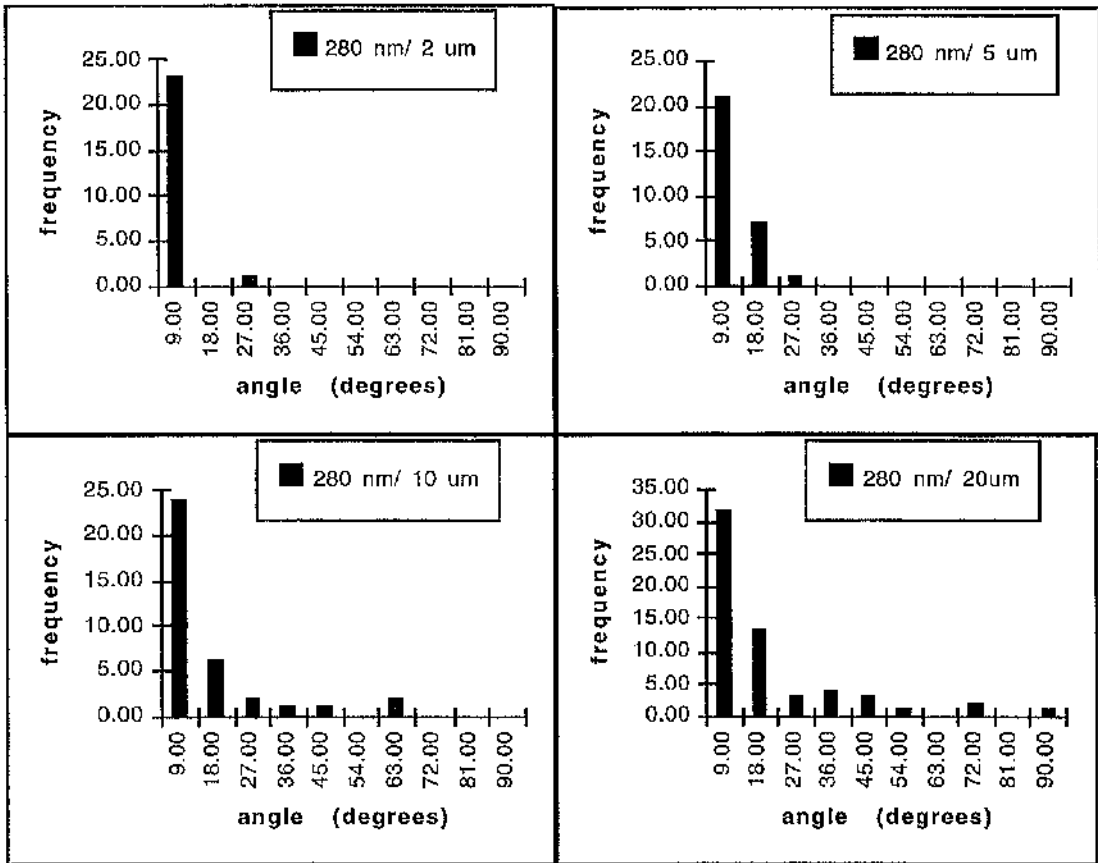


Figure 16: Osteoblast alignment on a structure with grooves 200 nm deeper than the structure results showed in grooved features. The alignment variability increased proportionally to groove width, but compared to **Figure 15**, the overall variability decreased significantly.

With the exception of cells on 80 nm deep/20 μm wide grooves, the cell length increased between 10 and 30 μm on grooved surfaces (**Table 10, Figure 17**). The minor axis of the cells decreased by roughly 10 μm or 50 % on all 2 μm wide grooves. As the grooves became deeper, the minor axis tended to decrease for all groove widths (**Table 10, Figure 18**). Influences on cell area did not become significant until grooves were deeper than 600 nm. Cell area was significantly ($P < 0.01$) decreased on structures df001, df002, and df009 (**Table 11**). Upon comparison to controls, differences in the major and minor axes of cells plated on grooved surfaces became apparent as well. All differences were significant ($P < 0.05$, most $P < 0.0001$) on any structure with a depth greater than or equal to 280 nm.

Structure	Groove width (μm)/ depth (nm)	Cell Major Axis (μm)	Standard deviation	Cell Minor Axis (μm)	Standard deviation
Flat Control		59.93	23.22	21.82	9.14
df005	2 / 80	80.91	42.31	12.62	6.83
	5 / 80	72.61	29.45	13.48	6.30
	10 / 80	71.81	26.49	20.88	9.53
	20 / 80	62.50	27.07	21.50	8.17
df007	2 / 280	75.15	32.75	11.66	4.60
	5 / 280	82.98	34.28	15.12	7.18
	10 / 280	76.59	40.28	15.70	8.40
	20 / 280	77.15	29.04	16.19	7.87
df008	2 / 670	90.84	35.12	11.93	5.12
	5 / 670	85.52	32.10	14.04	7.78
	10 / 670	80.04	37.56	14.83	7.63
	20 / 670	78.05	33.41	17.74	10.58
df009	2 / 670	85.08	35.44	10.54	4.24
	5 / 670	85.82	32.48	11.51	4.83
	10 / 670	76.92	30.74	11.77	5.35
	20 / 670	89.82	37.27	12.99	6.61
df001	12.5 / 600	88.95	35.17	11.65	5.58
df002	12.5 / 1100	83.43	39.45	12.22	4.39

Table 10: Cell major and minor axis lengths.

Structure	Groove width (μm)/ depth (nm)	Cell Area (μm^2)	Standard deviation	Cell Perimeter (μm)	Standard deviation
Flat Control		1068.76	574.43	223.09	107.86
df005	2 / 80	712.87	379.79	267.02	143.79
	5 / 80	706.89	323.61	241.61	95.34
	10 / 80	1150.23	658.24	277.95	127.90
	20 / 80	1024.59	565.86	245.96	98.70
df007	2 / 280	617.44	243.36	243.76	121.28
	5 / 280	919.27	467.39	297.56	144.06
	10 / 280	887.23	501.68	255.78	123.37
	20 / 280	926.00	467.47	278.90	120.03
df008	2 / 670	806.35	381.49	291.54	118.10
	5 / 670	866.52	422.11	297.56	128.91
	10 / 670	851.66	493.45	269.75	144.15
	20 / 670	977.32	641.24	272.79	116.53
df009	2 / 670	669.94	333.72	248.98	117.02
	5 / 670	761.88	433.40	266.34	121.11
	10 / 670	670.09	378.46	250.57	113.70
	20 / 670	830.01	401.43	302.00	136.73
df001	12.5 / 600	755.86	362.21	270.68	135.78
df002	12.5 / 1100	760.71	394.57	286.76	114.05

Table 11: Cell area and perimeter on various grooved features.

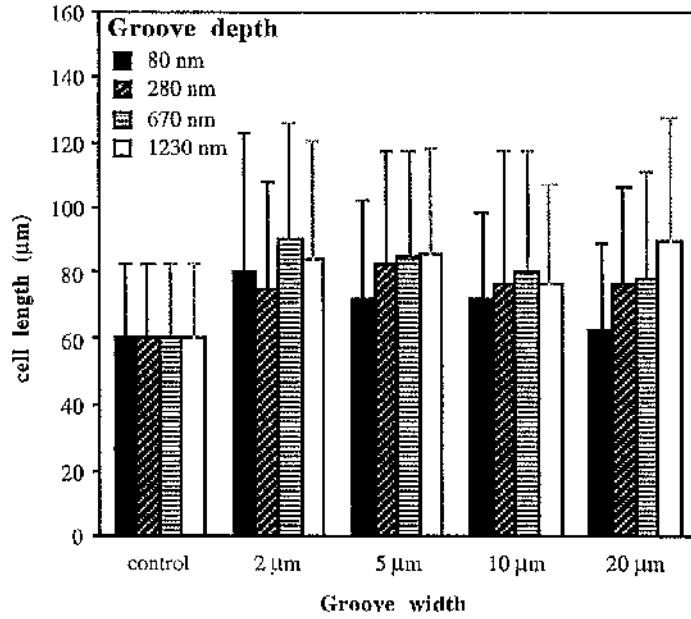


Figure 17: Osteoblast cell length on a range of groove widths and depths. Cell length tended to increase on most grooves.

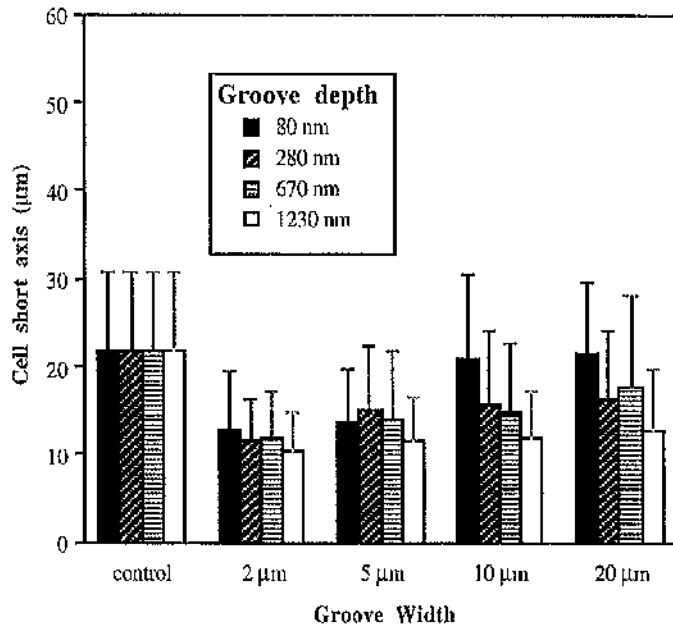


Figure 18: Osteoblast cell width generally decreased compared to the control.

Structure name	Groove (µm)	Groove Width (µm)	Cell Area	Major Axis	Minor Axis	Angle
df005	80	2	P<0.0001	P=0.0014	P<0.0001	P<0.0001
	80	5	P<0.0002	P=0.0147	P<0.0001	P<0.0001
	80	10	NS	P=0.0074	NS	P=0.0029
	80	20	NS	NS	NS	P=0.0065
df007	280	2	P<0.0001	P=0.0273	P<0.0001	P<0.0001
	280	5	NS	P=0.0007	P<0.0001	P<0.0001
	280	10	NS	P=0.0409	P<0.0001	P<0.0001
	280	20	NS	P<0.0001	P<0.0001	P<0.0001
df008	670	2	P=0.0167	P<0.0001	P<0.0001	P<0.0001
	670	5	NS	P<0.0001	P<0.0001	P<0.0001
	670	10	P=0.0062	P=0.0003	P<0.0001	P<0.0001
	670	20	NS	P<0.0001	P=0.0002	P<0.0001
df009	1230	2	P<0.0001	P<0.0001	P<0.0001	P<0.0001
	1230	5	P<0.0001	P<0.0001	P<0.0001	P<0.0001
	1230	10	P<0.0001	P<0.0001	P<0.0001	P<0.0001
	1230	20	P=0.0101	P<0.0001	P<0.0001	P<0.0001
df001	600	12.5	P=0.0004	P<0.0001	P<0.0001	P<0.0001
df002	1100	12.5	P=0.0025	P<0.0001	P<0.0001	P<0.0001

Table 12: Statistical results for quantitative response of osteoblasts to grooved surfaces of varying dimensions.

Extracellular matrix production

Grooved surfaces - polyurethane:

By Day 1, cells plated onto polyurethane structures had formed contacts with each other and the substrate. Cells formed numerous “islands” about 100-120 µm in diameter (Figure 19). The underlying cell-free surface was examined using SEM. Small mineralised globules ranging in size from 0.5 µm to 2.0 µm covered the polyurethane grooved surface (Figure 20) and were especially prevalent on the 2 µm grooved region (Figure 21).

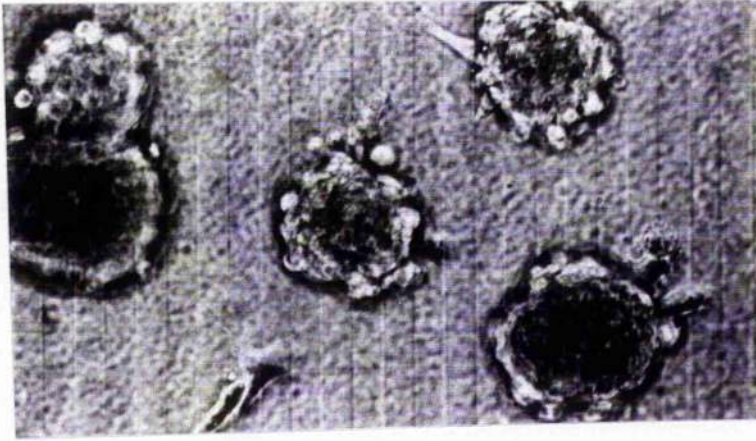


Figure 19: Phase contrast picture of live cells on a polyurethane surface (grooves 10 μm wide and 2 μm deep).



Figure 20: SEM photograph of a polyurethane surface (grooves 10 μm wide and 100 nm deep) after aggregates of cells were washed off during the fixing process. Numerous, mineral-like globules ranged in size from 0.5 - 2.0 μm .



Figure 21: SEM photograph of a polyurethane surface (grooves 2 μm wide and 1.23 μm deep) after aggregates of cells were washed off during the fixing process. Mineral-like globules ranged in size from 0.5 - 3.0 μm .

Grooved surfaces -fused silica:

In preliminary SEM studies, cells on grooves appeared to secrete more extracellular material. Both calvarial and bone marrow derived cells secreted mineral-like material (**Figures 22-26**). Orientation of extracellular material was influenced by groove width. Bone marrow cells plated on line spacings of 20 μm (**Figures 23-24**) produced material including collagen and calcium phosphate randomly oriented along groove and ridges. The same cells plated onto 5 μm wide grooves, however, aligned to the groove long axis and produced collagen also oriented along the groove axis (**Figures 25-26**). Cells examined on flat surfaces did not produce oriented extracellular material.

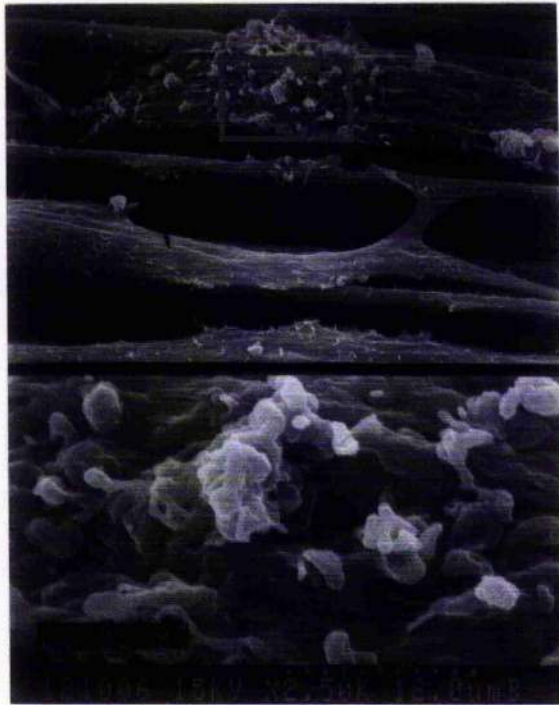


Figure 22: Rat calvarial osteoblasts after 11 days in culture aligned along a 5 μm wide, 6.0 μm deep grooved area. Cells are secreting mineral-like extracellular matrix. Inset close-up is at x12.5K magnification.



Figure 23: Bone marrow cells and some extracellular matrix found in a groove and across ridges of a 20 μm wide, 5.6 μm deep patterned mini-structure. Note no overall order of extracellular matrix or cells. Inset close-up is x6.0K magnification.



Figure 24: Bone marrow cells and mineral-like deposits on a 20 μm wide, 5.6 μm deep structure of fused silica.



Figure 25: Bone marrow cells on grooved surface (5.0 μm wide, 5.6 μm deep) after 3 days in culture. Cells aligned and formed a nodule which was manually disrupted in order to view the grooved interface. There was evidence of extracellular matrix production that looked like calcium phosphate and collagen (see close up at x2.5K).

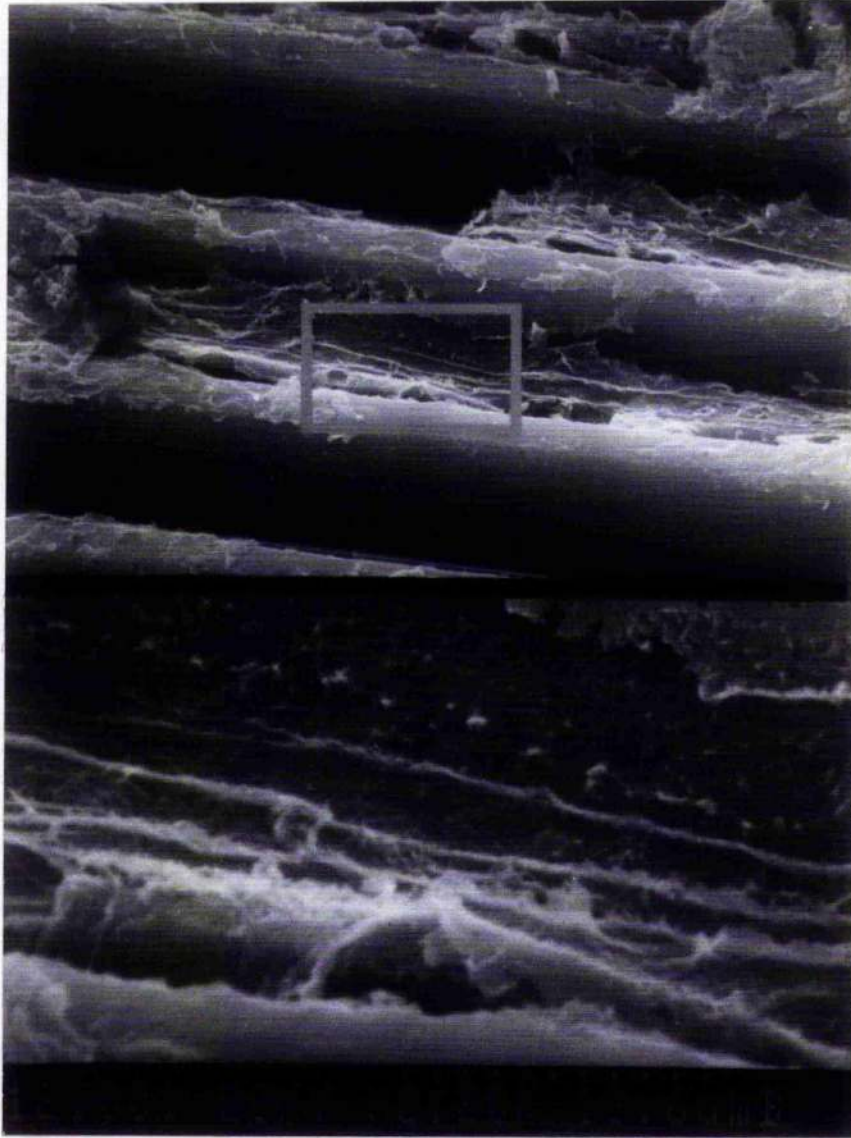


Figure 26: Along the periphery of the nodule (Figure 25), cells were highly aligned to the grooves (5.0 μm wide, 5.6 μm deep). Collagen-like fibrils (see inset for close-up at x11.0K) were found along cells and grooves. The overall direction of the fibrils was parallel to the grooves.

Atomic Force Microscopy & Polarised Microscopy Analysis:

Cells plated onto structures C, D, F, and G were examined for the presence of birefringent material using polarised light. Small strands of birefringent material was found along the 2

μm and $5 \mu\text{m}$ line spacing regions on structure F (depth = $3.3 \mu\text{m}$) (**Figure 27**). Birefringence was confirmed by rotation of the specimen through 360° . At 90° intervals the specimen alternated successively between a yellow colour complete extinction. This birefringent materials was not found on structures C, D, or G. AFM analysis of this structure revealed a crystalline material attached to the grooved surface (**Figures 28-30**). The ceramic nature of this material was confirmed after heating the specimen to approximately 900°C and re-examination under polarised light. The birefringent strands remained intact.

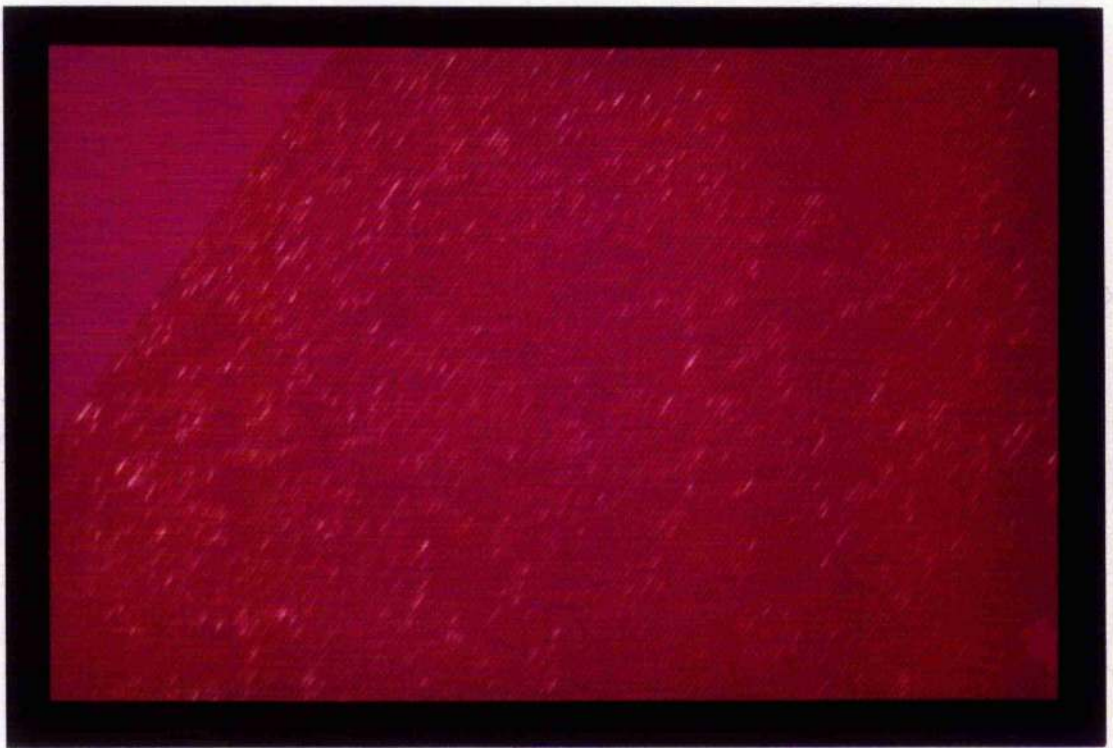


Figure 27: Grooved surface ($5 \mu\text{m}$ wide, $3.3 \mu\text{m}$ deep) exposed to polarised light after cell sheet removal. Birefringent material along grooves appeared yellow at 90° intervals. [Original magnification = 20x]

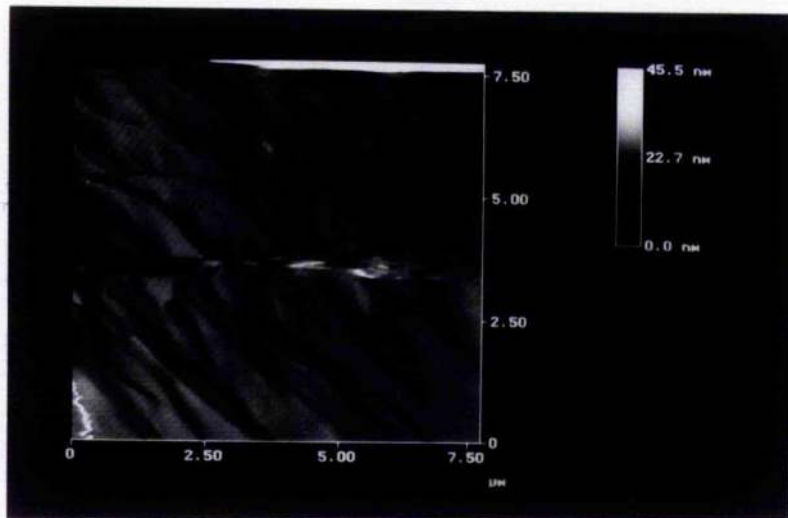


Figure 28: AFM overview scan of area along a groove or ridge on a 2 μm wide, 3.3 μm deep grooved region (Field area = 7.5 μm x 7.5 μm).

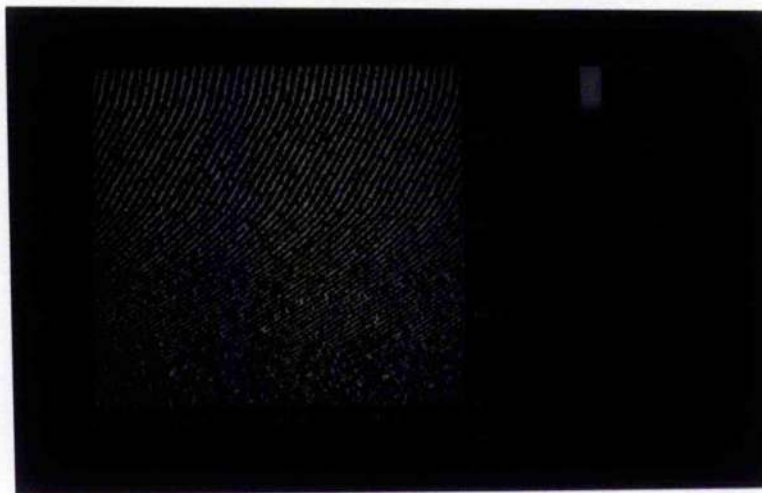


Figure 29: Close up scan of area explored in Figure 28 (Field area = 40 nm x 40 nm).

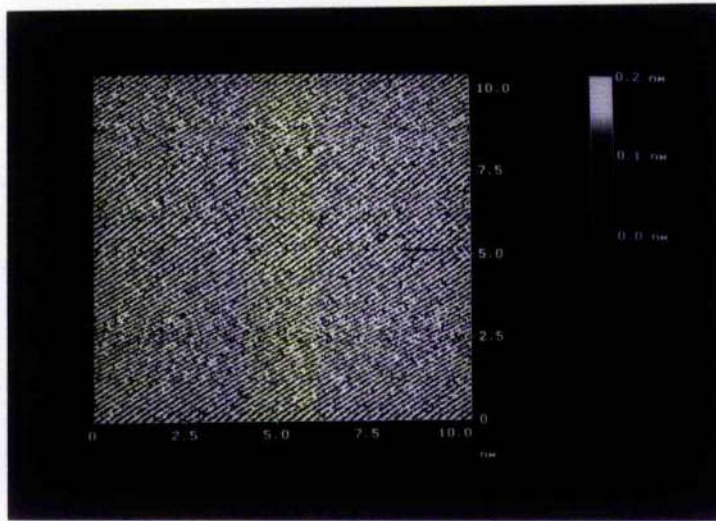


Figure 30: Fine view scan of the same region (Field area = 10 nm x 10 nm).

DISCUSSION

Quantitative response to topography

Various groups (Bellows, et al, 1986; Ricci, et al, 1994, Hunter, et al, 1995; Boyan, et al, 1995) have speculated on the interplay between cell shape, the biomaterial surface, and cell function. Most agree osteoblast shape helps determine cell phenotype and differentiation and ultimately their ability to build bone matrix and mineral.

Review of the literature revealed little information regarding quantitative analysis of osteoblast shape changes in response to grooved topography with the exception of a paper by Qu, et al, (1996). These authors only examined the effects of two surfaces with V-shaped grooves: 30 μm pitch/ 3 μm depth or 6-8 μm pitch / 3 μm depth. A wider array of grooved surfaces was analysed in this work ranging from depths of just 80 nm to 1.23 μm

and line spacings varying from 2 to 20 μm . These surfaces helped elucidate the effect of varying groove dimensions on cell alignment, area, length and width.

Although it was not surprising to discover rat primary calvarial cells reacted to grooved topography, details hitherto unknown regarding the sensitivity (defined here as significant changes in cell morphology compared to flat control cells) of that response were revealed in this work. When the groove is less wide than the average width of a bone cell (10 μm) cell sensitivity to very thin grooves (depth = 80 nm) is enhanced considerably compared to their response to 10 and 20 μm wide grooves. These results suggest that when designing an implant that will come in contact with bone cells, it may be advantageous to include features on that surface that the cells are most sensitive to in order to control cell function. What does this control of sensitivity mean in terms of the ability of these surfaces to influence extracellular matrix production?

Extracellular matrix production

Several groups have studied the influence of grooved substrata on osteoblast extracellular matrix (ECM) production (See Introduction, Chapter 1) both *in vitro* and *in vivo*. All groups, (Brunette, et al, 1991; Chehroudi, et al, 1992; Gray, et al, 1996; Qu, et al, 1996; Chehroudi, et al, 1997), reported the enhancement of mineralisation and ECM production of osteoblast cells seeded onto grooved topographical surfaces. Other than attempts to use digital radiography (Qu, et al. 1996; Chehroudi, et al, 1997) to assess "bone-like foci" orientation, and the suggestion by Chehroudi, et al (1992) that collagen was "probably oriented along the long axis of the grooves," no one has explicitly commented on the ability of grooved topography to influence ECM orientation.

This work presents evidence gained through SEM, PLM and AFM analysis that tantalisingly suggests that specific grooved surfaces do indeed influence ECM production. Fascinating evidence published by Martin, et al (1995) showed that osteoblasts cultured on “regular” rough surfaces produced more matrix than cells on randomly rough surfaces. Even more interesting is the dimensions of these “regular” surfaces were craters approximately 1 μm by 10 μm . These dimensions are similar in size to grooved dimensions reported in the next few sections that influence ECM production and mineralisation.

SEM Analysis:

What effect does altering the overall bulk material of the grooved surface have on ECM production? In this study, the flexibility of the surface changed dramatically, as did the surface chemistry with the production of polyurethane replicas of fused silica structures. Would osteoblasts favour the more biocompatible polyurethane surface?

The answers to these questions is not immediately clear from the results. SEM analysis of polyurethane grooved surfaces revealed the presence of small (0.5 - 3.0 μm) mineral-like globules similar to those reported in Chehroudi, et al (1992), who also found globular accretions on grooved and flat substrata either $> 10 \mu\text{m}$ or 0.5 - 3.0 μm in diameter. Furthermore, Davies (1996) showed that the initial layer along a bone/biomaterial interface is comprised of small, globular accretions.

Thus, there is evidence in the literature to support the production of mineralised globules by osteoblasts on grooved surfaces *in vitro*. However, the time frame (a few days) in which these accretions were made is much faster than those reported by Chehroudi, et al, (1992) whose cells took up to 30 days to lay down a mineralised matrix.

Did the polyurethane surface influence mineralisation? These numerous accretions were not found on fused silica surfaces after similar time in culture, thus, perhaps the grooved polyurethane surface positively influenced mineralisation.

Why did these cells form “islands” on the polyurethane surfaces and not on the fused silica ones? The most likely answer to this question is the slightly higher density these cells were plated out at onto structures. An environment was created where cells could spread out and adhere to each other just before or as they were coming in contact with the substrate. Because it is more natural for osteoblasts to adhere to other osteoblasts compared to an artificial biomaterial surface like polyurethane, it is hardly unsurprising that these cells acted in this manner. Another possible reason for “island” formation is that the inherent flexibility of these thin polyurethane replica surfaces caused the cells to behave differently. More experiments are necessary to confirm these hypotheses.

SEM analysis of rat calvarial derived osteoblasts and adult rat bone marrow cells unveiled the ability of some fused silica grooved surfaces of specific dimensions to influence ECM production. A few studies have hinted that collagen might be aligned to the grooves but no one has shown it explicitly. The fibrils pictured in **Figure 26** are similar in size to fibrils scattered throughout SEM photographs published by Davies and Mastuda (1988) and Davies (1996).

The fact that bone marrow cells formed nodules and produced ECM material on a grooved surface three days after plating is amazing. Normally, much longer times are needed in culture before mineralisation occurs *in vitro*. There are reported instances, however (Ecarot-Charrier, et al, 1988) where bone nodules have formed within 24 hours of the addition of β -glycerophosphate (β -GP) to confluent cell layers. The bone marrow cells

used in this work were cultured continuously in fresh ascorbic acid and β -GP. Taking into consideration the effect of ascorbic acid on osteoblasts in terms of an acceleration of differentiation, the availability of β -GP and the reasonably high density these cells were plated out at, it is not surprising that nodule formation and ECM production and alignment occurred so quickly.

The fact that these fibrils were only found on one structure suggests there is an optimum topography that influences ECM production. It is also fascinating to note that the dimensions of the structure that influenced cells to produce oriented collagen had a diameter (5 μ m) that these cells were quite responsive to in the quantitative topography study. This ability to control ECM orientation *in vitro* could lead to tissue engineering of organised bone and enhanced osseointegration of various implants.

Principle Behind PLM & the Detection Of Birefringence:

The property of birefringence has been used in biological optical microscopy to detect such structures as collagen, striated muscle fibres and chloroplasts. Furthermore, this material property can be used to determine the crystallinity of a sample with the use of a polarising microscope. Approximately 95% of all crystals are birefringent (Slayter, 1970). An important indicator of bone cell phenotype is their ability to produce extracellular matrix including a crystalline calcium phosphate, hydroxyapatite ($\text{Ca}_{10}(\text{PO}_4)_6(\text{OH})_2$) (Webster, 1988). Cells on grooved structures and tubes (Chapter 5 for tube results) were examined under polarised light for the production of hydroxyapatite.

Birefringence is a property of materials that possess patterned regions of varying refractive indices, i.e., an *anisotropic* material. It can also be defined as a property originating from the inherent asymmetry of the polarisability of chemical bonds. For

example, the ability to disrupt a carbon-carbon bond depends directly on the direction of disruption, i.e. it is easier to separate the bond between two carbons in a chain. This direction is defined as being more “polarisable,” and it follows that it has a higher index of refraction meaning light will travel more slowly in this direction.

Due to the differences in refractive indices in a birefringent material, light resolves into two mutually perpendicular vibration components the extraordinary ray (E ray) and the ordinary ray (O ray). These two beams are distinct physically because they travel at different velocities due to the difference in refractive indices. The velocity of the O ray remains constant with direction, while the velocity of the R ray varies. The birefringence of a material can be quantified as the difference between the refractive index for the ordinary ray and the refractive index for the extraordinary ray. It is important to note that upon viewing a birefringent material in a specific orientation, i.e. along its optical axis, the material itself appears isotropic.

The polarising microscope operates on the principle that by orientating light in a specific direction or plane through a sample, one can then detect the effect the light has on the sample in terms of absorption, reflection, etc. The polariser is responsible for filtering out all light oriented at right angles to one specific plane of light. The analyser is orientated in the polarising microscope such that when there is no specimen between the polariser and the analyser no light is transmitted, i.e. the polariser and analyser are “mutually oriented in a position of extinction.” Thus, when a birefringent specimen is placed in the microscope it shifts the light from the polariser such that the light *is* transmitted by the analyser.

The variation in overall colour seen in a birefringent sample results from the retardation of light through the sample which is directly related to the phase difference between the O and E rays and the thickness of the sample. When the sample is rotated through 360°, there are four positions of extinction and four positions of maximum brightness offset within each group by 90°.

Because biological samples do not retard light much more than 100m μ a red I plate is often used to detect interference colours. In this case, alternate addition and subtraction colours are observed at 90° rotation intervals depending on the retardation by the specimen and its orientation in relation to the plate. For example, if the slow direction of the specimen is perpendicular to the red I plate, a yellow colour is observed, whereas if the slow direction is parallel to the plate a blue colour can be seen.

All coverslip grooved samples were examined under polarised light and a red I plate. Analysis of the 2 and 5 μ m wide regions on structure F revealed the presence of small, yellow strands of material. It is assumed that this birefringent material is indeed a form of hydroxyapatite of calcium phosphate because it survived 900°C temperatures. Strands alternated as either all yellow or completely extinct upon 360° rotation which suggests all material was oriented in a similar manner and that grooved surfaces, once again, have the ability to influence ECM production and mineralisation. That fact that this material was only found on the 2 and 5 μ m grooves implies once again, that these groove widths are more influential than for example, 10 or 20 μ m wide ones.

AFM Analysis:

There are only a few reports in the literature regarding the detection and identification of biological crystalline material using atomic force microscopy (Blair, et al, 1995; Schaad, et

al, 1993). Schaad, et al, (1993) conclude that AFM is a “relevant tool” for the study of biological hydroxyapatite. Blair, et al, (1995) successfully used AFM as a tool for preliminary identification of microcrystals in patient synovial fluid, including hydroxyapatite.

In this work, we report nanometric resolution of what we believe to be a hydroxyapatite surface. Bres, et al, (1990) reported that hydroxyapatite has a dipyramidal hexagonal prismatic morphology with the follow spacings: $a_1 = a_2 = a_3 = 0.9432$ nm and $c = 0.6881$. The spacing between the 3 $\langle 100 \rangle$ planes = 0.82 nm (Lees, 1979). Also, in bone, the actual apatite crystals are 20 - 40 nm long and 1.5 - 3 nm wide. According to our AFM images, the crystalline material scanned has a spacing ranging from 0.3 nm to 6 nm, well within the range of parameters of hydroxyapatite. Furthermore, Voegel and Frank (1979) found some hydroxyapatite crystallites to be curved in an arc with a radius of 150-350 nm. The curved lines seen in **Figure 29** could be part of a larger arced structure.

CONCLUSIONS

The osteoblast response to grooved surfaces was elucidated further in this work. Rat osteoblasts were sensitive to features as tiny as 80 nm, and reacted more strongly in terms of ECM production and mineralisation to features with widths around 2 or 5 μm and similar depths. Preliminary studies using analytical techniques like SEM, PLM and AFM showed that grooves influenced ECM material alignment.

Chapter 5: *The Behaviour of Osteoblasts in Quartz Tubes*

INTRODUCTION.....	101
BACKGROUND.....	101
EXPERIMENTS.....	103
MATERIALS AND METHODS.....	104
EXPERIMENTS.....	104
VIDEO TIME LAPSE PHASE CONTRAST MICROGRAPHY.....	105
RESULTS.....	105
MORPHOLOGICAL BEHAVIOUR AND VIDEO TIME LAPSE PHASE CONTRAST MICROGRAPHY OBSERVATIONS	105
OSTEOCALCIN STAINING.....	112
POLARISED LIGHT AND QUANTITATIVE ANALYSIS OF UNSUPPLEMENTED CULTURES.....	113
POLARISED LIGHT AND QUANTITATIVE ANALYSIS OF SUPPLEMENTED CULTURES.....	116
DISCUSSION.....	118
CONCLUSIONS.....	120

INTRODUCTION

Background

The specific pore sizes that influence the migration of bone cells and enhance osseointegration of dental and orthopaedic implants continues to be debated. Because of fabrication conditions, a range of pore sizes is usually used, making it difficult to attribute implant results to a specific pore size or geometry. The well defined geometry and controlled culture conditions of small glass capillaries, however, circumvent these problems. The quartz tube is an ideal system to study the behaviour of osteoblasts for several reasons.

First of all, cells can be continuously monitored using basic phase contrast microscopy and video time lapse recording techniques. One has the unique opportunity to directly observe the cell's response to the curved, tubular environment, its interaction with other cells, and the formation of extracellular matrix. Secondly, the geometry is rigidly defined making it possible to differentiate differences in terms of extracellular matrix production and cell behaviour produced by varying the diameters and/or lengths of tubes. Thus, the study of osteoblasts in small diameter glass tubes provides more specific fundamental information regarding cell response to curved surfaces and microenvironments.

Interest in the area of porous surface coatings began with the advent of the cementless hip replacement in the early 1970s with researchers looking for surface geometries to encourage bone ingrowth and ideally osseointegration (Hungerford & Jones, 1988). Investigators believe there is an optimum pore size between 250 and 600 μm that provides enough space for preosteoblasts/osteoprogenitors to proliferate and form a dense mass of

cells, differentiate, and make bone (Gray, et al, 1996). Boyan, et al, (1996) hypothesise that the curvature of these pores may provide the optimum tension and compression for the cell's mechanoreceptors. There have been reports in the literature, however, of bone growing into pores as small in diameter as 40 μm (Brunette, 1988). In fact, one study determined that bone ingrowth stabilised the implant mechanically at earlier time points if the pore diameters ranging from either 45 - 150 μm or 150 - 300 μm .

In another study evaluating the effect of pore size, Eggl, et al, (1987) looked at bone formation over six months into hydroxyapatite (HA) and tricalcium phosphate (TCP) porous coated cylinders implanted into the metaphysis of the distal femur and proximal tibia of rabbits. Two ranges of pore sizes, either 50 - 100 μm or 200 - 400 μm were studied for each type of ceramic cylinder. After four weeks, the amount of bone ingrowth into the TCP 50 - 100 μm cylinder was 40%, whereas ingrowth into the small pore range HA cylinder was 24%. However, ingrowth into the 200 - 400 μm pore size implants was 19% and 17% for the HA and TCP cylinders respectively. Thus, there was significantly more bone ingrowth into the smaller pore range implants for both TCP and HA. The authors feel the larger amount of bone ingrowth into the 50-100 μm pore size TCP implants was enhanced by the presence of 20 μm wide interconnections, which created a favourable microenvironment for vascular and cellular invasion. However, the theory that bone ingrowth was enhanced by these interconnections is contradicted by the findings of Dennis, et al (1992). These authors found ceramics with pores 200-400 μm in diameter retained more cells and had more bone ingrowth than a coral-like continuous pore structure with an average diameter of 200 μm . Thus, there are conflicting reports in the literature regarding the best pore size for bone ingrowth and the effect of interconnectivity between

pores. Furthermore, none of these studies has the capability to visualise osteoblast behaviour and mineralisation continuously.

Finally, the last impetus for the study of bone formation in glass tubes *in vitro* stems from a report in the literature of ectopic bone formation in wide diameter tubes *in vivo*. Almost four decades ago, Seyle, et al, (1960) implanted pyrex glass tubes, 2 cm long and 3 cm wide subcutaneously into Sprague Dawley rats. Previous experiments established these cylinder dimensions to be the most favourable for bone formation in this situation. The von Kossa and van Gieson histological staining methods were used to ascertain the presence of calcium salts and collagen fibres respectively. These authors found that bone-like structures developed in the cylinders, complete with a marrow-like cavity and junction cartilage plates.

Experiments

Initially, two fundamental questions were addressed with the following experiments:

- How does cell behaviour differ in tubes compared to flat surfaces?
- Does the tubular environment effect extracellular matrix production in the absence of ascorbic acid and β -glycerophosphate, normal "mineralising supplements."?

Analytical techniques included time lapse video cinemicrography which enabled us to directly view in a continuous fashion the cell response to the three dimensional, tubular environment. Immunofluorescent and polarised light techniques enabled us to assess extracellular production. Findings included the tendency of cells in tubes greater than 150 μm to form dynamic contacts with each other and the walls of the tube, and to form dark, nodule-like structures similar to those found in normal confluent cell culture.

Whether or not the addition of β -glycerophosphate (β -GP) and ascorbic acid enhanced and/or influenced the extracellular matrix production and/or cell behaviour of osteoblasts was also investigated.

MATERIALS AND METHODS

*Note

Please refer to Chapters 2 and 4 for the cell isolation method and analytical techniques not mentioned but used in this chapter.

Experiments

Unsupplemented cultures

Rat calvarial osteoblasts were suspended in DMEM with 10% CS and 5% antibiotics and seeded at high density (approximately 3×10^6 cells/ml) by capillary action into 2 types of quartz tubes (Table 13). Cells in tubes and flat surfaces were videotaped after seeding and later analysed with immunofluorescent and polarised light microscopy techniques.

Tubes	Inner Diameter	Length
Group A	150 - 300 μ m	2 - 5 mm
Group B	700 μ m	0.5 - 2.3 cm

Table 13: Tube dimensions.

Supplemented cultures:

A 12 day experiment was conducted using 700 μ m wide tubes of varying lengths. β -GP (10 mM) and ascorbic acid (50 μ g/ml) were added to the media of half of the tubes on Day

7 and at every media change thereafter. Upon fixation in buffered formalin, tubes were examined under polarised light and the size and number of nodules were evaluated.

Video Time Lapse Phase Contrast Micrography

Osteoblasts were videotaped just after seeding for periods up to 12 days 37°C. Videos were recorded at 20X phase contrast objective magnification using a Cohu CCD camera or a Panasonic Neuvicon video camera under the lowest light level which would produce a good image. Images were stored on a Panasonic Model AG-6730 time-lapse video-recorder at one frame per minute.

RESULTS

Morphological Behaviour and Video Time Lapse Phase Contrast Micrography Observations

The behaviour of rat osteoblasts in tubular structures differed markedly from their behaviour on flat surfaces during similar time periods. Within a few hours of plating, cells stretched out and made contact with each other. The attachments formed spanned across the tube and along its length (**Figure 35**). Cells formed clumps or cords of cells which behaved as a dynamic system, detaching and reattaching along the tube wall constantly as a unit. Individual cells joined and detached from cords periodically.

Video time lapse phase contrast micrography revealed a higher level of activity of these cells compared to other cell types like endothelia, epitenon, and macrophages. (**Figures 31-34**). The period of activity of osteoblasts in tubes versus flat surfaces differed as well (data not shown). Cells on flat surfaces eventually spread out and formed a confluent, nondynamic mass of cells after 24 hours. In tubes, nodule-like structures formed after the

first 24 hours of seeding that resembled those found in confluent cell cultures on flat surfaces (Figures 31, 36, & 37).

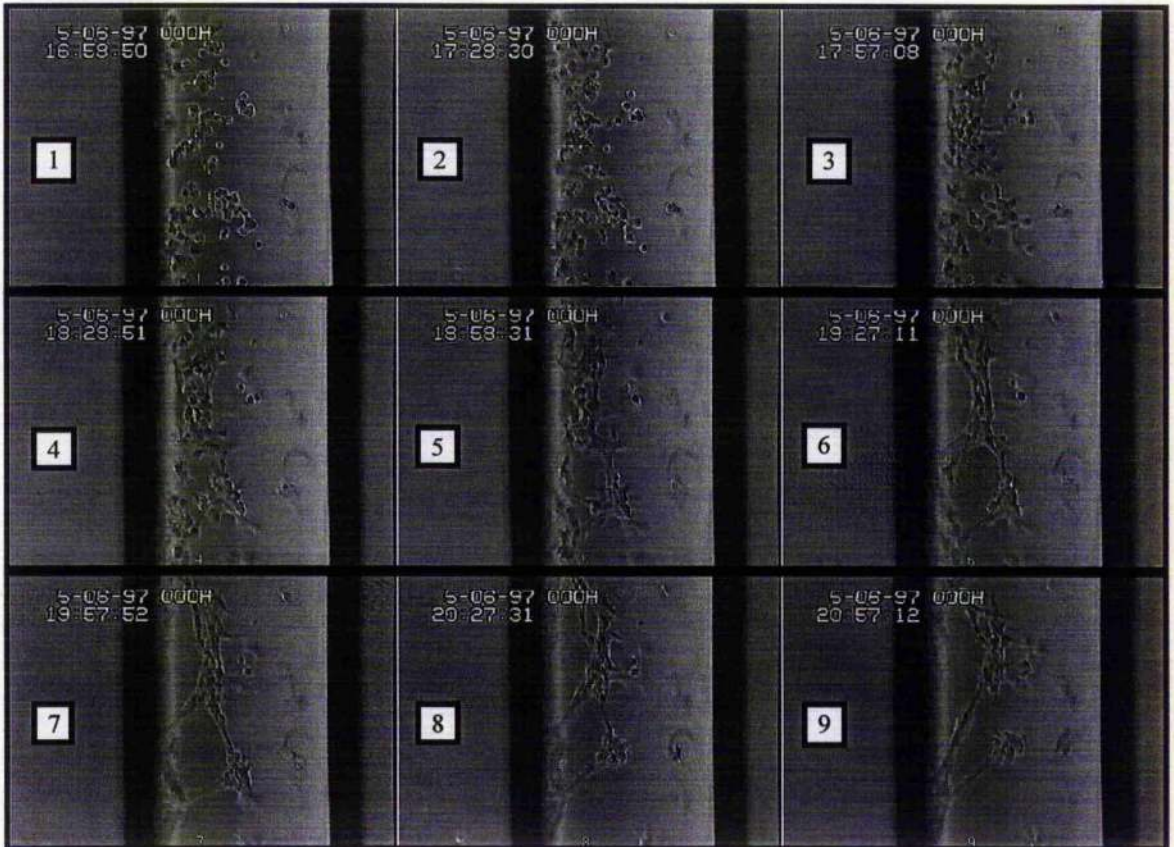


Figure 31: Time lapse cinemicrography of osteoblasts seeded into a 300 μm diameter tube. [Original magnification = 20x]. Frames shown are approximately 30 minutes apart. Frame 1 represents the time just after seeding. Note, cells do not spread out individually. By 1 hour after seeding (frame 3) cells had begun to reach out to each other and formed dynamic sheets/clusters of cells. Note the dynamic detachment from the tube of one side of the bottom clump of cells from frame 7 to frame 8. By frame 9 the bottom cluster had detached from the top cluster of cells as well.

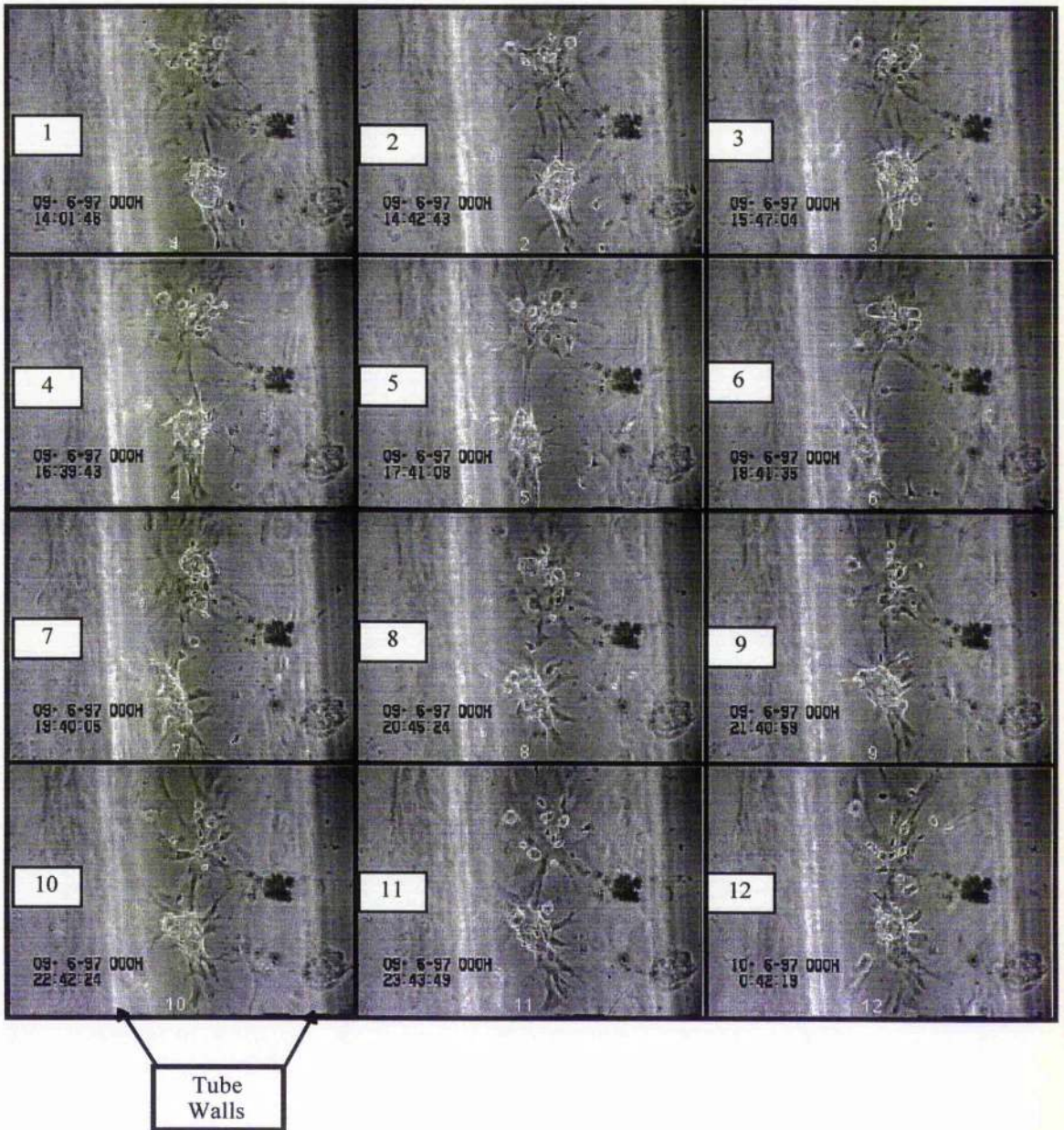


Figure 32: Time lapse video frames of osteoblasts after four days in culture in a 300 μm diameter quartz tube. Frames 1-12 are 1 hour apart with the exception of frames 1-2 (42 minutes apart). Note tendency of cells to form aggregate/nodule-like structures (frame 1) that move as a unit through out the tube and interact with other similar structures (frame 12). [Original magnification = 20x]

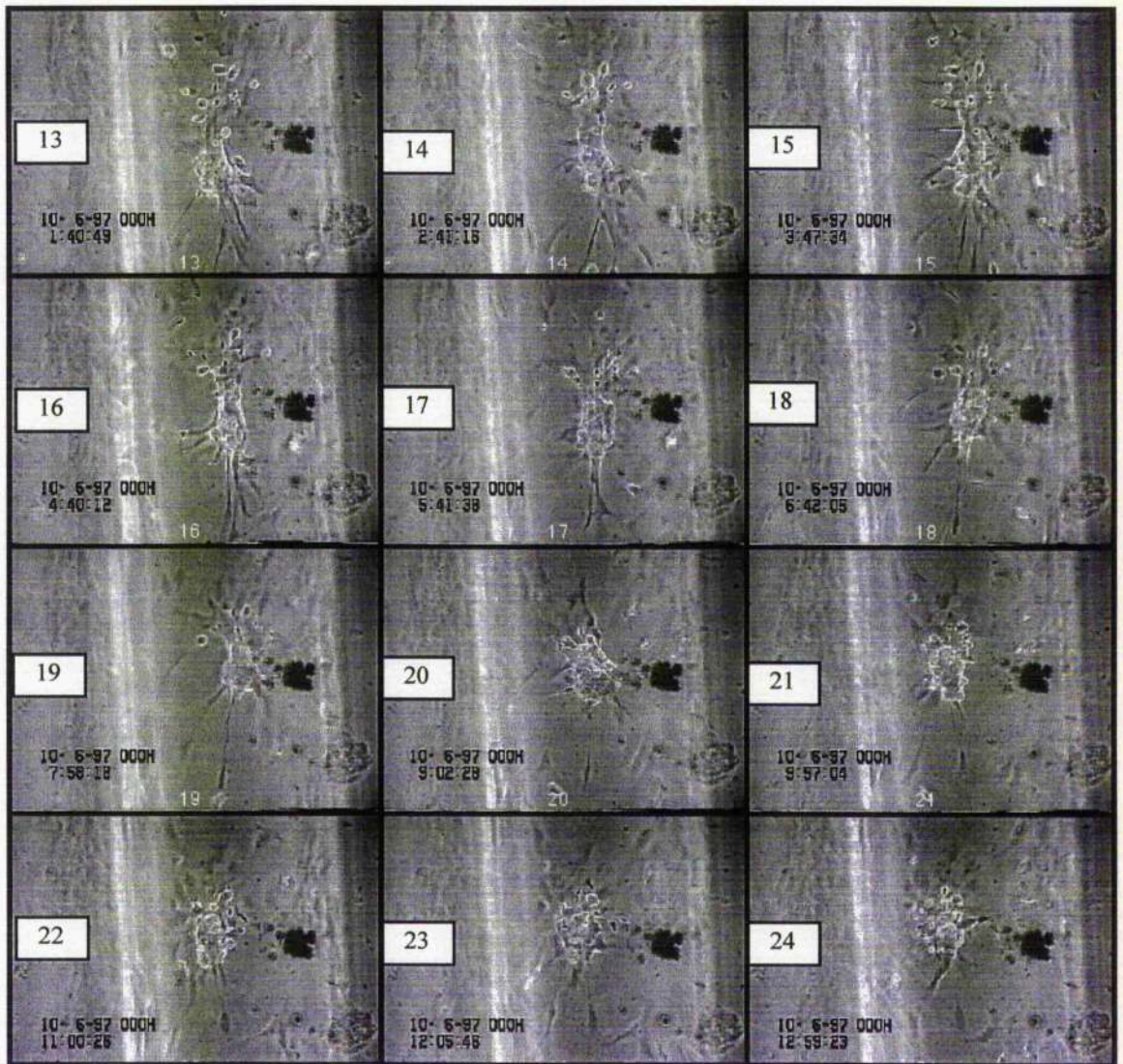


Figure 33: Continuation of frames in **Figure 32**. Frame 13 is 1 hour after frame 12 in time. Note dynamic movement of cells and cell clusters from frame 13 to frame 24. The two clusters actually merge by frame 14 and begin to move as a unit after frame 16. [Original magnification = 20x]

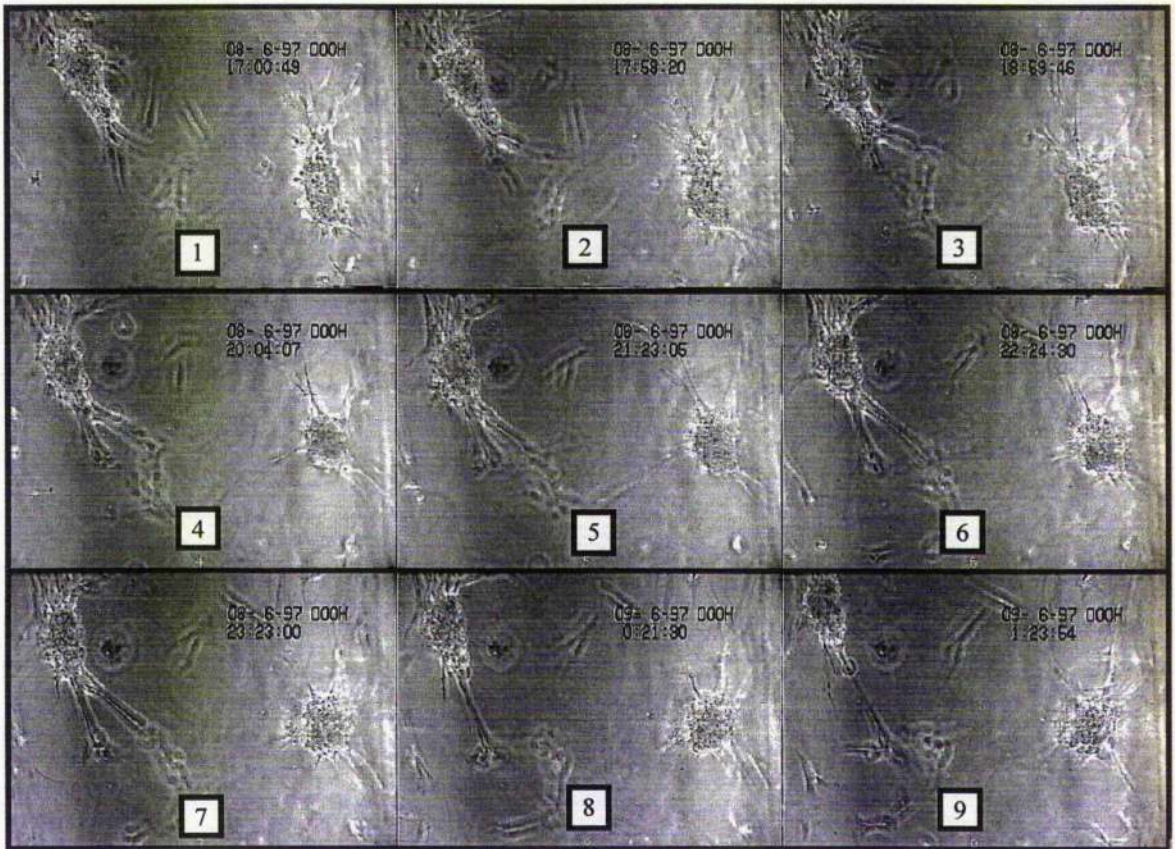


Figure 34: Time lapse cinemicrography of osteoblasts seeded into a 700 μm diameter tube after 72 hours in culture. [Original magnification = 20x]. Frames shown are approximately 1 hour apart. Note formation of cell clusters/ nodule-like structures similar to those found in 300 μm diameter tubes (**Figures 31-33**).

Viable cells filled the length of the tube, and the diffusion of nutrients was adequate for all of the tubes tested with the exception of long (2+ cm) 300 μm diameter tubes tested. The reaction of the cells to the tubular environment was governed by the diameter and length of the tube. In the smaller diameter tubes, i.e. 150 μm or less, cells formed cords that attached to each other and ran along the entire length of the tube, sometimes as long as 5 mm. Nodule-like structures were more likely to be formed in 250-280 μm diameter tubes in addition to cords spanning the tube diameter.

In the case of 700 μm wide tubes, the amount of nodule formation appeared to be directly correlated with the length of the tube. The longer the tube and the longer the

culture time, the more nodule-like formation seen. Also, some of the 700 μm tubes contained flared ends (diameter = 1.5 cm). In these regions with a larger radius of curvature, cells formed small cell aggregates or flattened against the surface of the wall. Cells have remained viable in these tubes for as long as 30 days and in some cases, filled the tube with more cells and extracellular matrix (**Figure 38**).

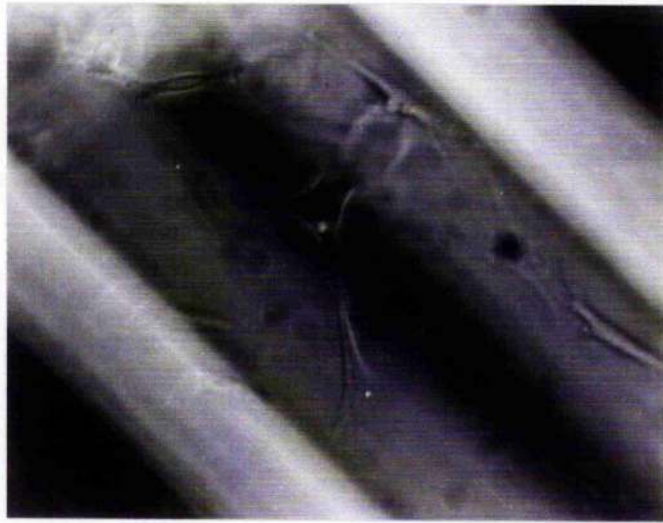


Figure 35: Phase contrast picture of cells in tube fixed after 18 days. Tube diameter = 270 μm . [Original magnification = 20x].

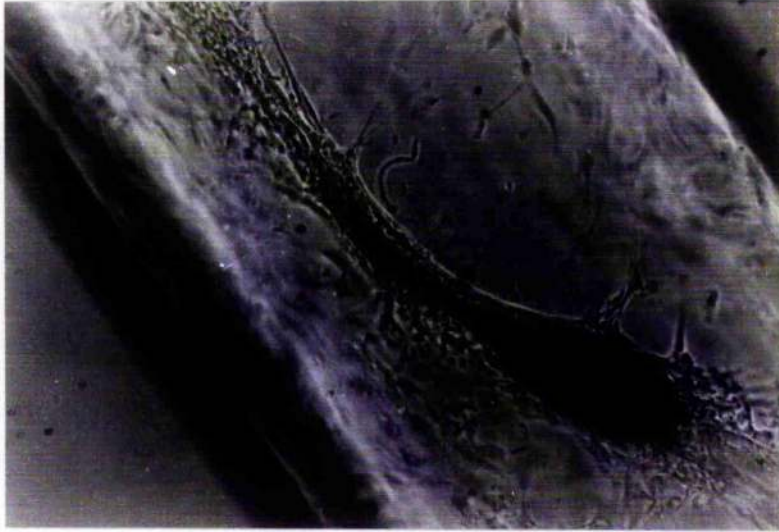


Figure 36: Nodule formation - phase contrast picture of live cells on Day 7 in a 700 μm diameter tube (tube length = 2.3 cm) [Original magnification = 10x].

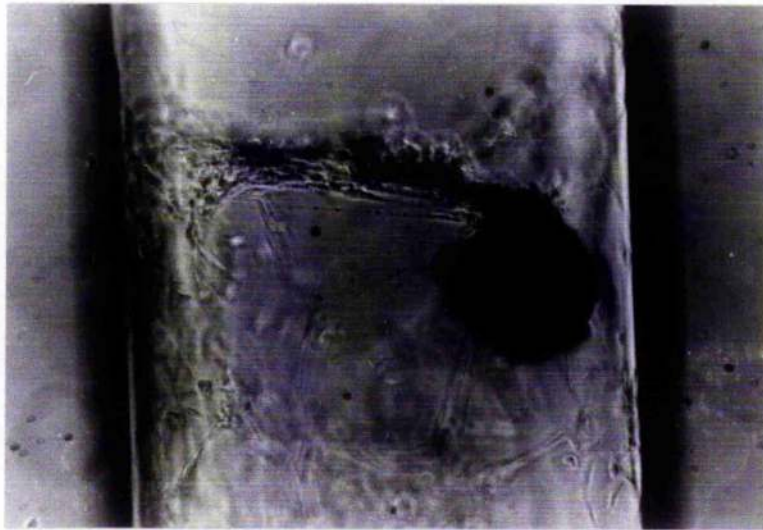


Figure 37: Nodule formation - phase contrast picture of live cells spanning the tube diameter (700 μm) on Day 7 (tube length = 1.7 cm) [Original magnification = 10x].



Figure 38: Tube (diameter = 220 μm) full of cells and extracellular material at Day 18. [Original magnification = 40x].

Osteocalcin staining

Cells and extracellular matrix in tubes stained positively for osteocalcin and were viewed by confocal laser scanning microscopy. Second antibody and autofluorescent controls were negative. Small globules along some cords of cells and particles lining the tube inner wall stained heavily for osteocalcin (**Figure 39 & 40**).



Figure 39: Cord of cells in a tube with an inner diameter of 280 μm fixed after 18 days in culture. Confocal laser scanning image [Original magnification: 40x]. Note the globules that formed along the cord and the highly stained particles along the inner wall of the tube (see bottom of picture).



Figure 40: Composite picture of osteocalcin staining of a cell cord (delineated by three white arrows) spanning across a 700 μm diameter tube. Cells were fixed at 12 days of culture after 5 days of exposure to supplemented media. Confocal laser scanning image [Original magnification: 40x].

Polarised light and quantitative analysis of unsupplemented cultures

The extracellular matrix production was enhanced by the tubular environment. Examination under polarised light revealed that some nodule-like groups of cells contained birefringent particles and regions (**Figures 41 & 42**). In 700 μm diameter tubes, cells formed nodules containing birefringent particles with an average area of $2.6 \times 10^3 \mu\text{m}^2$ (**Table 14 & 15**).

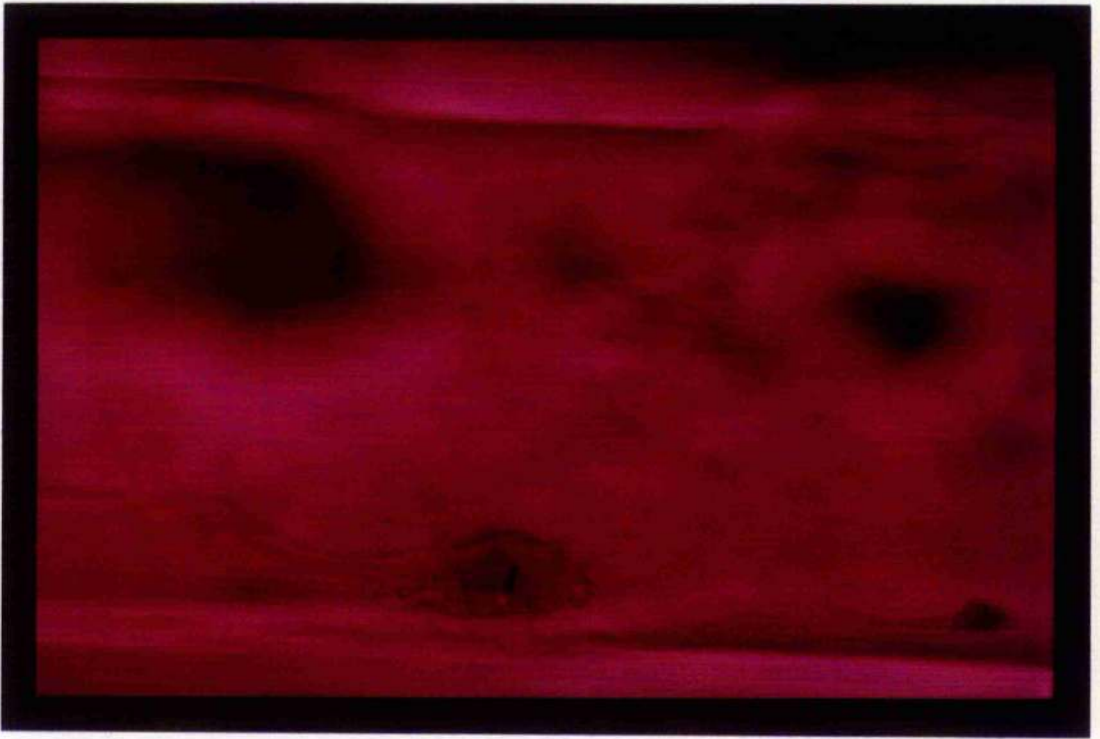


Figure 41: Photograph of nodule found in tube after 16 days of unsupplemented culture under polarised light [Original magnification = 20x]. Note yellow birefringent material in centre of nodule.



Figure 42: Photograph of the same nodule in **Figure 41** under polarised light and after 90° of rotation [Original magnification = 20x]. Note blue birefringent material in centre of nodule.

Tube Length (cm)	Nodule Number	Length (μm)	SD	Width (μm)	SD
0.7	0	-	-	-	-
0.7	7	121.63	62.01	69.30	25.56
2.0*	7	76.73	16.91	76.73	16.91
2.0*	7	100.98	32.38	87.12	12.91

Table 14: Nodule size and number in tubes with cells cultured in the absence of β -glycerophosphate and ascorbic acid. Note “*” denotes tube with flared end approximately 1.5 mm wide. All nodules presented were found in 700 μm wide end.

Tube length (cm)	Birefringent areas/ No. of nodules examined
1.5	4.5/6

Table 15: Polarised light analysis of tubes cultured in the absence of β -glycerophosphate and ascorbic acid.

Polarised light and quantitative analysis of supplemented cultures

The effect of tube length (diameter = constant) on nodule formation in terms of size and number is clear upon comparison of tubes (no flared end) in **Table 16**. Tubes twice as long had eight times as many nodules and an average nodule area almost three times greater. Furthermore, an overall comparison of nodule area (nonparametric) between supplemented and unsupplemented cultures reveals five times greater nodule area in supplemented cultures ($P < 0.0023$). In terms of birefringent areas per nodules examined, there is not a significant difference in number between supplemented and unsupplemented cultures among tubes of similar dimensions (**Table 15**, **Table 17**). In terms of birefringent area per nodule, however, some cells exposed to culture supplements had larger regions of birefringence (**Figure 44**).

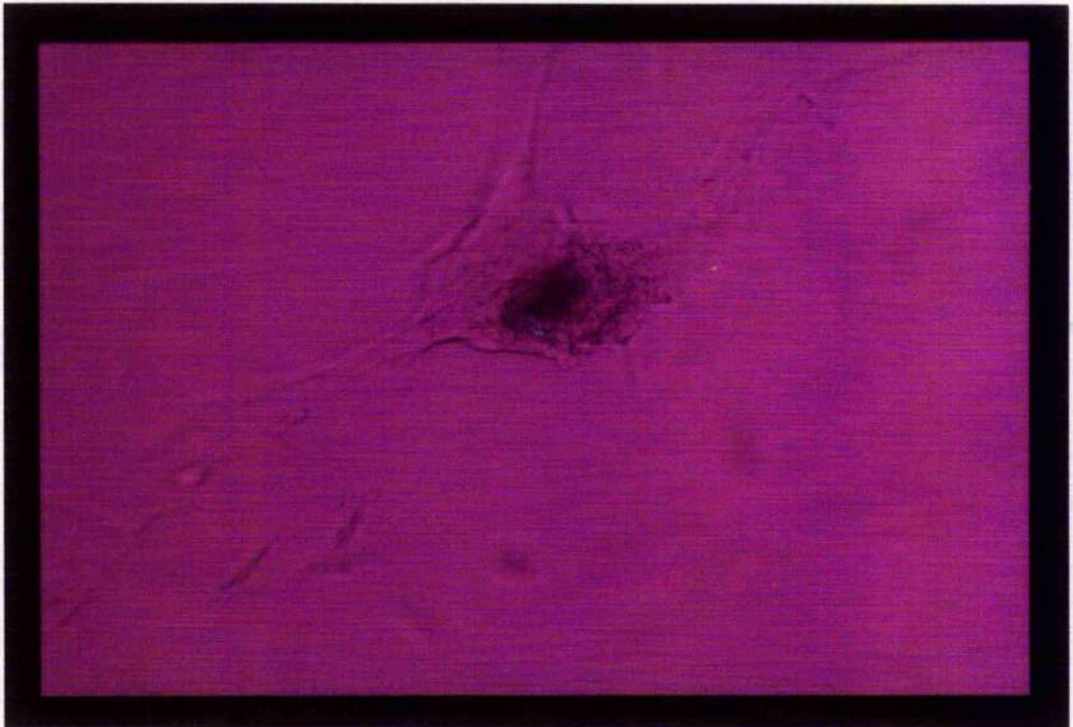


Figure 43: Nodule found in 700 μm diameter tube (length = 1.4 cm) after 12 days of culture and exposure to polarised light (ascorbic acid and β -glycerophosphate added at Day 5) [Original magnification = 20x]

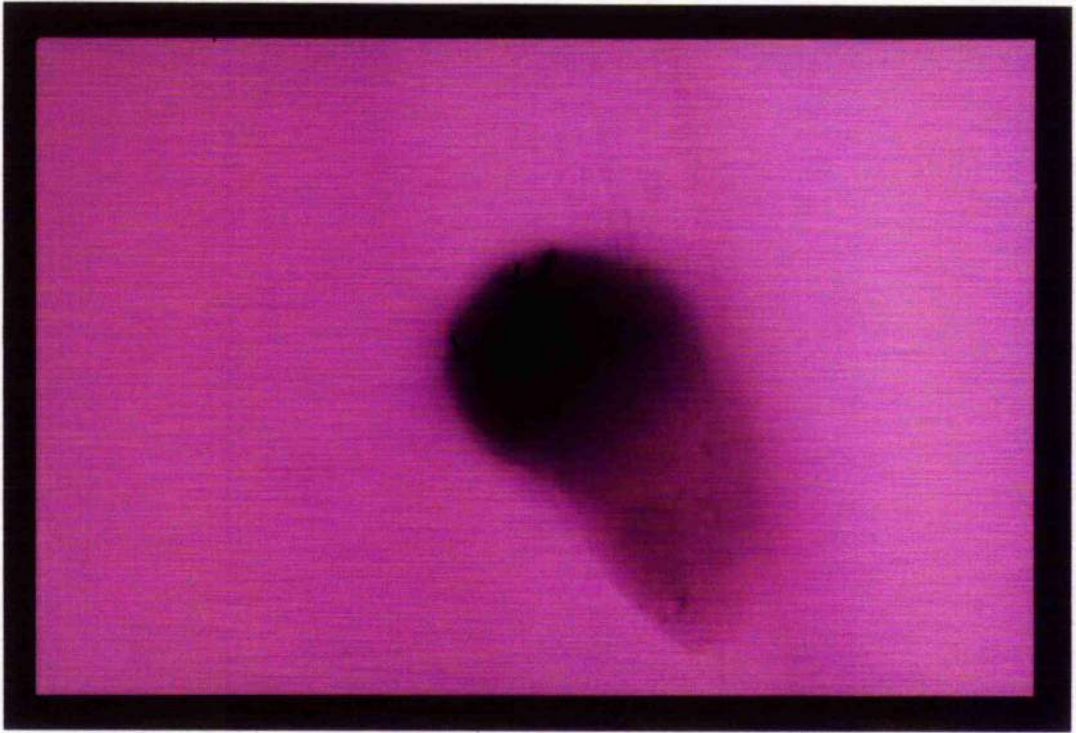


Figure 44: Photograph of large nodule found after 12 days of culture (ascorbic acid and β -glycerophosphate added at Day 5). After exposure to polarised light, most of nodule contained regions of birefringent material. Tube diameter = 700 μm , length = 1.5 cm. [Original magnification = 10x]

Tube Length (cm)	Nodule Number	Length (μm)	SD	Width (μm)	SD
0.6	1	158.4	-	74.25	-
1.2	3	280.5	57.16	135.3	82.43
1.2	5	198	166.84	85.14	23.84
2.5*	12	124.58	58.87	95.7	31.68

Table 16: Nodule size and number in tubes with cells cultured in the presence of β -glycerophosphate and ascorbic acid. Note “*” denotes tube with flared end approximately 1 mm wide. All nodules presented were found in 700 μm wide end.

Tube length (cm)	Birefringent areas/ No. of nodules examined
1.5	1/3
1.4	3/3
1.4	4/7

Table 17: Polarised light analysis of tubes exposed to β -glycerophosphate and ascorbic acid.

DISCUSSION

There are three mechanisms suggested in the literature by which surface topography may influence the osteoblast response to surfaces (Brunette, et al, 1992; Chehroudi, et al, 1997). It is hypothesised that control over cell polarity and shape could favour osteogenesis *in vivo*. Secondly, a “bone-inductive microenvironment” created by topography might promote bone formation. Finally, certain surface topography may favour the attachment of a particularly osteogenic cell population.

The behavioural differences of osteoblasts in tubes versus flat surfaces can be partially explained by the cellular condensation/microenvironment mechanism proposed in several papers by Chehroudi and Brunette (Brunette, et al, 1991; Chehroudi, et al, 1992; Qu, et al, 1996; Chehroudi, et al, 1997). These authors performed several studies to look at the influence of pitted surfaces on bone formation. Brunette, et al, (1991) studied pits with outer surface dimensions of 100 μm x 100 μm with walls tapering to an angle of 55° to the surface and an overall depth of 120 μm . Although they were unable to draw definite conclusions, preliminary work suggested that smaller, mineralised nodules appeared more frequently inside the pits. Chehroudi, et al, (1992), examined larger pits with an outer square with 270 μm sides. The results of *in vivo* experiments with implants placed in the

parietal region of rats revealed mineralization on some pitted surfaces after 8 weeks whereas no mineralization was observed next to smooth surfaces. *In vitro* experiments revealed the presence of some large ($> 10 \mu\text{m}$) globules on pitted surfaces. Only small ($0.5 - 3 \mu\text{m}$) globules were found on smooth culture surfaces. The authors concluded that the environment created by the topography of their implants positively influenced bone formation both *in vivo* and *in vitro*.

Qu, et al, (1996), looked at pits with dimensions of $175 \mu\text{m} \times 175 \mu\text{m}$ tapered at 125° to $100 \mu\text{m}$ in depth. The authors suggest that the restricted environment created by the pits may enhance bone formation by establishing a localised region of cytokines and extracellular matrix factors. Chehroudi, et al, (1997) suggest that the geometry of their pits, ranging from 3 to $120 \mu\text{m}$ deep and tapered at an angle of 125° to the surface, created an environment of increased cell density with little diffusion of regulatory molecules and limited proliferation. The constraint on growth felt by cells in high density environments has been linked to differentiation of various cell types (Boyan, et al, 1996). Thus, there is evidence in the literature for the osteoinductive potential of a localised environment similar to the one created inside tubes.

Further support for a bone inductive microenvironment created by topography like pits and cylinders in these experiments lies in the immunofluorescent results of osteocalcin. Osteocalcin is a late differentiation marker, appears concomitantly with mineralization, and has a role in mineral deposition and crystal growth (Robey, 1989; Gundberg, et al, 1984; Aubin, et al, 1995). When cells in tubes were examined for osteocalcin using confocal scanning laser microscopy, small globules lining the cords and tiny particles lining the tube interior stained heavily, and suggests that there is extracellular matrix production by these

cells in the tubes. Furthermore, given the fact that osteocalcin binds strongly to hydroxyapatite (Marks and Popoff, 1988), it seems to imply that the cells are producing small particles of hydroxyapatite.

CONCLUSIONS

The microenvironment created by small quartz tubes *in vitro*, influenced cell behaviour and extracellular matrix production. Cells exhibited an overall higher rate of activity and dynamic behaviour in all tube sizes examined. Tube diameter influenced whether cords or nodules were more likely to form and a combination of tube length and diameter determined the number of nodules that formed. Cells were able to form nodule-like structures with some regions of birefringence without media supplements, and displayed positively enhanced ECM production in supplemented cultures. This work examines for the first time osteoblast behaviour in a three dimensional space and the direct effects of varying that space.

SUMMARY

Numerous analytical approaches were used to evaluate the behaviour and functional changes of osteoblasts in response to well-defined regular rough (grooved) surfaces and extended concave surfaces (tubes). For example, for the first time in this kind of application, techniques like polarised light and atomic force microscopy were used to assess osteoblast extracellular matrix production. Furthermore, scanning electron microscopy allowed the close assessment of collagen orientation and matrix production, and time lapse video cinemicrography offered the unique opportunity to view firsthand the dynamic response and matrix formation by osteoblasts in a three dimensional environment. Thus, an array of techniques provided a new, more in depth look at osteoblast behaviour and function.

Although more knowledge was gained through this work, improvements could be made in a few areas and new experiments designed to learn more about the initial findings presented here in this work. For example, the grooved fused silica surface could be sputter coated with a thin (50 nm) layer of titanium to assess osteoblasts on a more adhesive and implant-like surface. Furthermore, the quartz tube could be used to screen other factors and modifications like fibronectin coatings, collagen matrices, growth factors or cytokines like BMPs, on osteoblasts in a confined, three dimensional environment.

In conclusion, this work demonstrated the ability of small, regular features and/or spaces to influence osteoblast behavior, morphology, and ECM production. The knowledge gained here could shed light on the parameters important in creating organised tissue leading to a new generation of more successful implants and repair constructs in dentistry and orthopaedics.

REFERENCES

- Aronow, M., Gerstenfeld, L., Owen, T., Tassinari, M., Stein, G., & Lian, J. (1990). Factors That Promote Progressive Development of the Osteoblast Phenotype in Cultured Fetal Rat Calvaria Cells. *Journal of Cellular Physiology*, 143, 213-221.
- Aubin, J. E., Liu, F., Malaval, L., & Gupta, A. K. (1995). Osteoblast and Chondroblast Differentiation. *Bone*, 17(2, Supplement), 77S-83S.
- Bancroft, J., H. Cook, and R. Stirling (1994). Manual of histological techniques and their diagnostic application. Edinburgh: Churchill Livingstone.
- Begley, C. T., Doherty, M. J., Hankey, D. P., & Wilson, D. J. (1993). The culture of human osteoblasts upon bone-graft substitutes. *Bone*, 14, 661-666.
- Bellows, C. G., Aubin, J. E., Heersche, J. N. M., & Antosz, M. E. (1986). Mineralized Bone Nodules Formed *In Vitro* from Enzymatically Released Rat Calvaria Cell Populations. *Calcified Tissue International*, 38, 143-154.
- Benayahu, D., Fried, A., Efraty, M., Robey, P. G., & Wientroub, S. (1995). Bone Marrow Interface: Preferential Attachment of an Osteoblastic Marrow Stromal Cell Line. *Journal of Cellular Biochemistry*, 59, 151-160.
- Bizios, R. (1994). Mini-Review: Osteoblasts: An In Vitro Model of Bone-Implant Interactions. *Biotechnology and Bioengineering*, 43, 582-585.
- Blair, J.M., Sorensen, L.B., Arnsdorf, M.F., Ratneshwar, L. (1995). The application of atomic force microscopy for the detection of microcrystals in synovial fluid from patients with recurrent synovitis. *Seminars in Arthritis and Rheumatism*, 24 (5), 359-369.
- Bobyn, J. D., Pilliar, R. M., Cameron, H. U., & Weatherly, G. C. (1980). The optimum pore size for the fixation of porous-surfaced metal implants by the ingrowth of bone. *Clinical Orthopaedics*, 150, 263-270.
- Boden, S.D., Mocuaig, K., Hair, G., Racine, M., Titus, L., Wozney, J.M., and Nanes, M.S. (1996). Differential Effects and Glucocorticoid Potentiation of Bone Morphogenetic Protein Action During Rat Osteoblast Differentiation in Vitro. *Endocrinology*, 137(8), 3401-3407.
- Boskey, A.L. (1989). Noncollagenous matrix proteins and their role in mineralization. *Bone and Mineral*, 6, 111-123.

- Bowers, K. T., Keller, J. C., Randolph, B. A., Wick, D. G., & Michaels, C. M. (1992). Optimization of Surface Micromorphology for Enhanced Osteoblast Responses In Vitro. *The International Journal of Oral & Maxillofacial Implants*, **7**(3), 302-310.
- Boyan, B.D., Hummert, T.A., Lieswetter, K., Schraub, D., Dean, D.D., and Schwarz, Z. (1995). Effect of titanium surface characteristics on chondrocytes and osteoblasts *in vitro*. *Cells and Materials*, **5**(4), 323-335.
- Boyan, B. D., Hummert, T. W., Dean, D. D., & Z., S. (1996). Role of material surfaces in regulating bone and cartilage cell response. *Biomaterials*, **17**(2), 137-146.
- Boyan, B.D., Hummert, T.A., Lieswetter, K., Schraub, D., Dean, D.D., and Schwarz, Z. (1995). Effect of titanium surface characteristics on chondrocytes and osteoblasts *in vitro*. *Cells and Materials*, **5**(4), 323-335.
- Bres, E.F., Voegel, J.C., Frank, R.M., (1990). High-resolution electron microscopy of human enamel crystals. *Journal of Microscopy*, **160** (2), 183-201.
- Brighton, C.T., Strafford, B., Gross, S.B., Leatherwood, D.I., Williams, J.L., and Pollack, S.R. (1991). The proliferative and synthetic response of isolated calvarial bone cells of rats to cyclic biaxial mechanical strain. *Journal of Bone and Joint Surgery, Series A*, **73**, 320-331.
- Brighton, C.T., Fisher, J.J., Levine, S.E., Corsetti, J.R., Reilly, T., Landsman, A.S., Williams, J.L., and Thibault, L.E. (1996). The biochemical pathway mediating the proliferative response of bone cells to a mechanical stimulus. *Journal of Bone and Joint Surgery Series A*, **78**, 1337-1347.
- Brighton, C.T., Sennett, B.J., Farmer, J.C., Iannotti, J.P., Hansen, C.A., Williams, J.L., and Williamson, J. (1992). The inositol phosphate pathway as a mediator in the proliferative response of rat calvarial bone cells to cyclical biaxial mechanical strain. *Journal of Orthopaedic Research*, **10**, 385-393.
- Bruder, S. P., Fink, D. J., & Caplan, A. I. (1994). Mesenchymal Stem Cells in Bone Development, Bone Repair, and Skeletal Regeneration Therapy. *Journal of Cellular Biochemistry*, **56**, 283-294.
- Brunette, D. M. (1988). The Effects of Implant Surface Topography on the Behavior of Cells. *The International Journal of Oral & Maxillofacial Implants*, **3**, 231-246.
- Brunette, D. M., Ratkay, J., & Chehroudi, B. (1991). Behaviour of Osteoblasts on Micromachined Surfaces. In J. E. Davies (Ed.), The Bone-Biomaterial Interface. Toronto: University of Toronto Press.
- Buckley, M.J., Banes, A.J., Levin, I.G., Sumpio, B.F., Sato, M., Jordan, R., Gilbert, J., Link, G.W., and Tran Son Tay, R. (1988). Osteoblasts increase their rate of division and align in response to cyclic, mechanical tension *in vitro*. *Bone and Mineral*, **4**, 225-236.
- Byers, P.D., Gray, J.C., Mostafa, A.G.S.A., and Ali, S.Y. (1981). The healing of bone and articular cartilage. In L.E. Glynn (Ed.), Tissue repair and regeneration. Amsterdam, New York, Oxford: Elsevier/North-Holland Biomedical Press.

- Chae, J.C., Collier, J.P., Mayor, M.B., Surprenant, V.A., and Dauphinais, L.A. (1992). Enhanced Ingrowth of Porous-Coated CoCr Implants Plasma-Sprayed with Tricalcium Phosphate, *Journal of Biomedical Materials Research*, **26**, 93-102.
- Chehroudi, B., Ratkay, J., & Brunette, D. M. (1992). The role of implant surface geometry on mineralization in vivo and in vitro - a transmission and scanning electron-microscopic study. *Cells And Materials*, **2**, 89-104.
- Chehroudi, B., McDonnell, D., & Brunette, D. M. (1997). The effects of micromachined surfaces on formation of bonelike tissue on subcutaneous implants as assessed by radiography and computer image processing. *Journal of Biomedical Materials Research*, **34**, 279-290.
- Chesmel, K.D. and Black, J. (1995a). Cellular responses to chemical and morphologic aspects of biomaterial surfaces. I. A novel in vitro model system. *Journal of Biomedical Materials Research*, **29**, 1089-1099.
- Chesmel, K.D., Clark, C.C., Brighton, C.T., and Black, J. (1995b). Cellular responses to chemical and morphologic aspects of biomaterial surfaces. II. The biosynthetic and migratory response of bone cell populations. *Journal of Biomedical Materials Research*, **29**, 1101-1110.
- Clark, P., Connolly, P., Curtis, A.S.G., Dow, J.A.T., and Wilkinson, C.D.W. (1987). Topographical Control of Cell Behaviour I. Simple step cues. *Development*, **99**, 439-448.
- Clark, P., Connolly, P., Curtis, A.S.G., Dow, J.A.T., and Wilkinson, C.D.W. (1990). Topographical Control of Cell Behaviour II. Multiple grooved substrata. *Development*, **108**, 635-644.
- Cooley, D.R., Van Dellen, A.F., Burgess, J., and Windeler, A.S. (1992). The advantages of coated titanium implants prepared by radio frequency sputtering from hydroxyapatite. *J. Prosthet. Dent.*, **67**, 93-100.
- Copley, L.A., Reilly, T.M., and Brighton, C.T. (1994). Integrins and the transduction of mechanical stress into proliferation in rat osteoblasts. *Trans Orthopaed Res Soc*, **19(1&2)**, 306(Abstract).
- Culling, C., Allison, R., & Barr, W. (1985). Cellular Pathology Technique (4th ed.). London: Butterworths.
- Curtis, A.S.G. and Varde, M. (1964). Control of Cell Behaviour: Topological Factors. *Journal of the National Cancer Institute*, **33(1)**, 15-26.
- Davies, J. E. (1996). In Vitro Modeling of the Bone/Implant Interface. *The Anatomical Record*, **245**, 426-445.
- Davies, J. E., & Matsuda, T. (1988). Extracellular Matrix Production by Osteoblasts on Bioactive Substrata *in vitro*. *Scanning Microscopy*, **2(3)**, 1445-1452.
- Dee, K.C., Rueger, D.C., Andersen, T.T., and Bizios, R. (1996). Conditions which promote mineralization at the bone-implant interface: A model *in vitro* study. *Biomaterials*, **17**, 209-215.

- Dennis, J., Haynesworth, S., Young, R., & Caplan, A. (1992). Osteogenesis in marrow-derived mesenchymal cell porous ceramic composites transplanted subcutaneously: Effect of fibronectin and laminin on cell retention and rate of osteogenic expression. *Cell Transplantation*, **1**, 23-32.
- Deodhar, A. A., & Woolf, A. D. (1996). Bone mass measurement and bone metabolism in rheumatoid arthritis: A review. *British Journal of Rheumatology*, **35**, 309-322.
- Dolce, C., Kinniburgh, A. J., & Dziak, R. (1995). Proto-oncogene activation in osteoblast cells due to mechanical stretching. *Journal of Dental Research*, **74**(Special Issue), 153(Abstract).
- Duncan, R.L. and Turner, C.H. (1995). Mechanotransduction and the Functional Response of Bone to Mechanical Strain. *Calcified Tissue International*, **57**, 344-358.
- Drury, R.A. and Wallington, E.A. (1967). Carleton's Histological Technique (4th ed.). New York, Toronto: Oxford University Press.
- Ecarot-Charrier, B., Shepard, N., Charette, G., Grynepas, M., & Glorieux, F. (1988). Mineralization in Osteoblast Cultures: A Light and Electron Microscopic Study. *Bone*, **9**, 147-154.
- Eggl, P. S., Mueller, W., & Schenk, R. K. (1987). The role of pore size on bone ingrowth and implant substitution in hydroxyapatite and tricalcium phosphate ceramics; A histologic and morphometric study in rabbits. In A. Pizzoferrato, P. G. Marchetti, A. Ravaglioli, & A. J. C. Lee (Eds.), Biomaterials and Clinical Applications (pp. 53-56). Amsterdam: Elsevier Science Publishers B.V.
- Friedman, R.J., Bauer, T.W., Garg, K., Jiang, M., Yuehuei, H., Draughn, R.A. (1995) Histological and Mechanical Comparison of Hydroxyapatite-Coated Cobalt-Chrome and Titanium Implants in the Rabbit Femur, *Journal of Applied Biomaterials*, **6**, 231-235.
- Gallagher, J. A., Gundle, R., & Beresford, J. N. (1996). Isolation and Culture of Bone-Forming Cells (Osteoblasts) from Human Bone. In G. E. Jones (Ed.), Methods in Molecular Medicine: Human Cell Culture and Protocols Totowa, NJ: Humana Press.
- Gomi, K., & Davies, J. E. (1993). Guided bone tissue elaboration by osteogenic cells in vitro. *Journal of Biomedical Materials Research*, **27**, 429-431.
- Gray, C., Boyde, A., & Jones, S. J. (1996). Topographically induced bone formation in vitro: Implications for bone implants and bone grafts. *Bone*, **18**, 115-123.
- Groessner-Schreiber, B., & Tuna, R. S. (1992). Enhanced extracellular matrix production and mineralization by osteoblasts cultured on titanium surface in vitro. *Journal of Cell Science*, **101**, 209-217.
- Gundberg, C. M., Hauschka, P. V., Lian, J. B., & Gallop, P. M. (1984). Osteocalcin: Isolation, Characterization, and Detection. *Methods in Enzymology*, **107**, 516-545.

- Hambleton, J., Schwartz, Z., Kharc, A., Windeler, S., Luna, M., Brooks, B., Dean, D., & Boyan, B. D. (1994). Culture surfaces coated with various implant materials affect chondrocyte growth and differentiation. *Journal of Orthopaedic Research*, **12**, 542-553.
- Hancin, D., Sabanay, H., Addadi, L., and Geiger, B. (1993). Differential adhesion of cells to enantiomorphous crystal surfaces. *Science*, **263**, 1413-1416.
- Harris, S. E., Bonewald, L. F., Harris, M. A., Sabatini, M., Dallas, S., Feng, J. Q., GhoshChoudhury, N., Wozney, J., & Mundy, G. R. (1994). Effects of transforming growth factor beta on bone nodule formation and expression of bone morphogenetic protein 2, osteocalcin, osteopontin, alkaline phosphatase, and type I collagen mRNA in long-term cultures of fetal rat calvarial osteoblasts. *Journal of Bone and Mineral Research*, **9**, 855-863.
- Harrison, R. (1911). On the stereotropism of embryonic cells. *Science*, **34**, 279.
- Hasegawa, S., Sato, S., Saito, S., Suzuki, Y., and Brunette, D.M. (1985). Mechanical Stretching Increases the Number of Cultured Bone Cells Synthesizing DNA and Alters Their Pattern of Protein Synthesis. *Calcified Tissue International*, **37**, 431-436.
- Hayashi, K., Matsuguchi, N., Uenoyama, K., Kanemaru, T. and Sugioka, Y. (1989) Evaluation of metal implants coated with several types of ceramics as biomaterials, *Journal of Biomedical Materials Research*, **23**, 1247-1259.
- Herbertson, A. and Aubin, J.E. (1995). Dexamethasone Alters the Subpopulation Make-Up of Rat Bone Marrow Stromal Cell Cultures. *Journal of Bone and Mineral Research*, **10**(2), 285-294.
- Hung, C. T., Pollack, S. R., Reilly, T. M., & Brighton, C. T. (1995). Real-time calcium response of cultured bone cells to fluid flow. *Clinical Orthopaedics and Related Research*, 256-269.
- Hungerford, D., & Jones, L. (1988). The Rationale of Cementless Revision of Cemented Arthroplasty Failures. *Clinical Orthopaedics and Related Research*, **October**, 12-24.
- Keller, J., & Young, F. (1987). Quantitative bone remodelling resulting from the use of porous dental implants. *Journal of Biomedical Materials Research*, **21**, 305-319.
- Kiernan, J. (1981). Histological and Histochemical Methods: Theory and Practice. Oxford: Pergamon Press.
- Lees, S. (1979). A model for the distribution of HAP crystallites in bone - An hypothesis. *Calcified Tissue International*, **27** (1), 53-56.
- Lillic, R., & Fullmer, H. (1976). Histopathologic Technique and Practical Histochemistry. New York: McGraw-Hill Book Co.
- Marieb, E. N. (Ed.). (1995). Human Anatomy and Physiology (Third ed.). New York: The Benjamin/Cummings Publishing Company, Inc.
- Marks, A. and Popoff, S. (1988). Bone Cell Biology: The Regulation of Development, Structure, and Function in the Skeleton. *The American Journal of Anatomy*, **183**, 1-44.

- Majeska, R., Nair, B., and Rodan, G. (1981). Glucocorticoid regulation of alkaline phosphatase in the osteoblastic osteosarcoma cell line ROS 17/2.8. *Endocrinology*, **116**, 170.
- Martin, J. Y., Schwartz, Z., Hummert, T. W., Schraub, D. M., Simpson, J., Lankford, J., Dean, D. D., Cochran, D. L., & Boyan, B. D. (1995). Effect of titanium surface-roughness on proliferation, differentiation, and protein-synthesis of human osteoblast-like cells (MG63). *Journal Of Biomedical Materials Research*, **29**, 389-401.
- McCabe, L. R., Last, T. J., Lynch, M., Lian, J., & Stein, G. (1994). Expression of cell growth and bone phenotypic genes during the cell cycle of normal diploid osteoblasts and osteosarcoma cells. *Journal of Cellular Biochemistry*, **56**, 274-282.
- Michaels, C. M., Keller, J. C., Stanford, C. M., & Solursh, M. (1989). In vitro cell attachment of osteoblast-like cells to titanium. *Journal of Dental Research*, **68**, 276.
- Mundy, G.R. (1993). Cytokines and growth factors in the regulation of bone remodeling. *Journal of Bone and Mineral Research*, **8**, S505-S510.
- Nimb, L., Jensen, J.S., Gotfredsen, K. "Interface mechanics and histomorphometric analysis of hydroxyapatite-coated and porous glass-ceramic implants in canine bone," *Journal of Biomedical Materials Research*, 1995, Vol. 29, 1477-1482.
- Owen, T., Aronow, M., Shalhoub, V., Barone, M., Wilming, L., Tassinari, M., Kennedy, M., Pockwinse, S., Lian, J., & Stein, G. (1990). Progressive Development of the Rat Osteoblast Phenotype In Vitro: Reciprocal Relationships in Expression of Genes Associated With Osteoblast Proliferation and Differentiation During Formation of the Bone Extracellular Matrix. *Journal of Cellular Physiology*, **143**, 420-430.
- Park, J. B., & Lakes, R. S. (1992). Biomaterials: An Introduction (2nd ed.). New York: Plenum Press.
- Pockwinse, S., Wilming, L., Conlon, D., Stein, G., & Lian, J. (1992). Expression of Cell Growth and Bone Specific Genes at Single Cell Resolution During Development of Bone Tissue-Like Organization in Primary Osteoblast Cultures. *Journal of Cellular Biochemistry*, **49**, 310-323.
- Pulco, D., Holleran, L., Doremus, R., & Bizios, R. (1991). Osteoblast responses to orthopaedic implant materials *in vitro*. *Journal of Biomedical Materials Research*, **25**, 711-723.
- Qu, J., Chehroudi, B., & Brunette, D. M. (1996). The use of micromachined surfaces to investigate the cell behavioural factors essential to osseointegration. *Oral Diseases*, **2**, 102-115.
- Rashmir-Raven, A.M., Richardson, D.C., Aberman, H.M., and DeYoung, D.J. (1995) The Response of Cancellous and Cortical Canine Bone to Hydroxylapatite-Coated and Uncoated Titanium Rods, *Journal of Applied Biomaterials*, **6**, 237-242.
- Reddi, A. (1997). Bone Morphogenesis and Modeling: Soluble Signals Sculpt Osteosomes in the Solid State. *Cell*, **89**, 159-161.
- Ricci, J., Alexander, H., Gona, A., & Lelah, M. (1990). In vitro tendon cell colony growth rates on synthetic fibers. *Journal of Applied Biomaterials*, **1**, 103-110.

- Ricci, J., Charvet, J., Chang, R., Howard, C., Green, W., Weiser, L., & Alexander, H. (1994). In vitro effects of surface microgeometry on colony formation by fibroblasts and bone cells, *presented at the 20th Annual Society for Biomaterials, Boston, MA*, 401.
- Robey, P. G. (1989). The Biochemistry of Bone. *Endocrinology and Metabolism Clinics of North America*, **18**(4), 859-901.
- Rubin, H. (1993). Spontaneous transformation as aberrant epigenesis. *Differentiation*, **53**, 123-137.
- Schaad P., Paris E., Cuisinier F.J., Voegel J.C. (1993) Atomic force microscopy study of human tooth enamel surfaces. *Scanning Microscopy*, **7**(4):1149-1152.
- Schmidt, R. and Kulbe, K.D. (1993). Long-term cultivation of human osteoblasts. *Bone and Mineral*, **20**, 211-221.
- Schulz, A. (1995). "True bone" in vitro? *Virchows Archiv*, **426**, 103-105.
- Selye, H., Lemire, Y., & Bajusz, E. (1960). Induction of bone, cartilage and hemopoietic tissue by subcutaneously implanted tissue diaphragms. *Roux' Archive fur Entwicklungsmechanik*, **151**, 572-585.
- Sherwood, L. (1993). *Human Physiology: From Cells to Systems* (2nd ed.). St. Paul: West Publishing Company.
- Slyter, E.M. (1970). *Optical Methods in Biology*. New York: Wiley-Interscience.
- Somjen, D., Binderman, I., Berger, E., and Harell, A. (1980). Bone remodelling induced by physical stress is prostaglandin E3 mediated. *Biochimica et Biophysica Acta*, **627**, 91-100.
- Stanford, C. and Keller, J. (1991). The Concept of Osseointegration and Bone Matrix Expression. *Critical Reviews in Oral Biology and Medicine*, **2**(1), 83-101.
- Stein, G.S., Lian, J.B., and Owen, T.A. (1990). Relationship of cell growth to the regulation of tissue-specific gene expression during osteoblast differentiation. *The FASEB Journal*, **4**, 3111-3123.
- Stein, G. S., Lian, J. B., Stein, J. L., Van, W. A., & Montecino, M. (1996). Transcriptional control of osteoblast growth and differentiation. *Physiological Reviews*, **76**, 593-629.
- Thomas, K., Kay, J., Cook, S., & Jarcho, M. (1987). The effect of surface macrotexture and hydroxylapatite coating on the mechanical strengths and histologic profiles of titanium implant materials. *Journal of Biomedical Materials Research*, **21**, 1395-1414.
- Tisdell, C.L., Goldberg, V.M., Parr, J.A., Bensusan, J.S., Staikoff, L.S., and Stevenson, S. (1994). The Influence of a Hydroxyapatite and Tricalcium-Phosphate Coating on Bone Growth into Titanium Fiber-Metal Implants. *The Journal of Bone and Joint Surgery, American Volume*, **76-A** (2), 159-171.
- Voegel, J.C., Frank, R.M. (1977). Stages in the dissolution of human enamel crystals in dental caries. *Calcified Tissue Research*, **24**(1), 19-27.
- Webster, S.S.J. (1988). The Skeletal Tissues. In: L. Weiss (Ed.), *Cell and Tissue Biology: A Textbook of Histology*. Baltimore/Munich: Urban & Schwarzenberg.

- Weiss, P. (1945). Experiments on Cell and Axon Orientation In Vitro: The Role of Colloidal Exudates in Tissue Organization. *Journal of Experimental Zoology*, **100**, 353-386.
- Weiss, P. and Taylor, A.C. (1956). Fish Scales as Substratum for Uniform Orientation of Cells In Vitro. *Anatomical Record*, **124**, 381.
- Wennerberg, A., Albrektsson, T., & Andersson, B. (1993). Design and Surface Characteristics of 13 Commercially Available Oral Implant Systems. *International Journal of Oral and Maxillofacial Implants*, **8**(6), 622-633.
- Wilkinson, C. and Curtis, A. (1996). Nanofabrication and its applications in medicine and biology. In R.R.H. Coombs and D.W. Robinson (Eds.), Nanotechnology in Medicine and the Biosciences. Gordon & Breach.
- Wojciak-Stothard, B., Curtis, A., Monaghan, W., McGrath, M., Sommer, I., and Wilkinson, C. (1995). Role of the cytoskeleton in the reaction of fibroblasts to multiple grooved substrata. *Cell Motility and the Cytoskeleton*, **31**, 147-158.
- Withold, W. (1996). Monitoring of bone turnover biological, preanalytical and technical criteria in the assessment of biochemical markers. *European Journal of Clinical Chemistry and Clinical Biochemistry*, **34**, 785-799.
- Wojciak, B. and Crossan, J. (1994). The effects of T Cells and their products on in vitro healing of epitenon cell microwounds. *Immunology*, **83**, 93-98.
- Wojciak, B., Crossan, J., Curtis, A.S.G., and Wilkinson, C.D.W. (1995). Grooved Substrata Facilitate In Vitro Healing of Completely Divided Flexor Tendons. *Journal of Materials Science: Materials in Medicine*, **6**, 266-271.
- Wojciak-Stothard, B., Madeja, Z., Korohoda, W., Curtis, A., and Wilkinson, C. (1995). Activation of macrophage-like cells by multiple grooved substrata. Topographical control of cell behaviour. *Cell Biology International*, **19**(6), 485-490.
- Wojciak-Stothard, B., Curtis, A., Monaghan, W., Macdonald, K., and Wilkinson, C. (1996). Guidance and Activation of Murine Macrophages by Nanometric Scale Topography. *Experimental Cell Research*, **223**, 426-435.
- Wong, M., Eulenberger, J., Schenk, R. and Hunziker, E. (1995) Effect of surface topology on the osseointegration of implant materials in trabecular bone, *Journal of Biomedical Materials Research*, **29**, 1567-1575.